DEVELOPMENT, CHARACTERIZATION AND SOLID PARTICLE EROSION RESPONSE OF POLYESTER BASED HYBRID COMPOSITES

A THESIS SUBMITTED IN PARTIAL FULFILMENT OF THE REQUIREMENT
FOR THE AWARD OF THE DEGREE OF

Doctor of Philosophy

in

MECHANICAL ENGINEERING

By

Amar Patnaik

Roll No. 50603005

Department of Mechanical Engineering
National Institute of Technology
Rourkela, India

AUGUST, 2008

DEVELOPMENT, CHARACTERIZATION AND SOLID PARTICLE EROSION RESPONSE OF POLYESTER BASED HYBRID COMPOSITES

A THESIS SUBMITTED IN PARTIAL FULFILMENT OF THE REQUIREMENTS FOR THE DEGREE OF

Doctor of Philosophy

in

Mechanical Engineering

Submitted to

National Institute of Technology, Rourkela
(Deemed University)

By

Amar Patnaik
(Roll No. 50603005)

Under the supervision of

Prof. S. S. Mahapatra
and
Prof. R. R. Dash

Department of Mechanical Engineering
National Institute of Technology
Rourkela, India
AUGUST, 2008

Dedicated to

My Grand Parents

Late Kristna Chandra Patnaik and

Late Chandrama Patnaik

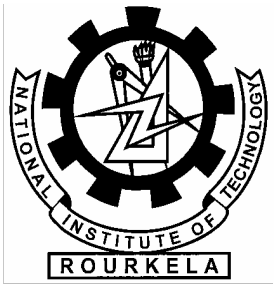

NATIONAL INSTITUTE OF TECHNOLOGY

ROURKELA

CERTIFICATE

This is to certify that the thesis entitled **DEVELOPMENT, CHARACTERIZATION AND SOLID PARTICLE EROSION RESPONSE OF POLYESTER BASED HYBRID COMPOSITES** being submitted by **Amar Patnaik** to the National Institute of Technology, Rourkela, INDIA, for the award of the degree of **Doctor of Philosophy** in Mechanical Engineering, is an authentic record of research work carried out by him under our supervision and guidance and the work incorporated in this thesis has not been, to the best of our knowledge, submitted to any other University or Institute for the award of a degree or diploma.

Rourkela	**Dr. Siba Sankar Mahapatra (Guide)**	**Dr. R.R.Dash (Guide)**
Date	N.I.T.Rourkela-769008	G.I.E.T.Gunupur-765022

acknowledgement

I would like to extend my sincere thanks to my supervisors Dr. S. S. Mahapatra and Dr. R. R. Dash for their able guidance and support throughout the research work.

I am grateful to **Professor Sunil Kumar Sarangi**, Director, National Institute of Technology, Rourkela who has been a constant source of inspiration for me. I am also grateful to **Professor R.K.Sahoo**, Head of the Department of Mechanical Engineering for his help and cooperation. I appreciate the encouragement from faculty members of the Mechanical Engineering Dept. of N.I.T. Rourkela.

I am grateful to Dr. Alok Satapathy and Dr. B.B. Verma, members of my doctoral scrutiny committee for being helpful and generous during the course of this work.

I am grateful to my parents and my sisters, for the tremendous amount of inspiration and moral support they have given me since my childhood. My special thanks go to Dr. Alok Satapathy for his support and encouragement in my work. I also thank my friends Dr. M.S.Khan, Dr. Sudhakar Pandian, Mahesh and Ms. Sandhyarani Biswas for their constant inspiration during my research work and all other technical staffs Samir and Rajesh who helped me directly and indirectly in my thesis work.

Finally, but most importantly, I thank God Almighty, my Lord for giving me the will power and strength to make it this far when I didn't see a light

Date :

N.I.T. Rourkela **(Amar Patnaik)**

LIST OF FIGURES

******

LIST OF TABLES

ABSTRACT

Erosive wear of engineering components caused by abrasive particles is a major industrial problem. Polymer composites are often used as engineering/ structural components where erosive wear occurs. Due to the operational requirements in dusty environments, the study of solid particle erosion characteristics of the polymeric composites becomes highly relevant. But, even today, the effect of fiber reinforcement and ceramic particulate filling on erosion characteristics of polyester composites has remained a much less studied area. Research in this respect is needed particularly with the inclusion of ceramic fillers both in view of the scientific and commercial importance. Moreover, a full understanding of the effects of all system variables on the wear rate is necessary in order to undertake appropriate steps in the design of machine or structural component and in the choice of materials to reduce/control wear.

The research reported in this thesis consists of two parts: The first part has provided the descriptions of the experimental program and has presented the mechanical characteristics of the hybrid composites under this study; the second part has reported the effect of different ceramic fillers on the solid particle erosion characteristics of glass-polyester composites. Two industrial wastes (flyash and cement by-pass dust) rich in metal oxides and two conventional ceramic powders (Al_2O_3 and SiC) have been used as the filler materials. The unfilled glass polyester composite has a strength of 349.6 MPa in tension and that this value drops to 304.5 MPa and 279.4 MPa with addition of 10 wt% and 20 wt% of flyash respectively. Among the four fillers taken in this study, the inclusion of alumina causes maximum reduction in the composite strength.

A theoretical model for the estimation of erosion wear rate based on the assumption that the kinetic energy of the erodent is utilized to cause micro-indentation leading to material loss has been developed. Then, a series of erosion experiments are conducted using an air jet type test rig on these composites under various test conditions. For this purpose, an experiment schedule is prepared following design of

experiments approach using Taguchi's orthogonal arrays in order to reduce the number of experiments without sacrificing the information to be extracted.

The analytical and experimental investigation suggests that successful fabrication of multi-component hybrid glass-polyester composites with reinforcement of ceramic fillers is possible. Incorporation of fillers modifies the tensile, flexural, impact and inter-laminar shear strengths of the glass polyester composites. The unfilled glass polyester composite has a strength of 349.6 MPa in tension and that this value drops to 304.5 MPa and 279.4 MPa with addition of 10 wt% and 20 wt% of flyash respectively. Among the four fillers taken in this study, the inclusion of alumina causes maximum reduction in the composite strength. The impact energy values of different composites recorded during the impact tests. It shows that the resistance to impact loading of glass-polyester composites improves with addition of particulate fillers. It is seen that with incorporation of CBPD particles the impact strength of unfilled glass fiber-polyester composite increases by about 15% - 20%. It is also noteworthy that the Al_2O_3 filled composites show 10% - 15% higher impact strength compared to the unfilled one. In case of the other two fillers (flyash and silicon carbide) the increment in impact strength is marginal.

The proposed theoretical model is found to perform well for the polymer based hybrid composites for normal as well as oblique impacts. The erosion efficiencies of these composites under normal impact vary from 3 to 6%, 6-9% and 9-12% for impact velocities 58m/sec, 45m/sec and 32m/sec respectively. The presence of particulate fillers in these composites improves their erosion wear resistance and this improvement depends on the type and content of the fillers.

Erosion characteristics of these composites have been successfully analyzed using Taguchi experimental design scheme. Significant control factors affecting the erosion rate have been identified through successful implementation of analysis of variance (ANOVA). Two predictive models - one based on artificial neural network (ANN) and the other one based on Taguchi approach are proposed. It has been demonstrated that these models reflect the effects of various factors on the erosion loss and their predictive results are consistent with theoretical observations.

*****

CONTENTS

*****

Chapter 1

Introduction

Chapter 1

INTRODUCTION

1.1 Background and motivation

Composites are materials consisting of two or more chemically distinct constituents, on a macro-scale, having a distinct interface separating them. One or more discontinuous phases are, therefore, embedded in a continuous phase to form a composite. The discontinuous phase is usually harder and stronger than the continuous phase and is called the *reinforcement*, whereas, the continuous phase is termed as the *matrix.* The matrix material can be metallic, polymeric or can even be ceramic. When the matrix is a polymer, the composite is called polymer matrix composite (PMC). The reinforcing phase can either be fibrous or non-fibrous (particulates) in nature. The fibre reinforced polymers (FRP) consist of fibres of high strength and modulus embedded in or bonded to a matrix with distinct interface between them. In this form, both fibres and matrix retain their physical and chemical identities. In general, fibres are the principal load carrying members while the matrix keeps them at the desired location and orientation, acts as a load transfer medium between them, and protects them from environmental damages [1].

Fibre reinforced polymer (FRP) composites have emerged from being exotic materials used only in niche applications following the Second World War to common engineering materials used in a diverse range of applications. Composites are now used in aircraft, helicopters, space-craft, satellites, ships, submarines, automobiles, chemical processing equipment, sporting goods and civil infrastructure, and there is the potential for common use in medical prosthesis and microelectronic devices. Composites have emerged as important materials because of their light-weight, high specific strength and stiffness, excellent fatigue resistance and outstanding corrosion resistance compared to most common metallic alloys such as steel and aluminium. Other advantages of composites include the ability to fabricate, directional mechanical properties, low thermal expansion coefficients and high dimensional stability. It is the combination of outstanding physical, thermal and mechanical properties that makes composites attractive to use in place of metals in many applications, particularly when weight-saving is critical. As already mentioned, FRP composites are simply multi-constituent materials that consist of reinforcing fibres

embedded in a rigid polymer matrix. The fibres used in FRP materials can be in the form of small particles, whiskers or continuous filaments. Most composites used in engineering applications contain fibres made of glass, carbon or aramid. A diverse range of polymers can be used as the matrix to FRP composites, and these are generally classified as thermoset (e.g. epoxy, polyester) or thermoplastic (e.g. polyether-ether-ketone, polyamide) resins. In almost all engineering applications requiring high stiffness, strength and fatigue resistance, composites are reinforced with continuous fibres rather than small particles or whiskers. Continuous fibre composites are characterized by a two-dimensional (2D) laminated structure in which the fibres are aligned along the plane (x- and y-directions) of the material. The use of FRP composites continues to grow at an impressive rate as these materials are used more in their existing markets and become established in relatively new markets such as biomedical devices and civil structures [2].

A judicious selection of matrix and the reinforcing phase can lead to a composite with a combination of strength and modulus comparable to or even better than those of conventional metallic materials [3]. The physical and mechanical characteristics can further be modified by adding a solid filler phase to the matrix body during the composite preparation. The improved performance of polymers and their composites in industrial and structural applications by the addition of particulate filler materials has shown a great promise and so has lately been a subject of considerable interest. Specific fillers (additives) are added to enhance and modify the quality of composites. The fillers play a major role in determining the properties and behaviour of particulate reinforced composite materials.

A possibility that the incorporation of both particles and fibres in polymer could provide a synergism in terms of improved properties and performance has not been adequately explored so far. However, some recent reports suggest that by incorporating filler particles into the matrix of fibre reinforced composites, synergistic effects may be achieved in the form of higher modulus and reduced material cost, yet accompanied with decreased strength and impact toughness [4-5]. Such multi-component composites consisting of a matrix phase reinforced with a fibre and filled with particulate matters are termed as *hybrid* composites.

Wear is damage to a solid surface usually involving progressive loss of materials, owing to relative motion between the surface and a contacting substance or substances [6]. It is a material response to the external stimulus and can be mechanical or chemical in nature. Wear is unwanted and the effect of wear on the reliability of industrial components is recognised widely and the cost of wear has also been recognised to be high. Systematic efforts in wear research were started in 1960s in industrialized countries. The direct costs of wear failures (i.e. wear part replacements), increased work and time, loss of productivity as well as indirect losses of energy and the increased environmental burden are real problems in everyday work and business. In catastrophic failures, there is also the possibility of human losses. Although wear has been extensively studied scientifically, still wear problems persist in industrial applications. This actually reveals the complexity of the wear phenomenon [7].

The factors affecting wear are [8]

- factors related to material properties, e.g., hardness, toughness, microstructure and chemical composition
- factors connected with operating conditions, e.g., contacting surfaces, contact pressure, relative velocity, operating temperature, and surface finish
- environmental conditions

There are quite a few terms to describe various wear modes; however, these modes can be clubbed into four principal categories [9]

1. abrasion
2. adhesion
3. erosion
4. surface fatigue

Abrasive wear: When two surfaces in contact move against each other, harder particles in one cut through the other. The mechanism of material removal may be the plastic deformation or fracture of the material ahead of the abradant, depending on material properties and sharpness of the abradant. Alternatively the abrasion can be brought about by a third particle entrapped between two rubbing surfaces. Abrasive wear comes into play when a tangential motion causes the material removal by the simultaneous micro-ploughing and micro-cutting [6].

Adhesive wear: This form of wear comes into play when two microscopically smooth bodies rub each other, the surface asperities at the contact point deform, and cold weld junctions form. Owing to a continued sliding, the older junctions shear off and new junctions form. If the cold junction shears off at a plane, material is transferred from one surface to the other. With further rubbing some of the transferred material gets detached and form loose wear debris [8]. Even the redeposition of worn particles to the original surface is also possible.

Erosion wear: In this mode of wear, a progressive loss of material occurs from a solid surface owing to a mechanical interaction between the surface and an impinging fluid stream [10]. The fluid stream may entrain the solid particles aiding the wear process.

Surface fatigue: The process in which tiny wear particles are dislodged from a surface by fracture on repeated rolling or sliding on the surface is known as surface fatigue. Owing to a repeated loading action subsurface cracks grow from pre existing defects. These cracks grow and join hands with other vicinal cracks and finally come to the surface removing a small chunk of material [9].

Solid particle erosion (SPE), a typical erosion wear mode, is the loss of material that results from repeated impact of small, solid particles. In some cases SPE is a useful phenomenon, as in sandblasting and high-speed abrasive water jet cutting but it is a serious problem in many engineering systems including steam and jet turbines, pipelines and valves carrying particulate matter, and fluidized bed combustion (FBC) systems. Solid particle erosion is to be expected whenever hard particles are entrained in a gas or liquid medium impinging on a solid at any significant velocity. In both cases, particles can be accelerated or decelerated and their directions of motion can be changed by the fluid.

Polymer composites are often used as engineering as well as structural components where erosive wear occurs. Due to the operational requirements in dusty environment, the study of solid particle erosion characteristics of the polymeric composites becomes highly relevant. Differences in the erosion behaviour of various types of composite materials are caused by the amount, type, orientation and properties of the reinforcement on the one hand and by the type and properties of the matrix and its adhesion to the fibres/fillers on the other hand. A full understanding

of the effects of all system variables on the wear rate is necessary in order to undertake appropriate steps in the design of machine or structural component and in the choice of materials to reduce/control wear [11].

The subject of erosion wear of polymer composites has not received substantial attention in past two decades. Interest in this area is commensurate with the increasing utilization of composites in aerospace, transportation and process industries, in which they can be subjected to multiple solid or liquid particle impact. Examples of these applications are pipe lines carrying sand slurries in petroleum refining, helicopter rotor blades [12], pump impeller blades, high speed vehicles and aircrafts operating in desert environments, water turbines, aircraft engines [13], missile components, canopies, radomes, wind screens [14] and outer space applications [15]. Resistance to rain and sand erosion is called among the major issues in the defence application of non-metallic materials [14]. Although a great amount of work has already been devoted to this topic many questions are still open. A comprehensive and systematic investigation of erosion in polymer composites has not been performed yet. Studies made on the erosive wear of composites refer more on fibre-reinforced polymer (FRP) and less on filler-reinforced-systems. The effect of fillers is considered more as modification of the matrix and less as reinforcement, possibly because of the low percentage of fillers. As a result, the effect of particulate fillers on erosion characteristics of hybrid composites has hardly received any research attention. There is no clear understanding of the mechanism of erosion and how the properties of the constituents and the interface affect the erosion behaviour of these composites. Extensive research is therefore needed to develop various methods and theoretical models for predicting erosion behaviour and its dependence on the proportion of the components and the composite micro-structure.

Statistical methods have commonly been used for analysis, prediction and/or optimization of a number of engineering processes. Such methods enable the user to define and study the effect of every single condition possible in an experiment where numerous factors are involved. Solid particle erosion is a complex wear phenomenon in which a number of control factors collectively determine the performance output (i.e. the erosion rate) and there is enormous scope in it for implementation of appropriate statistical techniques for process optimization. But unfortunately, such studies have not been adequately reported so far. The present work addresses to

this aspect by adopting a systematic statistical approach called Taguchi method to optimize the process parameters leading to minimum erosion of the polymer composites under study.

Against this background, the present work has been undertaken to investigate the erosion characteristics of polyester based hybrid composites. The focus has been on fabrication of a series of hybrid composites (glass-fibre-reinforced polyester composites with and without ceramic fillers), evaluation of their mechanical properties, development of a theoretical erosion model, assessment of their relative wear performance and on statistical interpretation of the various test results.

The objectives of this work are outlined as follows:

1. Fabrication of a series of glass fiber reinforced polyester matrix composites with and without ceramic fillers.
2. Characterization of mechanical properties such as tensile strength, flexural strength, tensile modulus, impact strength, inter-laminar shear strength and micro-hardness test of these composites.
3. Development of a theoretical model for estimation of erosion wear rate under multiple impact condition.
4. Parametric appraisal of erosion wear process of unfilled/particulate filled glass-fiber polyester composites and optimization.
5. Prediction of wear rate using artificial neural networks (ANN) and comparison with theoretical and experimental results.

1.2 Thesis outline

The remainder of this thesis is organized as follows:

Chapter 2: Includes a literature review designed to provide a summary of the base of knowledge already available involving the issues of interest. It presents the research works on fiber as well as particulate reinforced polymer composites by various investigators.

Chapter3: Includes a detailed description of the raw materials, test procedures, and design of experiments methodology. It presents the details of fabrication and characterization of the composites under investigation

and also an explanation of the Taguchi experimental design and neural computation.

Chapter 4: Presents the physical and mechanical properties of the composites under study.

Chapter 5: Proposes a theoretical model for estimation of erosion wear rate.

Chapter 6: Includes the erosion characteristics of glass-polyester-composites (without any particulate filler). It aims to validate the theoretical erosion model proposed in the previous chapter through experimental investigation. It also proposes a prediction model based on artificial neural networks (ANN) for estimation of erosion wear rate under different operating conditions and determines the optimal factor settings using genetic algorithm (GA).

Chapter 7: Includes the erosion characteristics of glass-polyester-composites (with different particulate fillers). It presents a detailed study on the effect of particulate fillers on the erosion behaviour of glass-polyester composites. The study includes the validation of theoretical model and the implementation of ANN and GA.

Chapter 8: Provides summary, specific conclusions drawn from both the experimental and analytical efforts and recommendations for future research.

Chapter 2

Literature Review

Chapter 2

LITERATURE REVIEW

Introduction

The purpose of literature review is to provide background information on the issues to be considered in this thesis and to emphasize the relevance of the present study. This treatise embraces various aspects of polymer composites with a special reference to erosion wear characteristics. The topics include brief review:

- On fiber/ particulate reinforced polymer composites
- On multiphase hybrid composites
- On mechanical properties of composites
- On wear analysis of composites
- On erosion wear characteristics of composites
- On erosion wear modeling
- On implementation of DOE and optimization techniques

At the end of the chapter a summary of the literature survey and the knowledge gap in the earlier investigations are presented.

2.1 On fiber reinforced polymer composites

Fiber reinforced polymer composites are now considered as an important class of engineering materials. They offer outstanding mechanical properties, unique flexibility in design capability and ease of fabrication. Additional advantages include light weight, corrosion and impact resistance and excellent fatigue strength. A fiber reinforced composite is not simply a mass of fibers dispersed within a polymer. It consists of fibers embedded in or bonded to a polymer matrix with distinct interfaces between the two constituent phases. The fibers are usually of high strength and modulus and serve as the principal load carrying members. The matrix acts as the load transfer medium between fibers and in less ideal cases where loads are complex, the matrix may even have to partly bear loads. The matrix also serves to protect the fibers from environmental damage before, during and after composite processing. In a composite, both fibers and matrix largely retain their identities and yet result in many properties that cannot be achieved with either of the constituents

acting alone. A wide variety of fibers are available for use in composites. The most commonly used fibers are various types of carbon, glass and aramid. Besides, natural fibers such as jute, sisal and ceramic fibers like alumina, silicon carbide, mullite and silicon nitride are also used in composite making. The unique combinations of properties available in these fibers provide the outstanding functional and structural characteristics such as high specific strength and specific stiffness to the fiber reinforced composites.

A key feature of fiber composites that makes them so promising as engineering materials is the opportunity to tailor the materials properties through the control of fiber and matrix combinations and the selection of processing techniques. In principle, an infinite range of composite types exists, from randomly oriented chopped fiber based materials at the low property end to continuous, unidirectional fiber composites at the high performance end.

2.2 On particulate filled polymer composites

Hard particulate fillers consisting of ceramic or metal particles and fiber fillers made of glass are being used these days to dramatically improve the wear resistance even up to three orders of magnitude [16]. Various kinds of polymers and polymer matrix composites reinforced with metal particles have a wide range of industrial applications such as heaters, electrodes [17], composites with thermal durability at high temperature [18] etc. These engineering composites are desired due to their low density, high corrosion resistance, ease of fabrication, and low cost [19-21]. Similarly, ceramic filled polymer composites have been the subject of extensive research in last two decades. The inclusion of inorganic fillers into polymers for commercial applications is primarily aimed at the cost reduction and stiffness improvement [22, 23]. Along with fiber-reinforced composites, the composites made with particulate fillers have been found to perform well in many real operational conditions. It is reported by Bonner [24] that with the inclusion of micro-sized particulates into polymers, a high filler content (typically greater than 20 vol.%) is generally required to bring the above stated positive effects into play. But at the same time, this may also have detrimental effects on some important properties of the matrix polymers such as processability, appearance, density and aging performance.

When silica particles are added into a polymer matrix to form a composite, they play an important role in improving electrical, mechanical and thermal properties of the composites [25, 26]. Currently, particle size is being reduced rapidly and many studies have focused on how single-particle size affects mechanical properties [27–33]. The shape, size, volume fraction and specific surface area of such added particles have been found to affect mechanical properties of the composites greatly. Yamamoto et al. [34] reported that the structure and shape of silica particle have significant effects on the mechanical properties such as fatigue resistance, tensile and fracture properties. Nakamura et al. [35–37] discussed the effects of size and shape of silica particle on the strength and fracture toughness based on particle-matrix adhesion and also found an increase of the flexural and tensile strength as specific surface area of particles increased. Moloney et al. [38–40] and Adachi et al. [41] found that the mechanical properties of epoxy composites were depended on volume fraction of particles. Furthermore, effects of different particle size of micron magnitude and nano-particles on the properties of the composites were discussed by Yuan et al. [42] and Ng et al. [43].

The filler plays a major role in determining the properties and behaviour of particulate composite materials containing a high content (over 60% by weight) of filler. Formulation and production of particulate composites can be based on two main principles, a filler theory and a mastic (filler matrix system) theory. The filler theory [44, 45] states that optimal composite properties are achieved when the particle size distribution permits a maximal packing of the filler particles. According to the mastic theory [44, 45], the matrix creates a coating on each filler particle with an optimal thickness. This provides a contact between the filler particles producing a rigid and stable composite mixture. Concerning these theories, two main parameters - the particle size distribution of the filler and the optimal matrix content for this distribution influence the behaviour of the composite. Other parameters affecting the mechanical behaviour of these composites are the wetting of the filler by the resin and the adhesion between the two components. Physico-chemical parameters of the filler which affect the initial behaviour and durability of the composite mixture include shape, surface activity and area, size and size distribution (gradation). A detailed discussion of these parameters has been reported by Karger and Stokes et al. [46, 47].

It has also been reported that the fracture surface energies of epoxy and polyester resin and their resistance to crack propagation are relatively low [47]. But if particulate filler is added to these resins, the particles inhibit crack growth. As the volume fraction of filler is varied, the fracture energy increases up to a critical volume fraction and then decreases again. Srivastava and Shembekar [48] showed that the fracture toughness of epoxy resin could be improved by addition of flyash particles as filler. The fillers also affect the tensile properties according to their packing characteristics, size and interfacial bonding. The maximum volumetric packing fraction of filler reflects the size distribution and shapes of the particles [49].

The mechanical properties of a thermoplastic polymer like Polypropylene (PP) have been modified by adding various mineral fillers such as talc and calcium carbonate [4, 50]. It has also been shown that such filler particles increase Young's modulus of PP, yet causing the decrease of the strength and the toughness. PP can also be reinforced with short glass fibres (SGF) to improve the stiffness and the fracture toughness. However, long glass fibres (LGF) are used more often as reinforcement since it is known that longer fibres with the same fibre diameter (i.e. with higher fibre aspect ratio) provide higher stiffness, tensile strength and toughness compared to shorter ones [5–8]. Recently, it has been observed that by incorporating filler particles into the matrix of fibre reinforced composites, synergistic effects may be achieved in the form of higher modulus and reduced material costs, yet accompanied with decreased strength and impact toughness [4, 5]. As already mentioned, such multi-component composites consisting of a matrix phase reinforced with a fiber and filled with particulate matters are termed as hybrid composites.

2.3 On multiphase hybrid composites

Garcia et al. [51, 52] are the first to suggest this kind of composite technique for improving the matrix-dominated properties of continuous fiber reinforced composites. In this technique, a supplementary reinforcement such as particulates, whiskers or micro fibers is added to the matrix prior to resin impregnation. Jang et al. [53, 54] found a significant improvement in impact energy of hybrid composites incorporating either particulates or ceramic whiskers. Attempts to understand the modifications in the tribological behaviour of the polymers with the addition of fillers or fiber reinforcements have been made by a few researchers [55, 56]. The enhancement in

tribological properties of Poly-phenylene-sulfide (PPS) has been reported with the addition of inorganic fillers [57] and fibers [58]. Bahadur et al. [59, 60] reported that the fillers such as CuS, CuF_2, CaS, and CaO reduced the wear rate of polyamide but many other fillers such as CaF_2 increased the wear rate. But most of the above studies are confined to dry sliding and abrasive wear behaviour of composites. The erosive wear behaviour of polyester composites reinforced with any fiber or particulate has not yet been reported in the literature.

Erosive wear of engineering components caused by abrasive particles is a major industrial problem. A full understanding of the effects of all system variables on the wear rate is necessary in order to undertake appropriate steps in the design of machine or structural component and in the choice of materials to reduce/control wear.

2.4 On erosion wear characteristics of composites

Erosion due to the impact of solid particles can either be constructive (material removal desirable) or destructive (material removal undesirable), and therefore, it can be desirable to either minimize or maximize erosion, depending on the application. Constructive applications include sand blasting, high-speed water-jet cutting, blast stripping of paint from aircraft and automobiles, blasting to remove the adhesive flash from bonded parts, erosive drilling of hard materials, and most recently, in the abrasive jet micromachining of silicon and glass substrates for optoelectronic applications, and the fabrication of components for micro-electro-mechanical-system (MEMS) and micro-fluidic applications. Solid particle erosion is destructive in industrial applications such as erosion of machine parts, surface degradation of steam turbine blades, erosion of pipelines carrying slurries and particle erosion in fluidized bed combustion systems. In most erosion processes, target material removal typically occurs as the result of a large number of impacts of irregular angular particles, usually carried in pressurized fluid streams. The fundamental mechanisms of material removal, however, are more easily understood by analysis of the impact of single particles of a known geometry. Such fundamental studies can then be used to guide development of erosion theories involving particle streams, in which a surface is impacted repeatedly.

After developing primitive fibre reinforced plastics (FRP) in 1940s, they have been widely used because of their superior specific strength and also high corrosion resistance. Initially FRP was composite reinforced with glass fibres (GFRP), however reinforcement of new fibres such as carbon/graphite and aramid have increased their importance recently. Following the development of these high-performance fibres, use of FRP into industrial applications such as load bearing parts of buildings, bridges, tank / vessels and transportations can be recognized [61,62]. To ensure the durability of FRPs for industrial applications, it is necessary to discuss the degradation behaviour and mechanism under various conditions such as stress, corrosion and erosion etc. Several parts and equipments are exposed to erosive conditions, for example pipes for hydraulic or pneumatic transportation [63–65], nozzle and impeller for sand-blasting facility [66], internal surface of vessels used for fluidized bed or with catalysis [67–69], nose of high-velocity vehicle [70], blades/propellers of planes and helicopters [71] etc., some of them made from fibrous composites.

Polymer composites with both discontinuous and continuous fibre reinforcement possess usually very high specific (i.e. density related) stiffness and strength when measured in plane. Therefore, such composites are frequently used in engineering parts in automobile, aerospace, marine and energetic applications. Due to the operational requirements in dusty environments, the study of solid particle erosion characteristics of the polymeric composites is of high relevance.

Polymers are finding an ever increasing application as structural materials in various components and engineering systems. The high specific strength and stiffness of polymers are primarily responsible for their popularity. However, the resistance of polymers to solid particle erosion has been found to be very poor [72], and in fact it is two or three orders of magnitude lower than metallic materials [73]. One possible way to overcome such a shortcoming is to introduce a hard second phase in the polymer to form polymer matrix composites (PMCs). A number of investigators [72-79] have evaluated the resistance of various types of PMCs to solid particle erosion. Tilly [72] and Tilly and Sage [74] tested nylon and epoxy reinforced with various fibres such as graphite, glass and steel and concluded that the reinforcement can either increase or decrease the erosion resistance depending on the type of fibres. Zahavi and Schmitt [73] tested a number of PMCs for erosion resistance and

concluded that glass-reinforced epoxy composite had a particularly good erosion resistance. Pool et al. [12] conducted erosion tests on four PMCs and inferred that wee-handled, ductile fibres in a thermoplastic matrix exhibit the lowest erosion rates. The above study was extended further by Tsiang [75]. He carried out sand erosion tests on a wide range of thermoset and thermoplastic PMCs having glass, graphite and Kevlar fibres in the forms of tape, fabric and chopped mat as reinforcements. Kevlar fibres in an epoxy resin provided the best erosion resistance. In a recent study, Mathias et al. [76] and also Karasek et al. [78] have evaluated the erosion behaviour of a graphite-fibre-reinforced bismaleimide polymer composite. These investigators observed the erosion rates of the PMC to be higher than the unreinforced polymer. Many of the investigators [73-76, 79] also consistently noted that the erosion rates of the PMCs were considerably larger than those obtained in metallic materials. In addition, composites with a thermosetting matrix mostly exhibited a maximum erosion rate at normal impact angles (i.e. a brittle erosion response) while for the thermoplastic polymer composites the erosion rate reached a maximum at an intermediate impact angle in the range 40^0-50^0 signifying a semi-ductile erosion response.

The wear behaviour of composite materials has received much less attention than that of conventional materials. However, as composites are utilized to an increasing extent in the aerospace, transportation and process industries, their durability may become a prime consideration. In erosion, material is removed by an impinging stream of solid particles. Studies to develop an understanding of the mechanisms of erosive wear have been motivated by reduced lifetimes and failures of mechanical components used in erosive environments e.g. in pipelines carrying sand slurries, in petroleum refining [80, 81] and in aircraft gas turbine/compressor blades [82, 79]. In addition to these studies, which were conducted to understand erosion behaviour in isotropic materials, there is increasing interest in understanding the erosion behaviour of anisotropic materials. Because of their very high specific stiffness and strength, composites are now used extensively in aircraft structures. The understanding of erosive wear behaviour is obviously important for such structures e.g. helicopter rotor blades. While polymeric coatings have been developed to protect composite aircraft structures from rain erosion [83, 84], there is little understanding of the mechanisms of erosive wear in these materials. For polymers

and composite materials, Tilly and Sage [74] investigated the influence of velocity, impact angle, particle size and weight of impacted abrasive for nylon, carbon-fiber-reinforced nylon, epoxy resin, polypropylene and glass-fiber-reinforced plastic. Their results showed that, for the particular materials and conditions of their tests, composite materials generally behaved in an ideally brittle fashion (i.e. maximum erosion rate occurred at normal impact). Fiber reinforcement may improve or worsen the resistance to erosion depending on the type of fibers used. In addition, the erosion rates in composites continued to increase with particle size in contrast with the independence of erosion rate on particle size found in steel with particle diameters greater than about 100 μm [74, 79]. Zahavi and Schmitt [85] performed erosion tests on a quartz-polyimide composite and a quartz-polybutadiene composite and again determined their behaviour to be like that of nearly ideally brittle materials. One interesting result was the behaviour of an E-glass-reinforced epoxy composite which exhibited erosion rates that were less than those of the other composites by a factor of 5. This was attributed to better adhesion between the matrix and the fibers and the lower porosity of this composite in comparison with the other composites. The E-glass-epoxy composite exhibited semi-ductile erosion behaviour with a maximum weight loss at an impingement angle of 45^0 - 60^0 while the others eroded in a brittle manner with the maximum weight loss occurring at 75^0 - 90^0.

The response of materials to solid particle erosion can be categorized as ductile or brittle depending on the variation in the erosion rate (E_r) with impact angle [86-88]. The impact angle is usually defined as the angle between the trajectory of the eroding particles and the sample surface. If E_r goes through a maximum at intermediate impact angles, typically in the range 15^0-30^0, the response of the eroding material is considered ductile. In contrast, if E_r continuously increases with increasing impact angle and attains a maximum at 90^0 (normal impact), the response of the eroding material is brittle. In addition, under ideally brittle erosion conditions the magnitude of E_r is determined only by the normal component of the impact velocity, and the size of the eroding particle strongly influences the erosion rate [86-89]. It is to be noted, however, that the above categorization of material behaviour as ductile or brittle is not absolute. For example, if spherical particles are used as the erodent instead of angular particles, the erosion rate exhibits a maximum at 90^0 even in the case of ductile materials such as copper and mild steel [90-93]. Similarly, even

a brittle material such as an inorganic glass exhibits ductile behaviour when impacted with very fine particles [94]. Erosion as well as abrasion experiments on metallic materials, ceramics and polymers have clearly indicated that the hardness of the eroding or abrading material by itself cannot adequately explain the observed behaviour [95-101]. As a result, combined parameters involving both hardness and fracture toughness have been utilized to correlate the erosion data of metals [95], ceramics [99, 100] and polymers [102]. In addition, correlation between the fatigue and the erosion or wear resistance has also been observed in the case of polymers [103]. The hardness is unable to provide sufficient correlation with erosion resistance, largely because it determines only the volume displaced by each impacting erodent particle and not really the volume removed (eroded). Thus a parameter which will reflect the efficiency with which the volume that is displaced is removed should be combined with hardness to obtain a better correlation.

Solid particle erosion is a dynamic process that leads to progressive loss of material from the target surface due to impingement of fast moving solid particles. This mode of wear is one of the important problems in various gas and liquid flow passages such as flow in pipes and pipe fittings (valves, bends, elbows, flow meters etc.), flow in pumps, turbines, compressors and many others. Erosion may cause equipment malfunctioning (vibration, leakage, excessive energy losses etc.) and may also lead to complete failure of machine components. Accurate prediction of the rate of erosion in a specific application is one of the very complicated problems since it requires detailed investigation of the solid particle motion before and after impact. The difficulty arises mainly from the fact that most flows occurring in industrial processes are turbulent which makes the particle trajectory and impact characteristics difficult to predict taking into consideration all fluid forces acting on the particle.

Erosion tests have been performed under various experimental conditions (erodent flux conditions, erosive particle characteristics) on different target composites. It has been concluded that composite materials present a rather poor erosion resistance [104–108]. A crucial parameter for the design with composites is the fibre content as it controls the mechanical and thermo-mechanical responses. In order to obtain the favoured material properties for a particular application, it is important to know how the material performance changes with the fibre content under given loading conditions. The erosive wear behaviour of polymer composite systems as a function

of fibre content has been studied in the past [109–111]. It was concluded that the inclusion of brittle fibres in both thermosetting and thermoplastic matrices leads to compositions with lower erosion resistance. Nevertheless, no definite rule is available to describe how the fibre content affects the erosion rate of a composite. An analytical approach was presented by Hovis et al. [112] which presumed that the erosion rate of a multiphase material depends on the individual erosion rate of its constituents. The linear (LROM) and inverse (IROM) rules of mixture were proposed and evaluated for a multiphase Al-Si alloy. The same rules of mixture were adopted by Ballout et al. [113] for a glass-fibre reinforced epoxy composite. These two rules of mixture were also proposed to model the abrasive wear of unidirectional (UD) fibre reinforced composite materials [114,115].

Information on the solid particle erosion of materials has been available for many years now [116]. Two erosion modes are often distinguished in the literature: brittle and ductile erosion. Brittle erosion deals with material removal due to crack formation, while ductile erosion deals with material removal due to cutting and ploughing. The difference manifests itself in the impact angle dependent erosion rate. When a brittle material is impacted by a hard sharp particle, the contact area is plastically deformed due to the high compressive and shear stresses and a radial crack is formed. After the impact, the plastic deformation leads to large tensile stresses that result in lateral cracks causing the material removal. As has been observed by some researchers, the composite materials present a rather poor erosion resistance [12, 79,117]. Thus, in order to obtain the desired material characteristics for a particular application, it is important to know how the composite performance changes with the fibre content under given loading conditions. The Influence of matrix modification on the solid particle erosion of glass/epoxy composites has also been studied in the past [118]. Miyazaki and Hamao [109] have examined the effect of fibre inclusion on the erosion behaviour by comparing the erosion rate of an FRP with that of a neat resin, which is the matrix material of the FRP. It was observed that the inclusion of brittle fibres in both thermosetting and thermoplastic matrices leads to compositions with lower erosion resistance. They have also studied the erosion behaviour of treated and untreated glass fibre reinforced epoxy resin composites. The results show the clear correlation between interfacial strength and erosion rate.

Thus, the erosion behaviour of polymeric materials depends first of all on their nature. Thermosetting polymers, such as epoxy (EP) and phenolic resins, show brittle erosion whereas the erosion response of thermoplastics is of ductile type [108]. The same categorization applies for the related composites. It was demonstrated that the maximum erosion rate is at an oblique impact angle of 30^0 and at 60^0–90^0 for polymers eroding in ductile and brittle manner respectively [104,116,119-121]. Rubbers, on the other hand, present a maximum erosion rate at 30^0, but the failure mechanisms differ from those of thermoplastic resins. It is, therefore, a great challenge to study the solid particle erosion of a system that may show both brittle and ductile erosion behaviour depending on its composition and structural characteristics.

Erosion of ductile materials by the impact of hard solid particles at low and moderate velocities (2-100 m/sec) can cause significant damage to structural components in many industrial applications. For example, erosion by non-combustible flyash particles causes premature material failures in the power generation industry [122]. During impact on the elastic–plastic target, particle energy transfers into rebound and plastic deformation of the target [123]. Rebound of the particle is caused by the elastic energy stored in the particle and target material and the magnitude of this energy is determined by the ratio of the rebound to the initial particle velocity. This ratio, called the restitution coefficient, depends on the mechanical properties of the target material and erodent, and impact parameters (i.e. velocity, impact angle, and particle size). The extent of erosion damage is related to the ability of the material to elastically recover and therefore, it is important to understand the effect of target mechanical properties, such as hardness, on the restitution coefficient. Several studies have been conducted to measure the restitution coefficient of various target-erodent systems [123–125]. However, these measurements are complicated and often inaccurate because of the difficulties involved in measuring rebound velocity of the particle.

As already mentioned, solid particle erosion is a general term used to describe mechanical degradation wear of a solid material subjected to a stream of abrasive erodent particles impinging on its surface. The effects of solid particle erosion have been recognized for a long time [126]. Damage caused by erosion has been reported in several industries for a wide range of situations. Examples can be cited for rocket

motor tail nozzles [127], helicopter rotors and gas turbine blades [128], parametric dependence of erosion wear for the parallel flow of solid–liquid mixtures [129], boiler tubes exposed to flyash [130]. The existing models of solid particle erosion treat ductile and brittle materials as separate and distinct, generating two basic theories. These include subsurface lateral crack propagation in brittle materials [131,132], and micro machining or damage accumulation and fatigue impact in ductile materials [133,134]. Sheldon [135] noted the importance of the tangential velocity component of the impacting particle and concluded that erosion occurs by a combination of ductile and brittle modes. Sheldon's conclusions are also supported by the work of Hockey et al. [136] on glass, silicon nitride and aluminium oxide. Previous results obtained by Sheldon and Finnie [137] demonstrate that glass and ceramics could present a ductile type of erosion behaviour under proper conditions. Neilson and Gilchrist [127] also support the idea that erosion mechanisms of any material are a linear combination of a ductile response and a brittle response and that the maximum erosion rate can be predicted at an intermediate angle. Furthermore, they have modified Finnie's equation to include the effect of the impingement angle upon ductile targets, to show the contribution of the tangential velocity component. As a continuation of these earlier works, Ballout [138] developed a new experimental technique (dynamic test) capable of controlling and separating the relative particle velocity components. This consists of a rotating disk with the samples held on it. The disk is mounted on a motor with adjustable speed and is positioned in front of an air-blast apparatus with its nozzle directed toward the sample at the top position on the disk. At a selected motor speed the linear velocity of the samples is known; also, the tangential velocity of the particles is calculated. The difference between both velocities is the relative tangential velocity of the particles. Because of the rotational speed given to the samples, this new technique is referred to as a 'dynamic test' compared to the conventional fixed samples placement in an air blasting erosion apparatus, which is referred to as a 'static test'. Ibrahim [139] demonstrated that by separating and controlling the tangential and the normal velocity component of the erodent particles, the erosion characteristics of ductile, semi-ductile, and brittle materials appear to follow a common law. The materials respond in a similar manner under the same conditions of testing. Ibrahim concluded that it is possible to unify the ductile and brittle models of solid particle erosion rates.

In general, the erosive wear behaviour of material depends on various operating parameters, such as velocity and angle of impact, particle size, shape, flux rate, etc. [140]. Literature on the effect of velocity of erodent on wear performance is sparse as compared to that on other parameters [141–145]. Earlier studies have shown that the value of the velocity exponent depends on the nature of both the target and the erodent. Tilly and Sage [74] reported a value of velocity exponent of 2.3 for 125–150 μm quartz erodents impacting a range of materials from metals to plastics. They also reported that the velocity exponent decreased with decreasing size of the erodent. In contrast, Finnie [117] reported a high velocity exponent of 6.5 for 575 μm steel spheres impacting glass. While studying the erosive wear behaviour of glass eroded by 300 μm size iron spheres, Dhar and Gomes [146,147] postulated that there was a threshold velocity value below which deformation was elastic and hence no damage occurred. Tilly [148] proposed that the threshold velocity depended on the particle size of the erodent and obtained a value of 2.7 m/s for 225 μm quartz against 11% chromium steel. Wiederhorn et al. [149] documented the velocity exponents for seven types of target materials having a wide range of brittleness indices and microstructures. Scattergood and Routbort [150] found that the velocity exponent increased with decreasing particle size of the erodent. While studying the erosive wear behaviour of amorphous polystyrene, Thai et al. [151] found that the velocity exponent was 3.69. Karasek et al. [152] observed almost linear correlation between the erosion rate of graphite fibre reinforced bismaleimide composite and the impinging velocity. Arnold and Hutchings [141] found that the erosion rate of natural rubber and epoxidized natural rubber had very strong dependence on the impinging velocity above 70 m/s. Rao et al. [153] reviewed the effect of impact velocity on the erosive wear of various polymers and composites. The influence of impact angle and dose of the erodent on the erosive wear behaviour of various poly-amides with different methylene to amide (CH_2 /CONH) ratio has also been reported [154]. Therefore, it is worthwhile to study the influence of various impact parameters like impinging angle, velocity, dose of the erodent etc. on the erosive wear behaviour of composites.

Available reports on the research work carried out on erosion can be classified under three categories; experimental investigations, erosion model developments and numerical simulations. Tilly [147] presented a thorough analysis of the various

parameters affecting erosion, including particle properties, impact parameters, particle concentration, material temperature and tensile stress. He also reviewed the different mechanisms of erosion, which were categorized into brittle and ductile behaviours. Ruff and Wiederhorn [155] presented another review of the solid particle erosion phenomena considering single and multiple particle models on erosion of metals and ceramics. The significant parameters for eroding particles and material characteristics were also presented. Humphrey [156] reported a more comprehensive review of the fundamentals of fluid motion and erosion by solid particles. The review includes a discussion of the experimental techniques and the various fundamental considerations relating to the motion of solid particles. An assessment of the fluid mechanics phenomena that can significantly influence erosion of material surfaces by impinging particles was also presented. Because of its direct relevance to gas and oil industries, erosion of pipes and pipe fittings attracted many researchers. Several experimental studies were conducted with the main objective being to determine the rate of erosion in such flow passages and its relation with the other parameters involved in the process. Among these studies are the works by Rochester and Brunton [157], True and Weiner [158], Glaeser and Dow [159], Roco et al. [160], Venkatesh [161], and Shook et al. [162]. Soderberg et al. [163,164] and Hutchings [165,166] reported the advantages and disadvantages of such experiments. The recent experimental study by McLaury et al. [167] on the rate of erosion inside elbows and straight pipes provided correlations between the penetration rate and the flow velocity at different values of the elbow diameter, sand rate and size. Edwards et al. [168] reported the effect of the bend angle on the normalized penetration rate. The objective of most of these experimental studies was to provide data for establishing a relationship between the amount of erosion and the physical characteristics of the materials involved, as well as the particle velocity and angle of impact. Blanchard et al. [169] carried out an experimental study of erosion in an elbow by solid particles entrained in water. The elbow was examined in a closed test loop. Electroplating the elbow surface and photographing after an elapsed period of time were carried out to show the wear pattern.

2.5 On erosion wear modeling

Several erosion models/correlations were developed by many researchers to provide a quick answer to design engineers in the absence of a comprehensive practical

approach for erosion prediction. The theoretical model developed by Rabinowicz [170] was used to calculate the volume of material removed from the target surface due to impact of solid particles entrained in a liquid jet. The results indicated that the sand particle trajectories appeared to be governed by the secondary flows and that there was no simple liquid velocity profile that can be used to calculate the particle trajectories in order to make an accurate prediction of the location of the point of maximum wear. One of the early erosion prediction correlations is that developed by Finnie [171] expressing the rate of erosion in terms of particle mass and impact velocity. In that correlation, the rate of erosion was proportional to the impact velocity squared. In a recent study, Nesic [172] found that Finnie's model over-predicts the erosion rate and presented another formula for the erosion rate in terms of a critical velocity rather than the impact velocity. The erosion model suggested by Bitter [173,174] assumed that the erosion occurred in two main mechanisms; the first was caused by repeated deformation during collisions that eventually results in the breaking loose of a piece of material while the second was caused by the cutting action of the free-moving particles. Comparisons between the obtained correlations and the test results showed a good agreement. It was concluded that cutting wear prevails in places where the impact angles are small (such as in risers and straight pipes) and it is sufficient to use hard material in such places to reduce erosion. Tilly [175] suggested another two-stage mechanism for explaining different aspects of the erosion process for ductile materials. In the first stage, the particles indent the target surface, causing chips to be removed and some material to be extruded to form vulnerable hillocks around the scar. The second stage was the one in which the particles break up on impact causing fragments to be projected radially to produce a secondary damage. A correlation was presented relating erosion to the energy required to remove a unit mass and the particle velocity and size. The calculated values of erosion were compared with the experimental data for different particle sizes and a reasonable agreement was found, however, the validity of the work was limited to ductile materials and could not be generalized to include other materials. Other erosion models were suggested by Laitone [176], Salama and Venkatesh [177], Bourgoyne [178], Chase et al. [179], McLaury [180], Svedeman and Arnold [181] and Jordan [182]. Recently, Shirazi and McLaury [183] presented a model for predicting multiphase erosion in elbows. The model was developed based on extensive empirical information gathered from many sources and it accounts for the

physical variables affecting erosion, including fluid properties, sand production rate and size and the fluid-stream composition. An important feature of this model was the use of the characteristic impact velocity of the particles. The method used for obtaining characteristic velocity for an elbow was an extension of a previous method introduced by the same authors for the case of a single-phase flow.

The use of computational methods in erosion prediction constitutes a combination of flow modeling, Lagrangian particle-tracking and the use of erosion correlations. The flow model is used to determine the flow field for a given geometry while the particle-tracking model is used to determine the particle trajectories for solid particles released in the flow. The particle impingement information extracted from the trajectories is used along with the empirical erosion equations to predict the erosion rates. Wang et al. [184] developed a computational model for predicting the rate of erosive wear in a 90^0 elbow for the two cases of sand in air and sand in water. The flow field was first obtained and then the particle trajectory and impacting characteristics were then determined by solving the equation of particle motion taking into consideration all the forces including drag, buoyancy and virtual mass effects with the assumption of a uniform distribution of the solid particles at the starting section. In a recent study by Edwards et al. [185], an erosion prediction procedure was developed and verified based on a computational fluid dynamics (CFD) code combining flow field analysis and particle-tracking for obtaining particle impingement data. The erosion rate was then computed using the empirical relations of Ahlert [186] and applied to predict erosion in a pipe bend fitting made of carbon steel.

In most erosion processes, target material removal typically occurs as the result of a large number of impacts of irregular angular particles, usually carried in pressurized fluid streams. The fundamental mechanisms of material removal, however, are more easily understood by analysis of the impact of single particles of a known geometry. Such fundamental studies can then be used to guide development of erosion theories involving particle streams, in which a surface is impacted repeatedly. Single particle impact studies can also reveal the rebound kinematics of particles, which are very important for models which take into account the change in erosive potential due to collisions between incident and rebounding particles [187,188]. A number of recent papers contain investigations of the rebound kinematics of spherical/angular

particles [189–193]. These are concerned with the identification and modelling of mechanisms of ductile target material removal due to the impact of single hard, angular particles. These works have demonstrated that, in this case, the trajectory of the particle while impacting the material surface is of prime interest in predicting the material loss, since this determines the manner in which a crater is carved out. In much of this work, the target material is assumed to be perfectly plastic (i.e. elastic rebound effects are ignored), with the impacting particle assumed to be non-deforming and the theory has thus come to be known as 'rigid-plastic.' Finnie's analysis [117, 171] of the cutting action of a single particle launched against a ductile target was the first such model capable of predicting material removal rate. In his model, the particles were assumed to be rigid and impact a target which reached a constant flow pressure immediately upon impact. Under the assumption that the particle did not rotate during the impact process, the particle was subjected to a resisting force vector of constant direction and Finnie was able to solve for the trajectory of the particle in closed form as it cut the surface and thus predict the size of the impact crater. An extension of Finnie's work, the rigid-plastic theory developed by Hutchings and co-workers [194–196] predicted the collision kinematics and crater dimensions for single impacts of square and spherical particles on ductile targets. The theory predicted the kinematics of the particle as it ploughed or cut through the target, under the assumption that the instantaneous resisting force could be calculated by multiplying a constant plastic flow pressure (i.e. the dynamic hardness) by the instantaneous contact area. In contrast to the constant direction force vector assumed in Finnie's work, in Hutchings' analysis, the particle was free to rotate and the resisting force vector could thus vary in both direction and magnitude. By examining the single impacts of the square and spherical particles, Hutchings identified two fundamental mechanisms of cutting erosion and a ploughing erosion mechanism, depending on both the particle shape and its orientation at the moment of impact [195]. In general, comparisons of experimentally measured crater volume, energy loss, and particle kinematics yielded acceptable agreement. For impacts involving spherical particles, the rigid plastic theory was later improved by Rickerby and Macmillan [197,198], to include a more accurate calculation of contact area. Sundararajan and co-workers [199–201] also used a similar theory to model ductile erosion and investigated the effect of material pile-up at the edge of the crater on the rebound kinematics of the spherical particles and the size of the resulting plastic

zone below the impact. In the case of the rigid-plastic impact of single angular particles, however, very little literature exists. A rigid-plastic theory developed by Papini and co-workers [202-205] generalized Hutchings' [195,196] rigid-plastic theory for square particles, so that particles of any shape impacting targets of arbitrary dynamic hardness and dynamic friction coefficient could be analysed. The specific case of two dimensional particles having rhomboidal shape (i.e. 'diamond shaped') of varying angularity was studied in detail by constructing a computer program capable of describing the trajectory of the particles as they formed impact craters, so that their size and shape could be predicted [204]. Dimensionless parameters were identified so that the results of a parametric study could be presented in a generally applicable form, fundamental erosion mechanisms were predicted, and it was postulated that for a given angle of attack, there was an optimum particle shape for the most efficient material removal [205]. Due to the difficulties associated with performing repeatable experiments involving the impact of angular particles, this model remained without experimental verification of any kind until very recently. Of particular difficulty was the design of the launching apparatus, so that the impacts all would occur in one plane. Very recently, an experimental apparatus capable of reliably launching two-dimensional rhomboidal particles was constructed and used to show that the model of Papini and Spelt could reasonably predict the rebound kinematics of particles launched at aluminium alloy targets [206]. Along with the erosion mechanisms identified by Hutchings, a previously unreported mechanism was also identified. While the agreement between measured and predicted results was encouraging, the experimental data were limited to measurements of rebound kinematics and not crater volume, and particles of only one angularity were used.

In order to develop a mathematical model, it is important to understand the mechanism responsible for solid-particle erosion of composite materials. For a composite material, its surface damage by solid-particle erosion depends on many factors, including the impact velocity, particle size and shape of the erodent, mechanical properties of both the target material and the erodent and the volume fraction, size and properties of the reinforcing phase as well as the bonding between the matrix and the reinforcing phase. The synergism of these factors makes it difficult to experimentally investigate the erosion mechanism for composite materials. Fortunately, computer simulation provides an effective and economic approach for

such investigation. Computer models proposed to simulate wear process may be classified into two groups: macro-scale models and atomic-scale models. The macro-scale models were proposed based on various assumptions or theories such as the cutting mechanism [171] and the platelet mechanism [207]. The cutting mechanism is based on the assumption that individual erodent particle impinges a target surface, cutting out a swath of the material. However, this mechanism is only suitable for ductile materials. Even for ductile materials, scanning electron microscope (SEM) observation of eroded surfaces has shown that erosion processes of metals involve extrusion, forging and fracture and that micro-cutting does not often occur [208]. Regarding the platelet mechanism, plastic deformation and work hardening prior to fracture are taken into account and this makes it closer to reality. However, this mechanism is also only suitable for ductile materials. Since there are many parameters influencing erosion, computer models based on the platelet mechanism are often used to treat special cases [209,210]. Furthermore, it is difficult to establish the relationship between erosion and microstructure based on these theories. Another method, finite element method (FEM), is also used for erosion simulation [211–213]. The FEM can provide information on the stress/strain distribution in surface layer, which helps to predict the initiation of surface failure. However, continuous changes in surface geometry during erosion lead to the difficulty in simulation of an entire erosion process using FEM. Although many models have been proposed to simulate erosion processes, lack of generality, flexibility or feasibility make these models difficult to be used to simulate erosion under different conditions and to investigate micro-structural effects on erosion. As a matter of fact, many wear models were proposed for mechanical design rather than for prediction of material performance. Therefore, they are not suitable for studying erosion processes in detail and for fundamentally investigating erosion mechanisms.

Another group of models developed based on fundamental physics laws are promising for wear modeling, such as the molecular dynamics simulation [214, 215] and the first-principle technique [216]. The molecular dynamic technique (MD) is one of the most powerful approaches for materials studies. However, the limited capability of current computing facilities makes it difficult to simulate an erosion process involving micro-structural effects, which requires handling a large number of atoms. Such simulation needs an unacceptable long computing time. A micro-scale

dynamic model (MSDM) was recently proposed for wear simulation, which has been applied to investigate abrasive wear [217,218]. This model was later applied to simulation of solid-particle erosion of homogeneous materials [219].

The correlations between wear resistance and characteristic properties of polymers have been discussed in terms of various semi-empirical equations by some pioneers. These include, e.g. the Ratner–Lancaster equation [220,221], i.e. the relationship of the single pass abrasion rate with the reciprocal of the product of ultimate tensile stress and strain or an equation used by Friedrich [222] to correlate the erosive wear rate of polymers with the quotient of their hardness to fracture energy. Although these equations are quite helpful to estimate the wear behaviour of polymers in some special cases, wear normally is very complicated and it therefore depends on many more mechanical and other parameters. This means that simple functions cannot always cover all the prevailing mechanisms under wear. For predictive purposes, an artificial neural network (ANN) approach has, therefore, been introduced recently into the field of wear of polymers and composites by Velten et al. [223] and Zhang et al. [224]. An ANN is a computational system that simulates the microstructure (neurons) of biological nervous system. The most basic components of ANN are modeled after the structure of the brain. Inspired by these biological neurons, ANN is composed of simple elements operating in parallel. ANN is the simple clustering of the primitive artificial neurons. This clustering occurs by creating layers, which are then connected to one another. How these layers connect may also vary. Basically, all ANN have a similar structure of topology. Some of the neurons interface the real world to receive its input, and other neurons provide the real world with the network's output. All the rest of the neurons are hidden from view. As in nature, the network function is determined largely by the interconnections between neurons, which are not simple connections, but some non-linear functions. Each input to a neuron has a weight factor of the function that determines the strength of the interconnection and thus the contribution of that interconnection to the following neurons. ANN can be trained to perform a particular function by adjusting the values of these weight factors between the neurons, either from the information of outside the network or by the neurons themselves in response to the input. This is the key to the ability of ANN to achieve learning and memory. The multi-layered neural network is the most widely applied neural network, which has been utilized in the most of the research works for

materials science reviewed by Zhang and Friedrich [225]. Back propagation algorithm can be used to train these multi-layer feed-forward networks with differentiable transfer functions to perform function approximation, pattern association and pattern classification. The term back propagation refers to the process by which derivatives of network error, with respect to network weights and biases, can be computed. The training of an ANN by back propagation involves three stages: (a) the feed-forward of the input training pattern, (b) the calculation and back propagation of the associated error and (c) the adjustment of the weights. This process can be used with a number of different optimization strategies.

2.6 On implementation of DOE and optimization techniques

Wear processes in composites are complex phenomena involving a number of operating variables and it is essential to understand how the wear characteristics of the composites are affected by different operating conditions. Although a large number of researchers have reported on properties, performance and on wear characteristics of composites, neither the optimization of wear processes nor the influence of process parameters on wear rate has adequately been studied yet. Selecting the correct operating conditions is always a major concern as traditional experiment design would require many experimental runs to achieve satisfactory result. In any process, the desired testing parameters are either determined based on experience or by use of a handbook. It, however, does not provide optimal testing parameters for a particular situation. Thus, several mathematical models based on statistical regression techniques have been constructed to select the proper testing conditions [226–231]. The number of runs required for full factorial design increases geometrically, whereas fractional factorial design is efficient and significantly reduces the time. This method is popular because of its simplicity, but this very simplicity has led to unreliable results and inadequate conclusions. The fractional design might not contain the best design point. Moreover, the traditional multi-factorial experimental design is the “change-one-factor-at-a-time” method. Under this method only one factor is varied, while all the other factors are kept fixed at a specific set of conditions. To overcome these problems, Taguchi and Konishi [232] advocated the use of orthogonal arrays and Taguchi [233] devised a new experiment design that applied signal-to-noise ratio with orthogonal arrays to the robust design of products and processes. In this procedure, the effect of a factor is measured by average

results and therefore, the experimental results can be reproducible. Phadke [234], Wu and Moore [235] and others [236–239] have subsequently applied the Taguchi method to design the products and process parameters. This inexpensive and easy-to-operate experimental strategy based on Taguchi's parameter design has been adopted to study effect of various parameters and their interactions in a number of engineering processes. It has been successfully applied for parametric appraisal in wire electrical discharge machining (WEDM) process, drilling of metal matrix composites, and erosion behaviour of metal matrix composites such as aluminium reinforced with red mud (240-246).

Chapter summary

This chapter has provided an exhaustive review of research works on fiber and particulate reinforced polymer composites reported by various investigators.

The literature survey presented above reveals the following knowledge gap that helped to set the objectives of this research work:

- Though much work has been reported on various wear characteristics of metals, alloys and homogeneous materials, comparatively less has been reported on the erosive wear performance of polymers and their composites and in fact no study has been found particularly on polyester based fiber/particulate reinforced composites.
- A possibility that the incorporation of both particles and fibers in polymer could provide a synergism in terms of improved wear resistance has not been adequately addressed so far and there is inadequate data available about phenomena behind the modified wear behaviour due to the addition of particulate fillers to the fiber reinforced polymer composites.
- As far as erosion study of polymer matrix composites is concerned, no specific theoretical model based on the assumption that the kinetic energy of the erodent is utilized to cause micro-indentation leading to material loss has been developed.
- Studies carried out worldwide on erosion behaviour of composites have largely been experimental and use of statistical techniques in analyzing wear characteristics is rare.

- Taguchi method, in spite of being a simple, efficient and systematic approach to optimize designs for performance, quality and cost, is used only in a limited number of applications worldwide. Its implementation in parametric appraisal of wear processes has hardly been reported.

The next chapter discusses experimental planning, the Taguchi method and neural computations.

*****

Chapter 3

Materials and Methods

Chapter 3

MATERIALS AND METHODS

Introduction

This chapter describes the materials and methods used for the processing of all the composites under this investigation. It presents the details of the characterization and erosion tests which the composite samples are subjected to. The methodology related to the design of experiment technique based on Taguchi method and the statistical analyses inspired by artificial neural networks are also presented in this part of the thesis.

3.1 Materials

Matrix Material

Unsaturated isophthalic polyester resin (density 1.35gm/cc, elastic modulus 3.25 GPa) supplied by Ciba-Geigy of India is the matrix material in the present investigation. Polyester is a category of polymers which contain the ester functional group in their main chain. The term unsaturated polyester resin is generally referred to the unsaturated (means containing chemical double bonds) resins formed by the reaction of dibasic organic acids and polyhydric alcohols. Polyester resin is also known as a thermosetting plastic, which implies the plastic sets at high temperatures as opposed to thermoplastics which can be formed at high temperatures. Polyester resin can attach things together to itself, creating a strong bond. Moreover, as it is a plastic it put against all elements as long as it has been produced to a high standard, without any problems of it falling apart. Polyester resins are the most economical and widely used resin systems, especially in the marine industry. Nearly one half million tons of this material is used annually in the United States in composite applications. Polyester resins can be formulated to obtain a wide range of properties ranging from soft and ductile to hard and brittle. Their advantages include low viscosity, low cost, and fast cure time. In addition, polyester resins have long been considered least toxic.

Fiber Material

In the present work, woven roving E-glass fibers (supplied by Saint Gobain Ltd. India) have been used as the reinforcing material in all the composites. Glass is the most common fiber used in polymer matrix composites. Its advantages include its

high strength, low cost, high chemical resistance and good insulating properties. The drawbacks include low elastic modulus, poor adhesion to polymers, high specific gravity, sensitivity to abrasion (reduces tensile strength), and low fatigue strength. The main types are E-glass (also called “fiber glass”) and S-glass. The “E” in E-glass (12 mm *diameter* and 120 mm *length*) stands for electrical because it is usually designed for electrical applications. However, it is used for many other purposes now, such as decorations and structural applications. The major constituents of E-glass are silicon oxide (54 wt %), aluminum oxide (15 wt %), calcium oxide (17 wt %), magnesium oxide (4.5 wt %) and boron oxide (8 wt %). E-glass fiber has an elastic modulus of 72.5 GPa and possess a density of 2.59 gm/cc.

Particulate Materials

Two conventional ceramic fillers: aluminum oxide and silicon carbide and two industrial wastes: flyash and cement by-pass dust (CBPD) are chosen to be used as particulate fillers in pre-determined proportions in various composites prepared for this investigation. While, Al_2O_3 and SiC have conventionally been used in many composite applications, the wastes flyash and cement by-pass dust (CBPD) can be considered as non-conventional materials for use as fillers in polymer composites. Here the fillers taken in this study are in the range of 80-100 μm**.**

Alumina is an inorganic material that has the potential to be used as filler in various polymer matrices. Aluminium oxide (Al_2O_3) commonly referred to as alumina, can exist in several crystalline phases which all revert to the most stable hexagonal alpha phase at elevated temperatures. This is the phase of particular interest for structural applications. Alumina is the most cost effective and widely used material in the family of engineering ceramics. It is hard, wear-resistant, has excellent dielectric properties, resistance to strong acid and alkali attack at elevated temperatures, high strength and stiffness. With an excellent combination of properties and a reasonable price, it is no surprise that fine grain technical grade alumina has a very wide range of applications.

Similarly, silicon carbide (SiC) is another ceramic material that too has the potential to be used as filler in various polymer matrices. It is an excellent abrasive and has been produced and made into grinding wheels and other abrasive products for over one hundred years. It is the only chemical compound of carbon and silicon. It was

originally produced by a high temperature electro-chemical reaction of sand and carbon. Today the material has been developed into a high quality technical grade ceramic with very good mechanical properties. It is used in abrasives, refractories, ceramics, and numerous high-performance applications. The material can also be made an electrical conductor and has applications in resistance heating, flame igniters and electronic components. Structural and wear applications are constantly developing. Silicon carbide is composed of tetrahedra of carbon and silicon atoms with strong bonds in the crystal lattice. This produces a very hard and strong material. It is not attacked by any acids or alkalis or molten salts up to 800°C. The high thermal conductivity coupled with low thermal expansion and high strength gives this material exceptional thermal shock resistant qualities. Silicon carbide has low density of about 3.1 gm/cc, low thermal expansion, high elastic modulus, high strength, high thermal conductivity, high hardness, excellent thermal shock resistance and superior chemical inertness.

The fly ash used here is of cenosphere type and has been collected from the Captive Power Plant of National Aluminium Co. (NALCO) located at Angul in India. Fly ash is a finely divided powder generated in huge quantities during power generation in coal based power plants. It is essentially a mixture of ceramic materials such as: SiO_2, Fe_2O_3, Al_2O_3 and TiO_2 etc.

Cement by-pass dust (CBPD) is a by-product of cement manufacturing. It is a fine powdery material similar in appearance to Portland cement. It is generated during the calcining process in the kiln. As the raw materials are heated in the kiln, dust particles are produced and then carried out with the exhaust gases at the upper end of the kiln. These gases are cooled and the accompanying dust particles are captured by efficient dust collection systems. Lime (CaO) constitutes about 40% of CBPD composition. Other compounds include SiO_2, Al_2O_3, Fe_2O_3, K_2O, Na_2O, Cl^-, etc. The chemical compositions/formulae and physical properties such as density and hardness of these particulate fillers are given in Table 3.1.

The composites prepared for this study are designated as A_1, B_1, C_1, C_2, C_3, C_4, C_5, C_6, C_7, C_8 and C_9 respectively. The detailed compositions along with the designation are presented in Table 3.2.

Table 3.1. Chemical compositions and Physical properties of filler materials

Filler	Composition/Chemical formula	Mean hardness (Hv)	Density (gm/cm^3)
Flyash*	SiO_2 (48.3%),Al_2O_3 (20.2%) Fe_2O_3 (6.4%),TiO_2 (1.9%)	725	3.15
Alumina	Al_2O_3	1175	3.89
Silicon Carbide	SiC	2800	3.22
CBPD**	CaO (40.5%), SiO_2 (14.5%), K_2O (4.66%) Al_2O_3(4.10%), Fe_2O_3 (2%),	695	2.40

Source: * Thermal spray coating of red mud on metals, Ph.D thesis, N.I.T.Rourkela, India (2005)
** Utilization of cement kiln dust (CKD) in cement mortar and concrete—an overview, Resources, Conservation and Recycling 48 (2006) 315–338.

Table 3.2. Designation and detailed compositions of the composites

Designation	Composition
A_1	Polyester +30wt% glass fiber
B_1	Polyester +40wt% glass fiber
C_1	Polyester +50wt% glass fiber
C_2	Polyester +50wt% glass fiber + 10wt% flyash
C_3	Polyester +50wt% glass fiber +20wt% flyash
C_4	Polyester +50wt% glass fiber +10wt% Alumina
C_5	Polyester +50wt% glass fiber +20wt% Alumina
C_6	Polyester +50wt% glass fiber +10wt% SiC
C_7	Polyester +50wt% glass fiber +20wt% SiC
C_8	Polyester +50wt% glass fiber +10wt% CBPD
C_9	Polyester +50wt% glass fiber +20wt% CBPD

3.2 Composite fabrication

Cross plied E-glass fibers are reinforced in unsaturated isophthalic polyester resin in three different weight proportions (30wt%, 40wt% and 50wt%) to prepare the composites A_1(Polyester +30wt% glass fiber), B_1 (Polyester +40wt% glass fiber) and C_1(Polyester +50wt% glass fiber) respectively. Each ply of glass-fiber is of dimension 200 × 170 mm^2. No particulate filler is used in these composites. The composite slabs are made by conventional hand-lay-up technique followed by light compression moulding technique. A stainless steel mould having dimensions of 210 × 180 × 20 mm^3 is used. A releasing agent (Silicon spray) is used to facilitate easy removal of the composite from the mould after curing. The curing of the polyester resin was done by incorporation of 2% cobalt nephthalate (as accelerator)

mixed thoroughly in the polyester resin and then 2% methyl-ethyl-ketone-peroxide (MEKP) as hardener prior to reinforcement. The mix is stirred manually to disperse the fibres in the matrix. Care is taken to ensure a uniform sample since fibres have a tendency to clump and tangle together when mixed. The cast of each composite was cured under light pressure of 0.0156 MPa for 24 h before it removed from the mould. Then this cast is post cured in the air for another 24 h after removing out of the mould. Specimens of suitable dimension are cut using a diamond cutter for physical characterization and mechanical testing. Utmost care has been taken to maintain uniformity and homogeneity of the composite although reproducibility is somewhat difficult in hand-lay up techniques.

The other composite samples C_2-C_9 with particulate fillers of fixed weight percentage are fabricated by the same technique. The fillers are mixed thoroughly in the polyester resin before the glass fiber mats (50 wt%) are reinforced in the matrix body. Composites C_2 and C_3 contain flyash particles in 10 wt% and 20wt% proportions respectively. Similarly C_4 and C_5, C_6 and C_7, C_8 and C_9 are the composites containing alumina, silicon carbide and cement by-pass dust fillers respectively along with 50wt% of glass fibers in them.

3.3 Mechanical characterization

Micro-hardness

Micro-hardness measurement is done using a Leitz micro-hardness tester. A diamond indenter, in the form of a right pyramid with a square base and an angle 136^0 between opposite faces, is forced into the material under a load F. The two diagonals X and Y of the indentation left on the surface of the material after removal of the load are measured and their arithmetic mean L is calculated. In the present study, the load considered F = 24.54N and Vickers hardness number is calculated using the following equation.

$$H_V = 0.1889 \frac{F}{L^2} \tag{3.1}$$

and $L = \frac{X + Y}{2}$

where, F is the applied load (N), L is the diagonal of square impression (mm), X is the horizontal length (mm) and Y is the vertical length (mm).

Density and void fraction

The theoretical density of composite materials in terms of weight fraction can easily be obtained as for the following equations given by Agarwal and Broutman [1].

$$\rho_{ct} = \frac{1}{\left(W_f / \rho_f\right) + \left(W_m / \rho_m\right)} \tag{3.2}$$

where, *W* and *ρ* represent the weight fraction and density respectively. The suffix *f, m* and *ct* stand for the fiber, matrix and the composite materials respectively.

The composites under this investigation consists of three components namely matrix, fiber and particulate filler. Hence the modified form of the expression for the density of the composite can be written as

$$\rho_{ct} = \frac{1}{\left(W_f / \rho_f\right) + \left(W_m / \rho_m\right) + \left(W_p / \rho_p\right)} \tag{3.3}$$

Where, the suffix '*p'* indicates the particulate filler materials.

The actual density (ρ_{ce}) of the composite, however, can be determined experimentally by simple water immersion technique. The volume fraction of voids (V_v) in the composites is calculated using the following equation:

$$V_v = \frac{\rho_{ct} - \rho_{ce}}{\rho_{ct}} \tag{3.4}$$

Tensile strength

The tensile test is generally performed on flat specimens. The commonly used specimens for tensile test are the dog-bone type and the straight side type with end tabs. During the test a uniaxial load is applied through both the ends of the specimen. The ASTM standard test method for tensile properties of fiber resin composites has the designation D 3039-76. The dimension of the specimen is 150 mm $\times$10 mm $\times$ (2.5 - 4) mm at a crosshead speed of 10 mm/min. As the thickness varies from 2.5 mm to 4mm, because for unfilled glass fiber reinforced polyester composite the fiber loading taken in this research are 30 wt%, 40 wt% and 50 wt %. Therefore, the thickness varies from 2.5 to 4 mm respectively. In case of particulate filled glass fiber reinforced polyester composites the length and width is same as the unfilled composites, whereas the thickness is 4mm for all the particulate filled composites. The tensile test is performed in the universal testing machine (UTM) Instron 1195 and results are analyzed to calculate the tensile strength of composite samples is shown in Figure 3.1. Here the test is repeated six times and the mean value of tensile strength is reported.

Flexural and inter-laminar shear strength

The short beam shear (SBS) tests are performed on the composite samples at room temperature to evaluate the value of inter-laminar shear strength (ILSS). It is a 3-point bend test, which generally promotes failure by inter-laminar shear. The SBS test is conducted as per ASTM standard (D2344-84) using the same UTM. The loading arrangement is shown in Figure 3.2. The dimension of the specimen is 40 mm $\times$10 mm $\times$ (2.5 - 4) mm at a crosshead speed of 10 mm/min. As the thickness varies from 2.5 mm to 4mm, because for unfilled glass fiber reinforced polyester composite the fiber loading taken in this research are 30 wt%, 40 wt% and 50 wt %. Therefore, the thickness varies from 2.5 to 4 mm respectively. In case of particulate filled glass fiber reinforced polyester composites the length and width is same as the unfilled composites, whereas the thickness is 4mm for all the particulate filled composites. The ILSS values are calculated as follows,

$$ILSS = \frac{3P}{4b.t} \tag{3.5}$$

Where, *P* is maximum load, *b* the width of specimen and *t* the thickness of specimen. The data recorded during the 3-point bend test is used to evaluate the flexural strength also. The flexural strength (F.S.) of any composite specimen is determined using the following equation. For both flexural and inter-laminar shear strength the test is repeated six times and the mean value is reported.

$$F.S = \frac{3PL}{2bt^2} \tag{3.6}$$

where, *L* is the span length of the sample

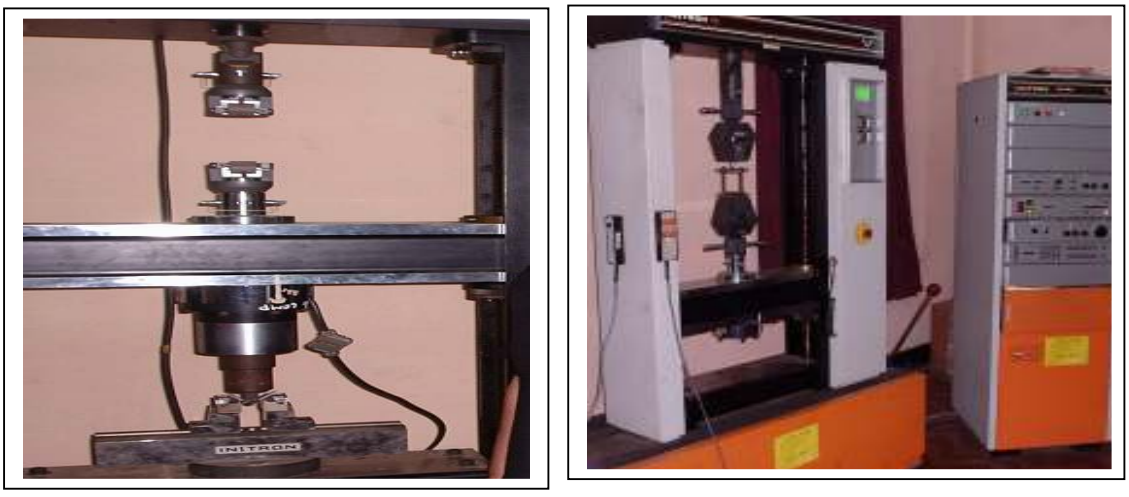

Figure 3.1. Photograph of Instron 1195 machine

Figure 3.2. Loading arrangement for the specimens

Impact strength

Low velocity instrumented impact tests are carried out on composite specimens. The tests are done as per ASTM D 256 using an impact tester (Figure 3.3). The pendulum impact testing machine ascertains the notch impact strength of the material by shattering the V-notched specimen with a pendulum hammer, measuring the spent energy, and relating it to the cross section of the specimen. The standard specimen for ASTM D 256 is same as the flexural and inter-laminar shear strength and the depth under the notch is 20 mm. Each test is repeated six times and the mean value of impact strength is reported. The machine is adjusted such that the blade on the free-hanging pendulum just barely contracts the specimen (zero position). Since there are practically no losses due to bearing friction, etc. (< 0.3 %), the testing conditions may be regarded as ideal. The specimens are clamped in a square support and are struck at their central point by a hemispherical bolt of diameter 5 mm. Raising the pendulum gives it the requisite energy of deformation (potential energy, e_p) as the product of reaction force (F) times the relative height (h).

$$e_p = F.h = F.\ L\ (1-\cos\alpha) \qquad [Nm] \tag{3.7}$$

The reaction force (F) is measured with the pendulum in the precisely horizontal position at a distance L from the fixed point. The height of fall (h):

$$h = L\ (1-\cos\alpha) \qquad [m] \tag{3.8}$$

The length L is the distance between the pendulum axis and the point of impact of the hammer's blades at the center of the specimen.

Upon release of the pendulum, the potential energy is converted into kinetic energy by acceleration due to gravity. At the moment it passes the zero position, the pendulum constitutes the potential energy (e_p) engraved on the hammer.
As it shatters a specimen, the pendulum is braked by the impact, losing part of its velocity and, hence, part of its potential energy (e_p), namely the impact-energy component (e_1).

$$e_1 = F.h_1 = F.L\ (1-\cos\alpha) \quad [\text{Joules}] \tag{3.9}$$

The amount of impact energy (e_1) thusly consumed is the difference between the potential energy (e_p) and the surplus energy (e_s).

$$e_1 = e_p - e_s \quad [\text{Joules}] \tag{3.10}$$

The respective values of impact energy of different specimens are recorded directly from the dial indicator.

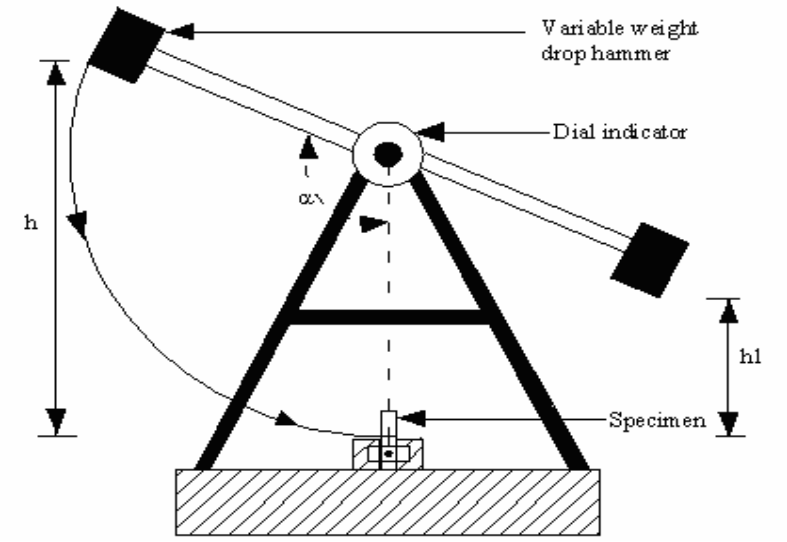

Figure 3.3. Schematic diagram of an impact tester

3.4 Scanning electron microscopy

The surfaces of the specimens are examined directly by scanning electron microscope JEOL JSM-6480LV as shown in Figure 3.4. The composite samples are mounted on stubs with silver paste. To enhance the conductivity of the samples, a thin film of platinum is vacuum-evaporated onto them before the photomicrographs are taken.

Figure 3.4. Scanning Electron Microscope (JEOL JSM-6480LV)

3.5 X-Ray diffraction studies

The composites are examined for the identification of the (crystalline) phases with a Philips X Ray Diffractometer. The X ray diffractograms on the eroded and uneroded surfaces are taken using Cu Kα radiation.

3.6 Erosion test apparatus

The set up used in this study for the solid particle erosion wear test is capable of creating reproducible erosive situations for assessing erosion wear resistance of the prepared composite samples. It consists of an air compressor, an air particle mixing chamber and accelerating chamber. The schematic diagram of the erosion test rig is given in Figure 3.5 and pictorial view is presented in Figure 3.6.

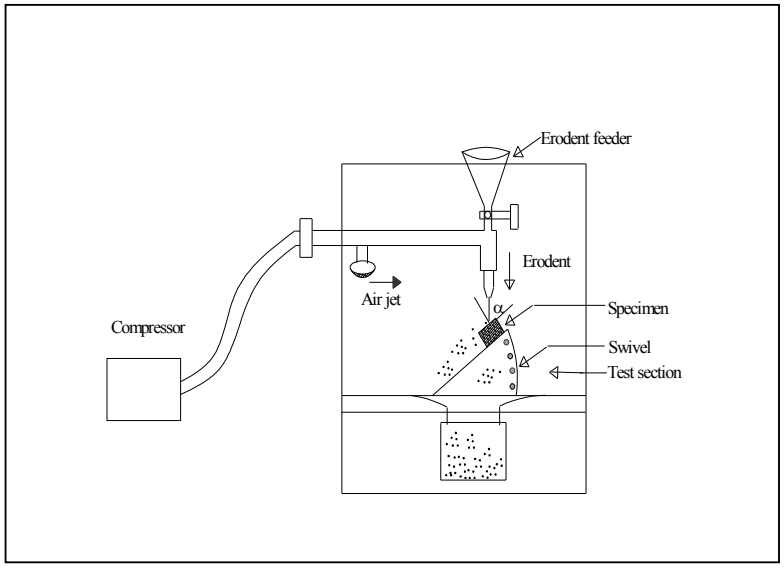

Figure 3.5. A schematic diagram of the erosion test rig

Figure 3.6. Solid particle erosion test set up

Dry compressed air is mixed with the erodent particles which are fed at constant rate from a sand flow control knob through the nozzle tube and then accelerated by passing the mixture through a convergent brass nozzle of 3mm internal diameter. These particles impact the specimen which can be held at different angles with respect to the direction of erodent flow using a swivel and an adjustable sample clip. Square samples of size 40mm×40mm are cut from the plaques for erosion tests**.** The velocity of the eroding particles is determined using standard double disc method [247]. The conditions (confirming to ASTM G 76 test standards) under which erosion tests are carried out are listed in Table 3.3. In the present study, dry silica sand (spherical) of different particle sizes (300μm, 500 μm and 800μm) are used as erodent. A standard test procedure is employed for each erosion test. The samples are weighed to an accuracy of ± 0.1 mg using an electronic balance, eroded in test rig for 5 min and then weighed again to determine the weight loss. The ratio of weight loss to the weight of the eroding particles causing loss (i.e. testing time ×particle feed rate) is then computed as the dimensionless incremental erosion rate. This procedure repeated till the erosion rate attains a constant steady-state value.

3.7 Process optimization and Taguchi method

Statistical methods are commonly used to improve the quality of a product or process. Such methods enable the user to define and study the effect of every single condition possible in an experiment where numerous factors are involved. Solid particle erosion is such a process in which a number of control factors collectively

determine the performance output i.e the erosion rate. Hence, in the present work a statistical technique called Taguchi method is used to optimize the process parameters leading to minimum erosion of the polymer composites under study. This part of the chapter presents the Taguchi experimental design methodology in detail.

Table 3.3. Parameter settings for erosion test.

Control Factors	Symbols	Fixed parameters	
Velocity of impact	Factor A	Erodent	Silica sand
Fiber/Filler loading	Factor B	Erodent feed rate (g/min)	10.0 ± 1.0
Stand-off distance	Factor C	Test temperature	RT
Impingement angle	Factor D	Nozzle diameter (mm)	3
Erodent size	Factor E	Length of nozzle (mm)	80

Taguchi Experimental Design

Taguchi technique is a powerful tool for design of high quality systems based on orthogonal array experiments that provide much-reduced variance for the experiments with an optimum setting of process control parameters. It introduces an integrated approach that is simple and efficient to find the best range of designs for quality, performance and computational cost. From a scientific viewpoint, these experiments are either one or a series of tests to either confirm a hypothesis or to understand a process in further detail. Experiments from a manufacturing point of view, however, are concerned with finding the optimum product and process, which is both cost effective and of a high quality. In order to achieve a meaningful end result, several experiments are usually carried out. The experimenter needs to know the factors involved, the range of these factors are varied between, the levels assigned to each factor as well as a method to calculate and quantify the response of each factor. This one factor at a time approach will provide the most favorable level for each factor but not the optimum combination of all the interacting factors involved. Thus, experimentation in this scenario can be considered as an iterative process. Although it will provide a result, such methods are not time or cost effective. But the design of experiments is a scientific approach to effectively plan and perform experiments, using statistics. In such designs, the combination of each factor at every level is studied to determine the combination that would yield the best result.

The advantage of such design schemes is that it will always determine the effect of factors and possible interactions (between factors) on the result.

Taguchi design of experiment is a powerful analysis tool for modeling and analyzing the influence of control factors on performance output. The most important stage in the design of experiment lies in the selection of the control factors. Therefore, initially a large number of factors are included so that non-significant variables can be identified at earliest opportunity. Exhaustive literature review on erosion behaviour of polymer composites reveal that parameters viz., impact velocity, impingement angle, fiber loading, filler content, erodent size and stand-off distance etc largely influence the erosion rate of polymer composites [248, 249]. In the present work, the impact of five such parameters are studied using L_{27} (3^{13}) orthogonal design. The operating conditions under which erosion tests are carried out are given in Table 3.4. The tests are conducted at room temperature as per experimental design given in Table 3.5.
Five parameters viz., impact velocity, fiber/filler loading, stand-off distance, impingement angle and erodent size, each at three levels, are considered in this study. In Table 3.4, each column represents a test parameter and a row gives a test condition which is nothing but combination of parameter levels. Five parameters each at three levels would require 3^5 = 243 runs in a full factorial experiment whereas Taguchi's factorial experiment approach reduces it to 27 runs only offering a great advantage.

Table 3.4. Levels for various control factors

Control factor	Level			
	I	II	III	Units
A: Velocity of impact	32	45	58	m/sec
B: Fiber loading (for composites A_1,B_1, C_1)	30	40	50	wt%
B: Filler content (for composites C_1-C_9)	0	10	20	wt%
C: Stand-off distance	120	180	240	mm
D: Impingement angle	30	60	90	degree
E: Erodent size	300	500	800	μm

This method achieves the integration of design of experiments (DOE) with the parametric optimization of the process yielding the desired results. The orthogonal array (OA) requires a set of well-balanced (minimum experimental runs)

experiments. Taguchi's method uses a statistical measure of performance called signal-to-noise ratio (S/N), which is logarithmic function of desired output to serve as objective functions for optimization. The S/N ratio considers both the mean and the variability into account. It is defined as the ratio of the mean (signal) to the standard deviation (noise). The ratio depends on the quality characteristics of the product/process to be optimized. The three categories of S/N ratios are used: lower-the-better (LB), higher-the-better (HB) and nominal-the best (NB). The experimental observations are transformed into a signal-to-noise (S/N) ratio. There are several S/N ratios available depending on the type of characteristics. The S/N ratio for minimum erosion rate coming under smaller is better characteristic, which can be calculated as logarithmic transformation of the loss function as shown below.

Smaller is the better characteristic: $\frac{S}{N} = -10 \log \frac{1}{n}\left(\sum y^2\right)$ (3.11)

where n the number of observations, and y the observed data. "Lower is better" (LB) characteristic, with the above S/N ratio transformation, is suitable for minimizations of erosion rate. The standard linear graph by Peace [233] and Phadke [234], as shown in Figure 3.7, is used to assign the factors and interactions to various columns of the orthogonal array.

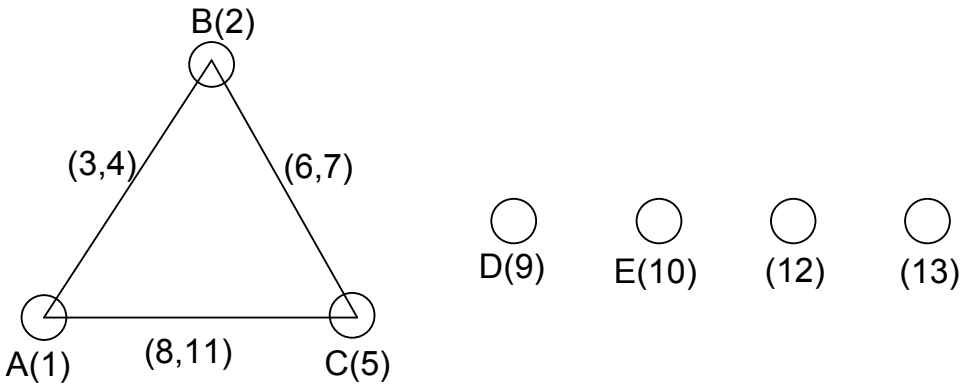

Figure 3.7. Linear graphs for L_{27} orthogonal array

The plan of the experiments is as follows: the first column was assigned to impact velocity (A), the second column to fiber/filler loading (B), the fifth column to stand-off distance (C), the ninth column to impingement angle (D) and tenth column to erodent size (E), the third and fourth column are assigned to $(A \times B)_1$ and $(A \times B)_2$, respectively to estimate interaction between impact velocity (A) and fiber loading (B), the sixth and seventh column are assigned to $(B \times C)_1$ and $(B \times C)_2$ respectively, to estimate interaction between the fiber loading (B) and stand-off distance (C), the eighth and

eleventh column are assigned to $(A\times C)_1$ and $(A\times C)_2$ respectively, to estimate interaction between the impact velocity (A) and stand-off distance (C). The remaining columns are assigned to error columns respectively.

Table 3.5. Orthogonal array for L_{27} (3^{13}) Taguchi Design

$L_{27}(3^{13})$	1 A	2 B	3 $(AxB)_1$	4 $(AxB)_2$	5 C	6 $(BxC)_1$	7 $(BxC)_2$	8 $(AxC)_1$	9 D	10 E	11 $(AxC)_2$	12	13
1	1	1	1	1	1	1	1	1	1	1	1	1	1
2	1	1	1	1	2	2	2	2	2	2	2	2	2
3	1	1	1	1	3	3	3	3	3	3	3	3	3
4	1	2	2	2	1	1	1	2	2	2	3	3	3
5	1	2	2	2	2	2	2	3	3	3	1	1	1
6	1	2	2	2	3	3	3	1	1	1	2	2	2
7	1	3	3	3	1	1	1	3	3	3	2	2	2
8	1	3	3	3	2	2	2	1	1	1	3	3	3
9	1	3	3	3	3	3	3	2	2	2	1	1	1
10	2	1	2	3	1	2	3	1	2	3	1	2	3
11	2	1	2	3	2	3	1	2	3	1	2	3	1
12	2	1	2	3	3	1	2	3	1	2	3	1	2
13	2	2	3	1	1	2	3	2	3	1	3	1	2
14	2	2	3	1	2	3	1	3	1	2	1	2	3
15	2	2	3	1	3	1	2	1	2	3	2	3	1
16	2	3	1	2	1	2	3	3	1	2	2	3	1
17	2	3	1	2	2	3	1	1	2	3	3	1	2
18	2	3	1	2	3	1	2	2	3	1	1	2	3
19	3	1	3	2	1	3	2	1	3	2	1	3	2
20	3	1	3	2	2	1	3	2	1	3	2	1	3
21	3	1	3	2	3	2	1	3	2	1	3	2	1
22	3	2	1	3	1	3	2	2	1	3	3	2	1
23	3	2	1	3	2	1	3	3	2	1	1	3	2
24	3	2	1	3	3	2	1	1	3	2	2	1	3
25	3	3	2	1	1	3	2	3	2	1	2	1	3
26	3	3	2	1	2	1	3	1	3	2	3	2	1
27	3	3	2	1	3	2	1	2	1	3	1	3	2

3.8 Neural Computation

Erosion wear process is considered as a non-linear problem with respect to its variables: either materials or operating conditions. To obtain minimum wear rate, combinations of operating parameters have to be planned. Therefore a robust methodology is needed to study these interrelated effects. In this work, a statistical method, responding to the constraints, is implemented to correlate the operating parameters. This methodology is based on artificial neural networks (ANN), which is a technique that involves database training to predict input-output evolutions. The details of this methodology are described by Haykin S [251]. In the present analysis, the velocity of impact, filler content, stand-off distance, impingement angle and erodent size are taken as the five input parameters. Each of these parameters is characterized by one neuron and consequently the input layer in the ANN structure has five neurons. The database is built considering experiments at the limit ranges of each parameter. Experimental result sets are used to train the ANN in order to understand the input-output correlations. The database is then divided into three categories, namely: (i) a training category, which is exclusively used to adjust the network weights and (ii) a test category, which corresponds to the set that validates the results of the training protocol. Usually seventy five percent data (patterns) is used for training and twenty five percent for testing [251]. The input variables are normalized so as to lie in the same range group of 0-1. The output layer of the network has only one neuron to represent wear rate. To train the neural network used for this work, about 135 data sets obtained during erosion trials on different composites are taken. Different ANN structures (Input-Hidden-Output nodes) with varying number of neurons in the hidden layer are tested at constant cycles, learning rate, error tolerance, momentum parameter, noise factor and slope parameter. Based on least error criterion, one structure, shown in Table 3.5, is selected for training of the input-output data. The learning rate is varied in the range of 0.001-0.100 during the training of the input-output data. Neuron number in the hidden layer is varied and in the optimized structure of the network, this number is 12 for a typical case. The number of cycles selected during training is high enough so that the ANN models could be rigorously trained.

The C^{++} coding used for neural computing developed by Haykin S [251] using back propagation algorithm is used as the prediction tool for erosion wear rate of different

composites under various test conditions. The three-layer neural network having an input layer (I) with five input nodes, a hidden layer (H) with twelve neurons and an output layer (O) with one output node employed for this work is shown in Fig. 3.8.

Table 3.6. A typical case of Input parameters selected for training

Input Parameters for Training	**Values**
Error tolerance	0.01
Learning rate (ß)	0.01
Momentum parameter(α)	0.03
Noise factor **(NF)**	0.01
Number of epochs	20,0000
Slope parameter (£)	0.6
Number of hidden layer	12
Number of input layer neuron **(I)**	5
Number of output layer neuron **(O)**	1

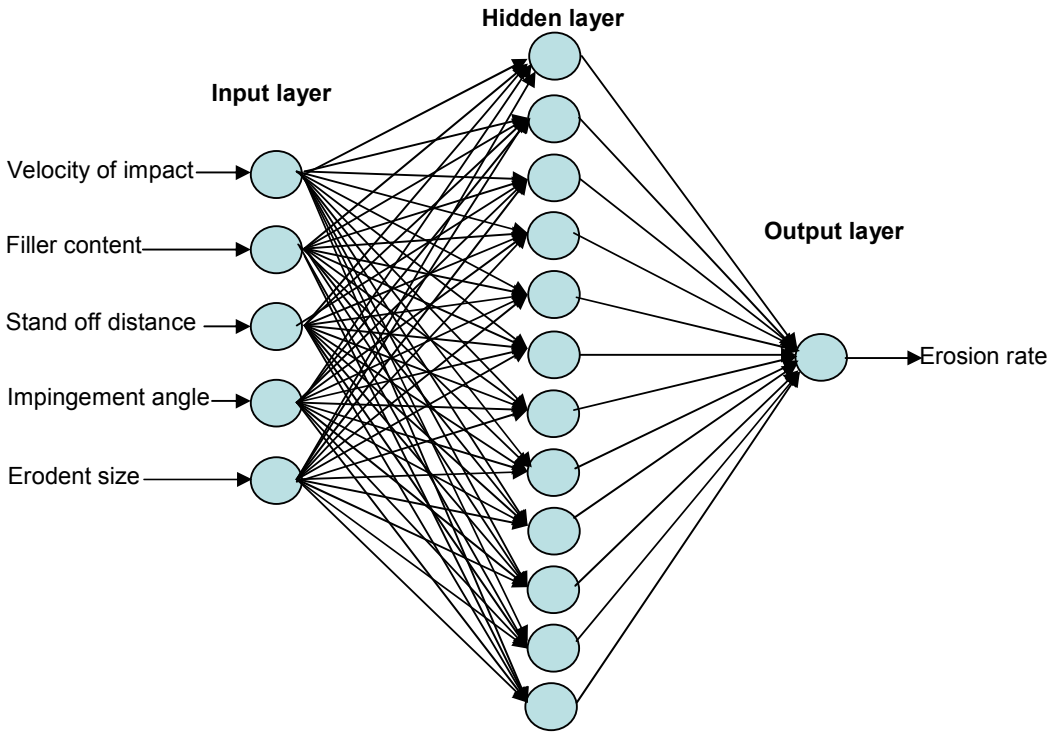

Figure 3.8. The neural network architecture

Chapter summary

This chapter has provided:

- The descriptions of materials used in the experiments
- The details of fabrication and characterization of the composites
- The description of erosion wear test
- An explanation of the Taguchi experimental design and neural computation.

The next chapter presents the physical and mechanical properties of the polymer composites under study.

****

Chapter 4

Mechanical Characterization of the Composites

Chapter 4

MECHANICAL CHARACTERIZATION OF THE COMPOSITES

Introduction

This chapter presents the physical and mechanical properties of the glass fiber reinforced polyester composites prepared for this work. The interpretation of the results and the comparison among various composite samples are also presented. This chapter consists of two parts: one for the glass-polyester composites without particulate filling (A_1, B_1 and C_1) and the other for the particulate filled composites (C_1-C_9).

Part I

4.1 Glass fiber-polyester composites (A_1, B_1 and C_1)

Density and volume fraction of voids

The theoretical and measured densities along with the corresponding volume fraction of voids are presented in Table 4.1. It may be noted that the composite density values calculated theoretically from weight fractions using Eq.(3) are not equal to the experimentally measured values. This difference is a measure of voids and pores present in the composites. It is clearly seen that with the increase in fiber content from 30 wt% to 50 wt%, there is a decrease in the void fraction. This is due to fibre-fibre interactions and fibre constraint on packing. These effects can lead to the swelling of the composite and reduce density. However, in all the three composites A_1, B_1 and C_1, the volume fractions of voids are reasonably small (< 2.5%) and this can be attributed to the absence of particulate fillers in these composites.

Table 4.1. Measured and Theoretical densities of the composites (without particulate fillers)

Composites	Measured density (g/cc)	Theoretical Density (g/cc)	Volume fraction of voids (%)
A_1 (Polyester +30wt% glass fiber)	1.738	1.776	2.411
B_1 (Polyester +4wt% glass fiber)	1.874	1.845	1.497
C_1 (Polyester +5wt% glass fiber)	1.932	1.950	1.020

Micro-hardness

The variation of composite micro-hardness with the weight fraction of glass fiber is shown in Figure 4.1. For the composite A_1 (30 wt% of GF), the micro-hardness value is recorded as 32 Hv while for C_1 (50 wt% of GF) this value is measured to be 39 Hv. It is thus seen that with the increase in fiber content in the composite, the hardness improves although the increment is marginal.

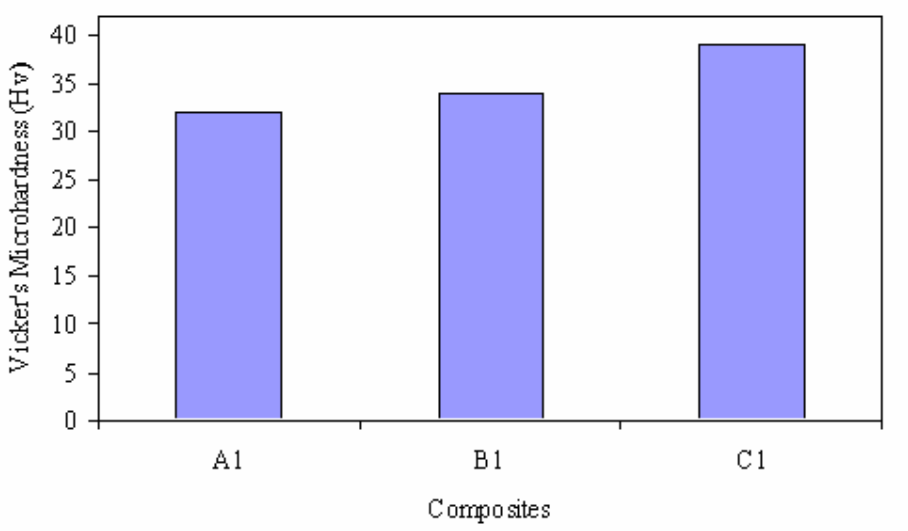

Figure 4.1. Micro-hardness vs. fiber loading for glass polyester composites

Tensile and flexural strength

It is well known that the strength properties of composites are mainly determined by the fiber content and the fiber strength. So the variation in composite strength with different fiber loading is obvious. These variations in tensile and flexural strengths of the composites A_1, B_1 and C_1 are shown in Figure 4.2. A gradual increase in both tensile strength as well as flexural strength with the fiber weight fraction is noticed. It clearly indicates that inclusion of glass fiber improves the load bearing capacity and the ability to withstand bending of the composites. Similar observations have been reported by Harsha et al. [249] for fiber reinforced thermoplastics such as polyaryletherketone composites. It may be mentioned here that both tensile and flexural strengths are important for structural applications.

Inter laminar shear strength (ILSS)

The stresses acting on the interface of the two adjacent laminae in a layered composite are called inter laminar composites. These stresses cause relative deformations between the consecutive laminae and if these stresses are sufficiently

high they may cause failure along the mid-plane between two adjacent laminae. It is therefore of considerable interest to evaluate inter laminar shear strength through tests in which failure of the laminates of the composite initiates in a shear (delamination) mode. In the present work the ILSS values are measured for unfilled glass-polyester composites A_1, B_1 and C_1 and an improvement is recorded in the ILSS of the composites with increase in the fiber content in them. The values are illustrated graphically in Figure 4.3.

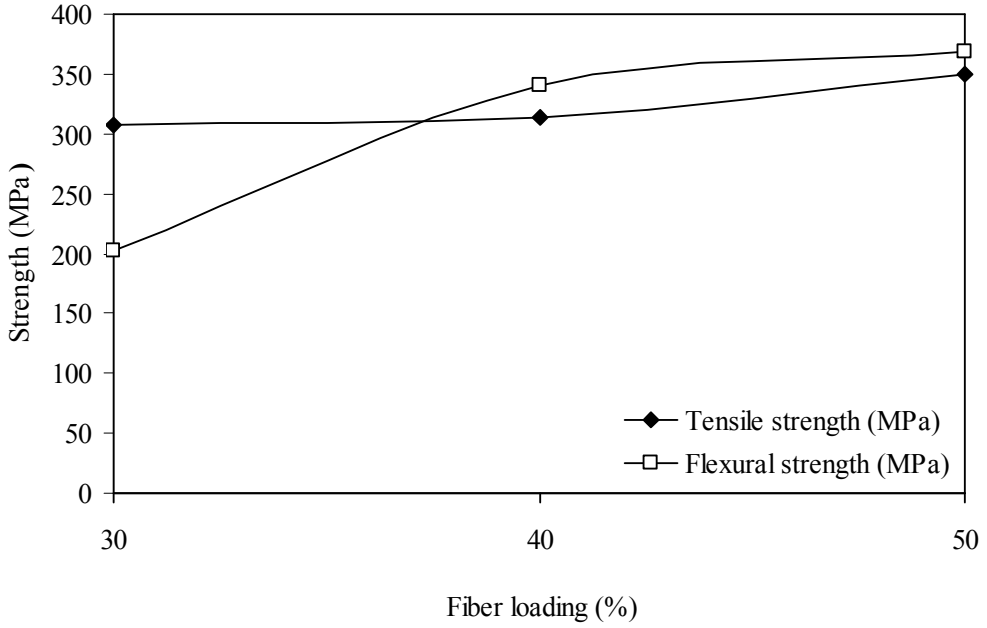

Figure 4.2. Fiber loading vs. strengths of glass fiber polyester composites

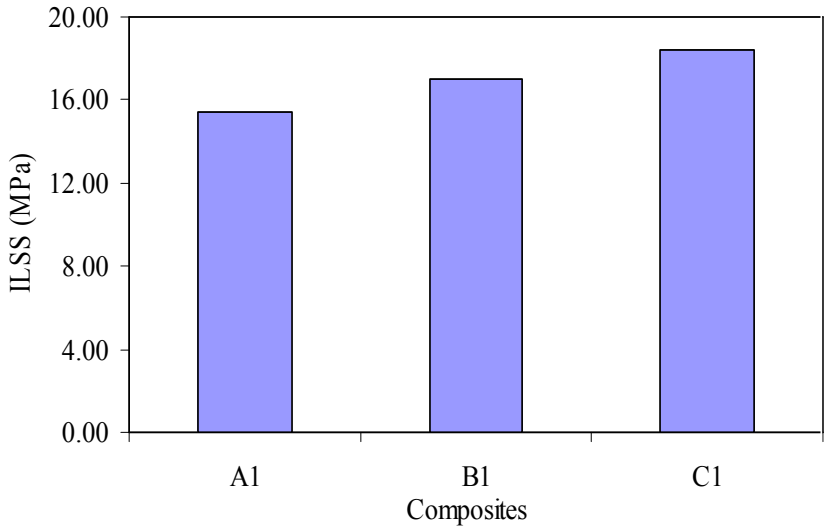

Figure 4.3 Fiber loading vs. inter-laminar shear strength of glass fiber polyester Composites

Impact strength

The study of impact behaviour of fibrous composite material is essential before recommending then for structural / engineering applications. The strength, orientation and weight fraction of fiber largely influence the impact strength of any fiber reinforced composite. In the present investigation, since the orientation of glass fiber is kept unchanged in all the three samples, the difference in impact energy values with different fiber content is obvious. This variation is clearly shown in Figure 4.4. A significant increase in this property can be observed with the increase in fiber content (50 wt%) in comparison to lower fiber content. This confirms the efficiency of these fibers as reinforcement for polyester resin composites. For contents above 50 wt. %, the impact property value decreases reported by Al Emran Ismail and Nor Azila Zamani [250]. This fact can be related with the high content of fiber and the poor dispersion and distribution of the fibers in the matrix. It seems that 50 wt. % of fiber constitutes a limit value to increase the properties.

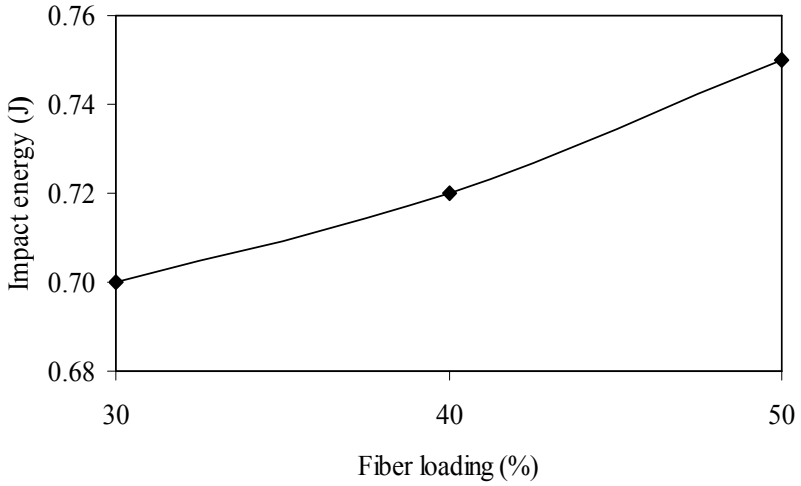

Figure 4.4. Fiber loading vs. impact energy of glass fiber polyester composites

Part II

4.2 Particulate filled glass-polyester composites (C_1-C_9)

The characterization of the composites reveals that inclusion of any particulate filler has strong influence on the physical and mechanical properties of composites. The modified values of the properties of the particulate filled / unfilled glass-polyester composites under this investigation are presented in Table 4.2.

Table 4.2. Mechanical properties of the composites

Composites	Hardness (Hv)	Tensile strength (MPa)	Tensile modulus (GPa)	Flexural strength (MPa)	ILSS (MPa)	Impact energy (J)
C_1 (Polyester +50wt% glass fiber)	39	349.6	5.7	368	18.42	0.75
C_2(Polyester +50wt% glass fiber + 10wt% flyash)	45	304.5	5.92	451.84	22.57	0.76
C_3 (Polyester +50wt% glass fiber +20wt% flyash)	37	279.4	6.07	297.82	18.99	0.78
C_4(Polyester +50wt% glass fiber +10wt% Alumina)	38	240.8	3.35	417	23.46	0.83
C_5 (Polyester +50wt% glass fiber +20wt% Alumina)	36.5	206	4.187	362.92	19.60	0.85
C_6 (Polyester +50wt% glass fiber +10wt% SiC)	43	282.6	5.81	353.8	24.17	0.77
C_7 (Polyester +50wt% glass fiber +20wt% SiC)	47	251.7	6.02	309.2	20.32	0.78
C_8 (Polyester +50wt% glass fiber +10wt% CBPD)	43.5	322.6	5.98	463.34	24.86	0.86
C_9 (Polyester +50wt% glass fiber +20wt% CBPD)	40	297	6.31	327.2	21.14	0.89

Density

The theoretical and measured densities along with the corresponding volume fractions of voids are presented in Table 4.3. It may be noted that the composite density values calculated theoretically from weight fractions using Eq. (3) are not exactly same as the measured values. This difference is a measure of voids and pores present in the composites. It is clear from Table 4.3 that in C_1 the volume fraction of voids is negligible and this is due to the absence of particulate fillers. With the addition of filler materials more voids are found in the composites. As the filler content increases from 10 wt% to 20 wt% the volume fraction of voids is also found to be increasing. This is due to the irregular shape of the fillers and presence of empty spaces near sharp edges of the filler particles. This trend is observed in all the particulate filled composites (C_2-C_9) irrespective of the filler material.

Table 4.3. Measured and Theoretical densities of the composites (with particulate fillers)

Composites	Measured density (gm/cc)	Theoretical density (gm/cc)	Volume fraction of voids (%)
C_1	1.932	1.950	1.020
C_2	1.780	1.930	7.700
C_3	1.710	2.100	18.57
C_4	1.765	1.930	8.200
C_5	1.730	2.167	19.96
C_6	1.752	1.960	10.71
C_7	1.739	2.120	17.92
C_8	1.809	1.917	5.630
C_9	1.882	2.028	7.190

Density of a composite depends on the relative proportion of matrix and reinforcing materials and this is one of the most important factors determining the properties of the composites. The void content is the cause for the difference between the values of true density and the theoretically calculated one. The voids significantly affect some of the mechanical properties and even the performance of composites. Higher void contents usually mean lower fatigue resistance, greater susceptibility to water penetration and weathering [1]. The knowledge of void content is desirable for estimation of the quality of the composites. It is understandable that a good composite should have fewer voids. However, presence of void is unavoidable in composite making particularly through hand-lay-up route.

Micro-hardness

The measured micro-hardness values of all the nine composites are presented in Fig. 4.5. It can be seen that the hardness is affected only marginally by the addition of alumina particles. It is further observed that flyash addition beyond 10 wt% also shows a minor change in the hardness. The composite C_2 with 10 wt% flyash content is found to exhibit some improvement in hardness compared to the unfilled composite C_1. The mean hardness of flyash as well as alumina particle are generally high like any other oxide ceramic and so with their inclusion, the composite

hardness is expected to increase. But the measured values do not show consistency with this theory. The low or marginal effect of these particulate fillers on composite micro-hardness may be due to the presence of pores and voids. However, as expected the hardness values of SiC-GF-Polyester composites (C_6 and C_7) are found to be higher than that of composite (C_1). Here the hardness is seen to have improved with increase in SiC content (Fig. 4.5). Similarly, the addition of cement by-pass dust has also resulted in improved hardness of the composites. It is evident from Figure 4.5 where it can be seen that the hardness values of C_8 and C_9 are not only higher than that of the unfilled composite (C_1) but also Al_2O_3 filled composites (C_4 and C_5).

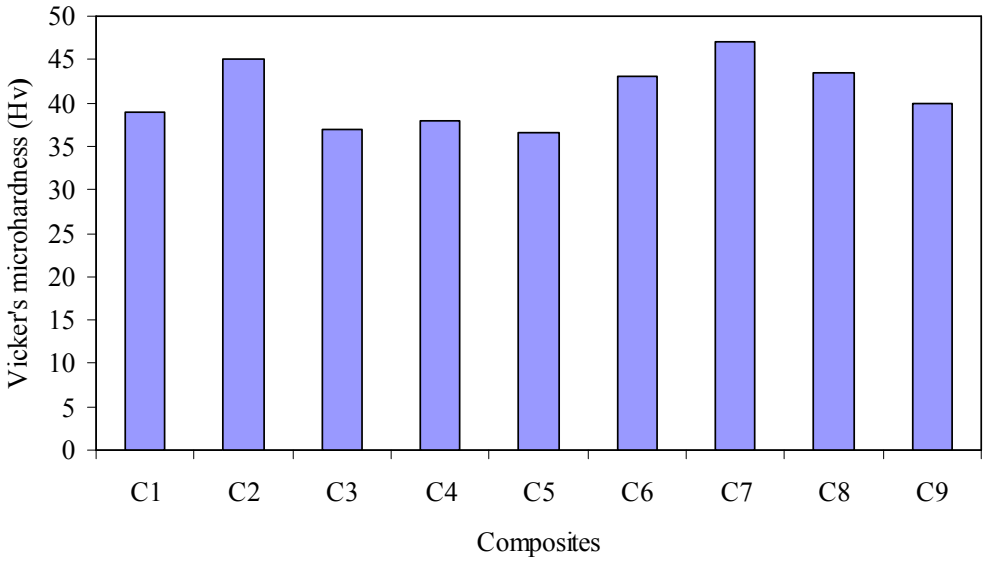

Figure 4.5. Comparison of hardness values of different composites

Tensile properties

The test results for tensile strengths and moduli are shown in Figs. 4.6 and 4.7 respectively. It is seen that in all the samples irrespective of the filler material the tensile strength of the composite decreases with increase in filler content. The unfilled glass polyester composite (50wt% Fiber loading)has a strength of 349.6 MPa in tension and it may be seen from Table 4.2 that this value drops to 304.5 MPa and 279.4 MPa with addition of 10 wt% and 20 wt% of flyash respectively. Among the four fillers taken in this study, the inclusion of alumina causes maximum reduction in the composite strength. There can be two reasons for this decline in the strength properties of these particulate filled composites compared to the unfilled one. One

possibility is that the interface bonding between the filler particles and the matrix may be too weak to transfer the tensile stress; the other is that the corner points of the irregular shaped particulates result in stress concentration in the polyester matrix. These two factors are responsible for reducing the tensile strengths of the composites so significantly. The tensile strengths are different with different filler materials as their compatibility with the matrix and irregularities in shape are different from one another. Similar property modification has been previously reported for Al_2O_3 particles reinforced in polyurethane matrix [252].

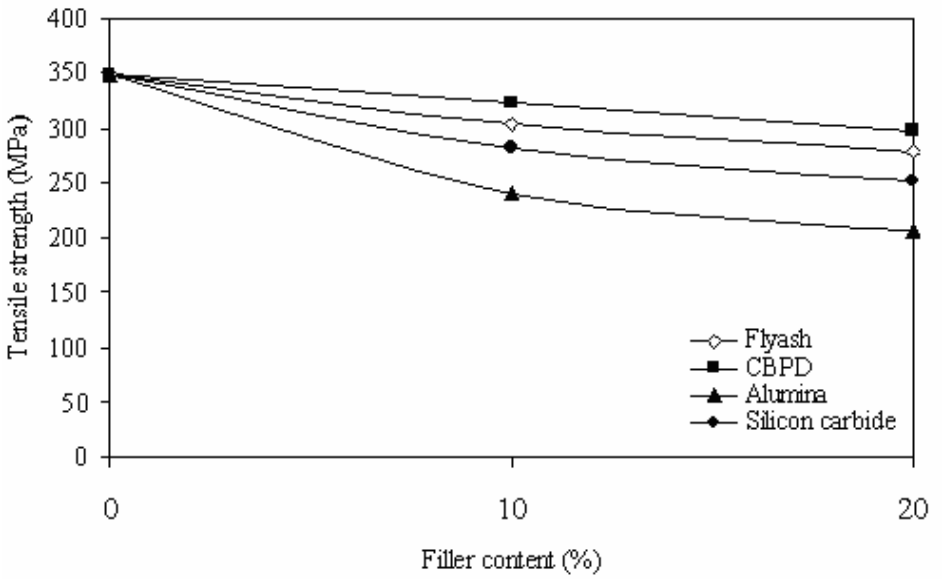

Figure 4.6. Variation of tensile strength of composites with filler type and content

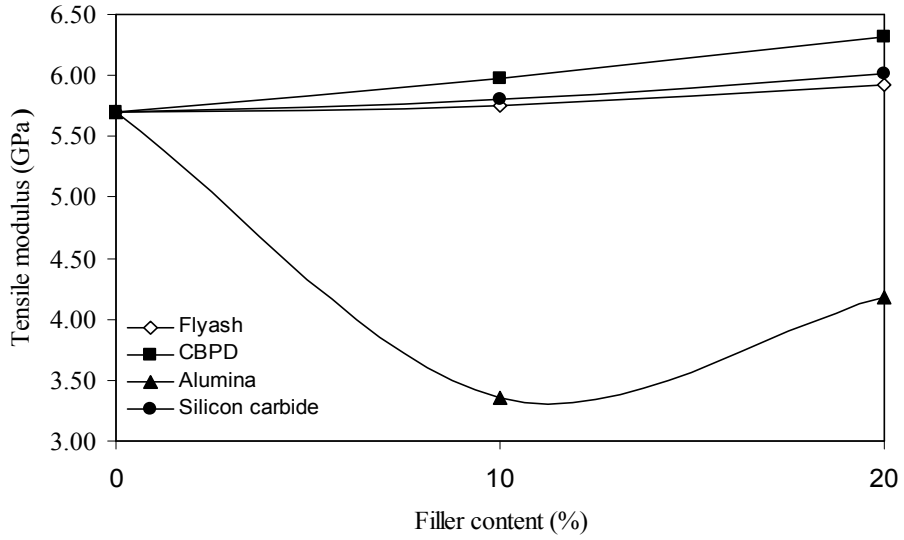

Figure 4.7. Variation of tensile modulus of composites with filler type and content

The compatibility of alumina particles in polyester resin seems to be not as good as that of flyash, as a result of which the percentage reduction in tensile strength is highest in the former case. The tensile moduli of these alumina filled composites C_4 and C_5, are also found to be less than the modulus of the unfilled one. On the contrary the experimental findings suggest that with addition of flyash, SiC and CBPD, the tensile moduli of the glass polyester composites improve reasonably (Fig. 4.7). This improvement is attributed to the relatively lower strain rates of composites C_2, C_3, C_6,C_7, C_8 and C_9 during the tensile test.

Flexural and Inter-laminar shear strength

Figure 4.8 shows the comparison of flexural strengths of the composites obtained experimentally from the 3-point bend tests. It is interesting to note that composites (C_2,C_4 and C_8) with addition of small amount (10 wt%) of fly ash, alumina and CBPD exhibited improved flexural strength compared to the unfilled glass-polyester composite (C_1). But for the composite samples (C_3,C_5 and C_9) with 20 wt% of these fillers lower values of the flexural strength are recorded. However, this trend is not found in the composites (C_6 and C_7) with silicon carbide particles, where the flexural strength of the glass-polyester system declines monotonically with filler content.

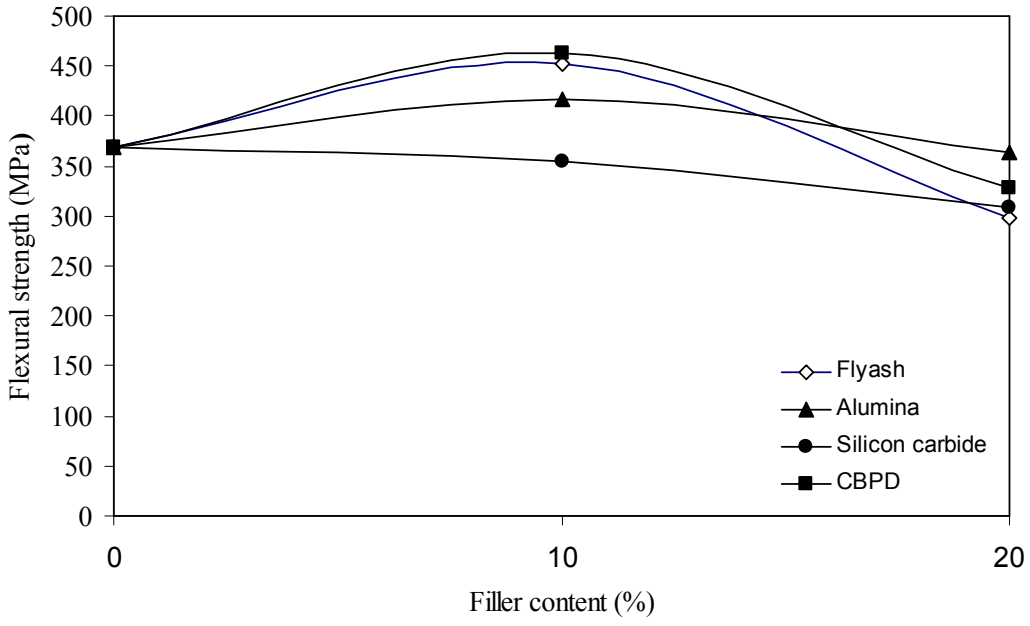

Figure 4.8. Variation of flexural strength of composites with filler type and content

The flexural properties are of great importance for any structural element. Composite materials used in structures are prone to fail in bending and therefore the development of new composites with improved flexural characteristics is essential. From the results it may now be suggested that alumina, fly ash and CBPD are potential candidates to be used as fillers in making high flexural strength composites.

The inter-laminar shear strength values of the particulate filled composites are shown along with that of the unfilled glass polyester composite (C_1) in Figure 4.9. It is seen that there is improvement of ILSS of glass-reinforced polyester composite with particulate filling irrespective of the filler type. Incorporation of silicon carbide is seen to have caused the maximum increase in the strength compared to the other fillers. It can also be noticed that with increase in filler content from 10 wt% to 20 wt% there is invariably a drop in the inter-laminar shear strength.

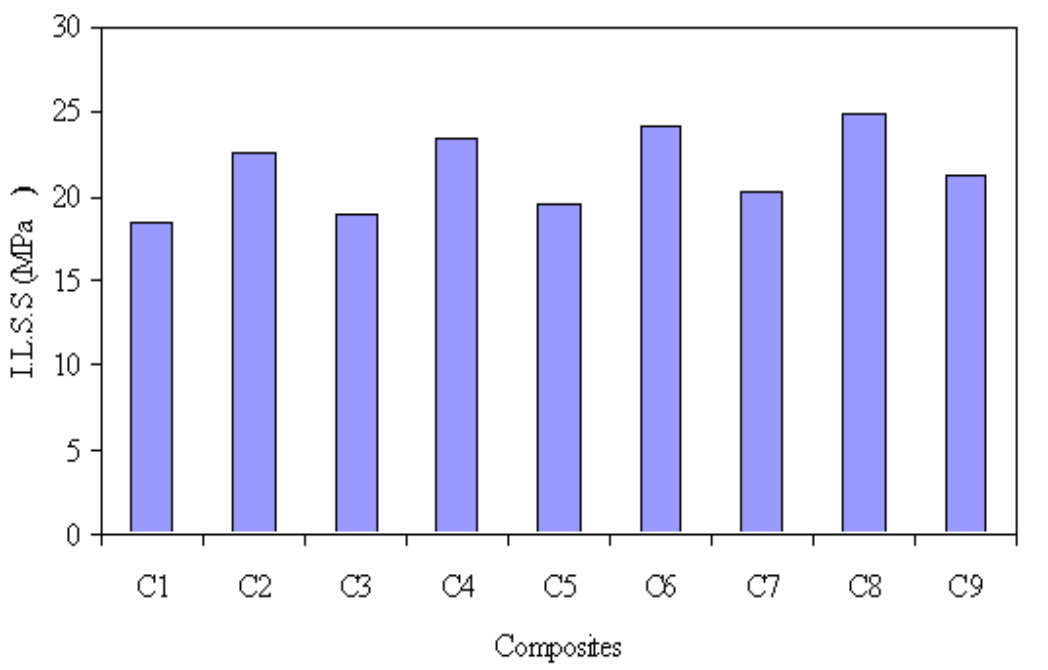

Figure 4.9. Inter-laminar shear strength of different composites

The stresses acting on the interface of two adjacent laminas are called inter-laminar shear stress. The stresses cause relative deformation between the lamina and if these are sufficiently high, they may cause failure along the common plane between the laminas. It is therefore, of considerable interest to evaluate inert-laminar shear strength through tests in which failure of laminates initiates in a shear (delaminating) mode. In the present investigation, during flexural test, the span length is very short

(40 mm). A large span to depth ratio in bending test increases the maximum normal stress without affecting the inter-laminar shear stress and thereby increases the tendency for longitudinal failure. If the span is short enough, failure initiates and propagates by inter-laminar shear failure. The maximum shear stress in a beam occurs at the mid plane. So in the shear test, failure consists of a crack running along the mid plane of the beam so that crack plane is parallel to the longitudinal plane.

Impact strength

The impact energy values of different composites recorded during the impact tests are given in Table 4.2. It shows that the resistance to impact loading of glass-polyester composites improves with addition of particulate fillers. It is seen that with incorporation of CBPD particles the impact strength of unfilled glass fiber-polyester composite increases by about 15% - 20% . It is also noteworthy that the Al_2O_3 filled composites show 10% - 15% higher impact strength compared to the unfilled one. In case of the other two fillers (flyash and silicon carbide) the increment in impact strength is marginal.

High strain rates or impact loads may be expected in many engineering applications of composite materials. The suitability of a composite for such applications should therefore be determined not only by usual design parameters, but by its impact or energy absorbing properties. Thus, it is important to have a good understanding of the impact behaviour of composites for both safe and efficient design of structures and to develop new composites having good impact properties. The results of impact tests in the present study reveal that CBPD and Al_2O_3 are promising filler materials in future hybrid composites.

Chapter summary

This chapter summarises that:

- Successful fabrication of glass-polyester composites with reinforcement of conventional ceramic fillers like: Al_2O_3 and SiC is possible.
- Industrial wastes like fly ash and cement by-pass dust (CBPD) can also be gainfully utilized for the composite making purpose.
- Incorporation of these fillers modifies the tensile, flexural, impact and inter-laminar shear strengths of the glass polyester composites.

- The micro-hardness and density of the composites are also greatly influenced by the type and content of fillers.

The next chapter presents the development of a theoretical model for estimation of wear rate of polymer composites during solid particle erosion.

****

Chapter 5

Development of a Theoretical Model for Erosion Wear Rate Estimation

Chapter 5

DEVELOPMENT OF A THEORETICAL MODEL FOR EROSION WEAR RATE ESTIMATION

Introduction

This chapter presents the development of a mathematical model for estimating the rate of erosion wear caused by solid particle impact.

5.1 Nomenclature

The following symbols are used in this thesis:

2r	chord length of the indentation (m)
d	erodent diameter (m)
δ	indentation depth (m)
e_v	volumetric wear loss per particle impact (m^3)
E_V	total volumetric erosion wear rate (m^3/sec)
α	angle of impingement (degree)
V	impact velocity (m/sec)
P	force on the indenter (N)
H_v	hardness (N/m^2)
m	mass of single erodent particle (kg)
M	mass flow rate of the erodent (kg/sec)
N	number of impact per unit time (sec^{-1})
ρ_c	density of composite (kg/m^3)
ρ	density of erodent (kg/m^3)
η_{normal}	erosion efficiency with normal impact
η	erosion efficiency
E_{rth}	erosion wear rate (kg/kg)

5.2 Development of theoretical model

Solid particle erosion is a wear process in which the material is removed from a surface by the action of a high velocity stream of erodent particles entrained in a high velocity fluid stream. The particles strike against the surface and promote material

loss. During flight, a particle carries momentum and kinetic energy which can be dissipated during the impact due to its interaction with a target surface. As far as erosion study of polymer matrix composites is concerned, no specific model has been developed and thus the study of their erosion behaviour has been mostly experimental. However, Mishra [253] proposed a mathematical model for material removal rate in abrasive jet machining process in which the material is removed from the work piece in a similar fashion. This model assumes that the volume of material removed is same as the volume of indentation caused by the impact. This has a serious limitation as in a real erosion process the volume of material removed is actually different from the indentation volume. Further, this model considers only the normal impact i.e α = 90^0 whereas in actual practice, particles may impinge on the surface at any angle ($0^0 \le \alpha \le 90^0$). The proposed model addresses these shortcomings in an effective manner. It considers the real situation in which the volume of material removed by erosion is not same as the volume of material displaced and therefore, additional term "erosion efficiency (η)" is incorporated in the erosion wear rate formulation. In the case of a stream of particles impacting a surface normally (i.e. at α=90^0), erosion efficiency (η_{normal}) defined by Sundararajan et. al [254] is given as

$$\eta_{normal} = \frac{2ErHv}{\rho V^2} \tag{5.1}$$

But considering impact of erodent at any angle α to the surface, the actual erosion efficiency can be obtained by modifying Eq. (5.1) as

$$\eta = \frac{2ErHv}{\rho V^2 Sin^2\alpha} \tag{5.2}$$

The model is based on the assumption that the kinetic energy of the impinging particles is utilized to cause micro-indentation in the composite material and the material loss is a measure of the indentation. The erosion is the result of cumulative damage of such non-interacting, single particle impacts. The model further assumes the erodent particles to be rigid, spherical bodies of diameter equal to the average grit size. It considers the ductile mode of erosion and assumes the volume of material lost in a single impact is less than the volume of indentation. The model is developed with the simplified approach of energy conservation which equals the erodent kinetic energy with the work done in creating the indentation.

The model for ductile mode erosion proceeds as follows.

From the geometry of Figure 5.1, $r^2 = d \times \delta$

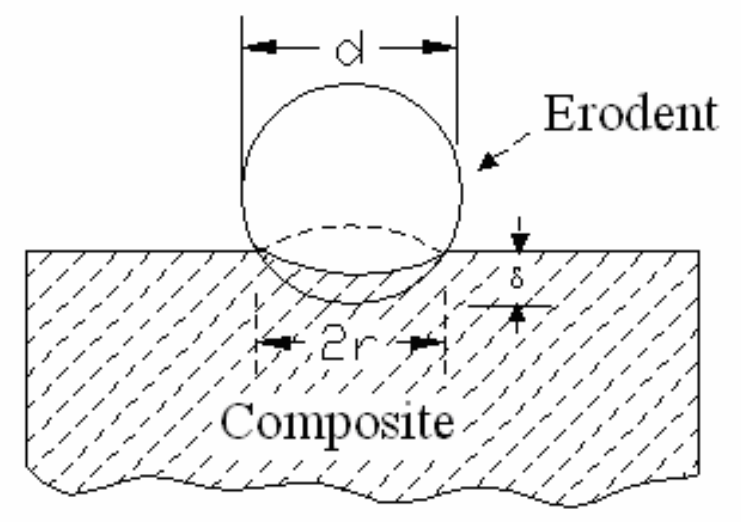

Figure 5.1. Scheme of material removal mechanism

The volume of indentation = $\pi\delta^2\left[\frac{d}{2}-\frac{\delta}{3}\right]$

So, the volumetric wear loss per particle impact is given by

e_v = Volume of indentation $\times$ η

= η $\times$ $\pi\delta^2\left[\frac{d}{2}-\frac{\delta}{3}\right]$ and neglecting δ^3 terms

$= \frac{\pi .d .\delta^2}{2} \times \eta$

Since δ represents a very small depth of indentation, δ^3 term can be neglected.

Considering N number of particle impacts per unit time, the volumetric erosion wear loss will be

$$E_V = \frac{\pi.d.\delta^2}{2} N \times \eta \qquad (5.3)$$

The impact velocity will have two components; one normal to the composite surface and one parallel to it. At zero impact angles, it is assumed that there is negligible wear because eroding particles do not practically impact the target surface [255]. Consequently, there will be no erosion due to the parallel component and the indentation is assumed to be caused entirely by the component normal to the composite surface as shown in Figure 5.2.

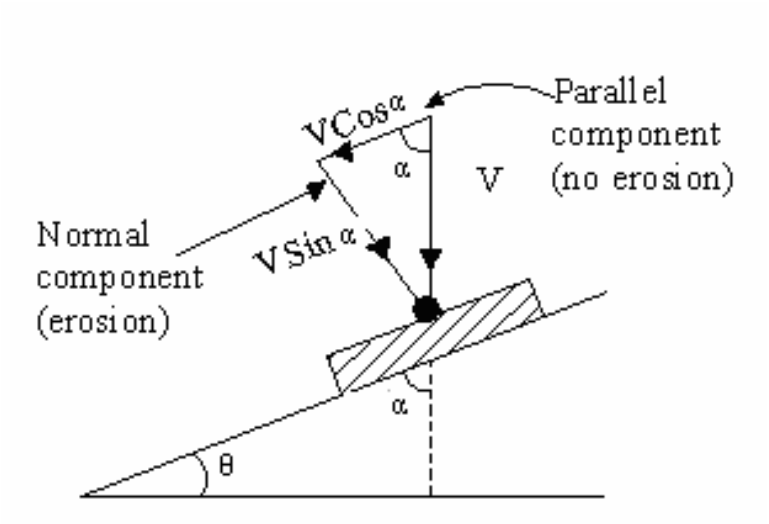

Figure 5.2. Resolution of impact velocity in normal and parallel directions.

Now applying conservation of energy to the single impact erosion process, kinetic energy associated with the normal velocity component of a single erodent particle is equal to the work done in the indentation of composite. The energy of impact introduces a force P on the indenter to cause the indentation in the composite. Thus,

$$\frac{1}{2}mv^2\sin^2\alpha = \frac{1}{2}.P.\delta \tag{5.4}$$

So, $\frac{1}{2}(\frac{\pi d^3}{6})\rho v^2\sin^2\alpha = \frac{1}{2}(\pi r^2 H_V)\delta$

On solving;

$$\delta^2 = \frac{\rho.V^2 d^2\sin^2\alpha}{6H_V} \tag{5.5}$$

The number of erodent particle impacting the target is estimated from the known value of erodent mass flow rate, M as

$$N = \frac{M}{\frac{\pi d^3}{6}\rho} \tag{5.6}$$

Substituting the value of δ in Eq. (5.3)

$$E_V = \frac{\pi.d.d^2.V^2.Sin^2\alpha.\rho}{2\times 6H_V}.\frac{M.6}{\pi.d^3\rho}.\eta$$

$$E_V = \frac{V^2.Sin^2\alpha}{2H_V}.\eta\ .M$$

Erosion rate (Er) defined as the ratio of mass lost due to erosion to the mass of erodent is now expressed as:

$$E_R = \frac{\rho_C . \eta . V^2 . Sin^2 \alpha}{2H_V} \tag{5.7}$$

The mathematical expression in Eq. (5.7) can possible be used for predictive purpose to make an approximate assessment of the erosion damage from the composite surface.

Chapter summary:

- This chapter has provided a theoretical model for estimation of wear rate in an erosion process. But since, material removal by impact erosion wear involves complex mechanisms; a simplified theoretical model for such a process may appear inadequate unless its assessment against experimental results is made. So for the validation of the proposed model, erosion tests on the composites are to be conducted at various operating conditions.

The next chapter presents the erosion test results of the polyester composites under this study.

****

Chapter 6

Study on Erosion Wear Characteristics of Glass-Fiber Polyester Composites

Chapter 6

STUDY ON EROSION WEAR CHARACTERISTICS OF GLASS-FIBER POLYESTER COMPOSITES

Introduction

The objective of this chapter is to validate the theoretical erosion model proposed in the previous chapter through experimental investigation. The test results of erosion trials carried out on the three glass-polyester composites A_1, B_1 and C_1 (without particulate filling) are given. The Taguchi analysis and the artificial neural network (ANN) implementation are also presented followed by a genetic algorithm (GA) approach.

6.1 Erosion test results

Steady state erosion

The erosion curves are plotted (Figure 6.1) from the results of erosion tests conducted for different impingement angle keeping all other parameters constant (impact velocity = 32m/sec, stand-off distance = 120 mm and erodent size = 300 μm). It can be seen that the peaks of erosion rates are located at an angle of 60^0 for all the samples irrespective of fiber content. This shows semi-ductile erosion behaviour of the composite. It is further noted in Figure 6.1 that with increased fiber content the erosion rate of the composites is greater. This can be attributed to the fact that the harder the material, larger is the fraction of the crater volume that is removed [254]. In this investigation higher hardness values have been recorded for composites with higher fiber loading and this is one reason why the composites exhibit declining erosion resistance with the increase in fiber content.

Erosion wear behaviour of materials can be grouped as ductile and brittle categories although this grouping is not definitive. Thermoplastic matrix composites usually show ductile behaviour and have the peak erosion rate at around 30^0 impingement angle because cutting mechanism is dominant in erosion. While the thermosetting ones erode in a brittle manner with the peak erosion occurring at normal impact. However, there is a dispute about this failure classification as the erosive wear behaviour depends strongly on the experimental conditions and the composition of

the target material [256]. Figure 6.1 also shows the dependence of the erosion rate of polyester composites with different fiber content on the impingement angle. The curves are plotted with the results of erosion tests conducted for different impingement angle keeping all other parameters constant (impact velocity = 32m/sec, stand-off distance = 120mm and erodent size = 300μm). It can be seen that the peaks of erosion rates are located at an angle of 60^0 for all the samples irrespective of fiber content. This shows semi-ductile erosion behavior of the composite. It is further noted (Fig. 6.1) that the erosion rate increases with increase in fiber content. Sundararajan et al. [210] concluded that this behavior is attributed to the fact that the harder the material, larger is the fraction of the crater volume that is removed. In this investigation higher hardness values have been noted for composites with higher fiber loading and this is therefore the reason why the composites exhibit declining erosion resistance with the increase in fiber content.

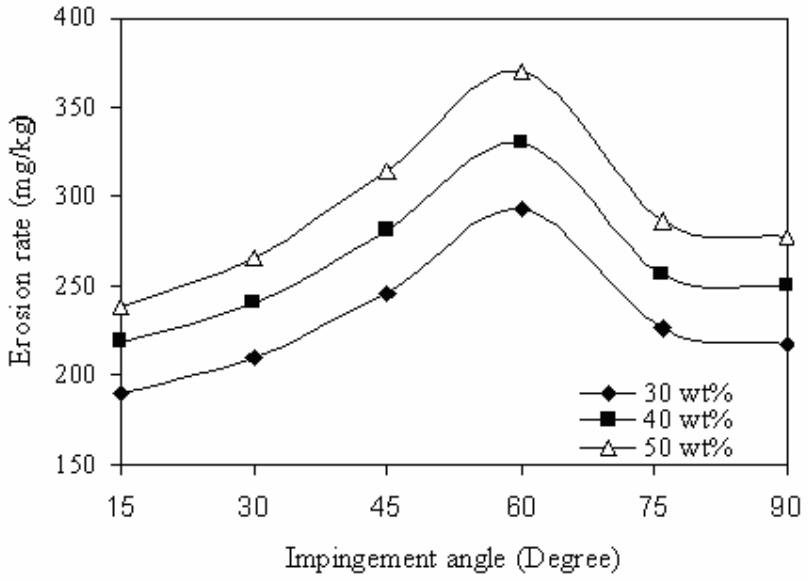

Figure 6.1. Erosion rate vs. Angle of impingement for different fiber loading

6.2 Surface morphology

To identify the mode of material removal, the morphologies of eroded surfaces are studied under scanning electron microscope. Figure 6.2 presents the microstructure of the composite eroded at high impact velocity (58m/sec), at lower stand-off distance (120mm) and at an impingement angle of 60^0. It shows local removal of resin material from the impacted surface resulting in exposure of the fibers to the erodent flux. This micrograph also reveals that due to sand particle impact on fibers there is formation of transverse cracks that break these fibers. Figure 6.3 presents

the magnified microstructure of the composite eroded at the same conditions. Here the propagation of crack along transverse as well as longitudinal direction is well visualized. On comparing this micro-structure with that of the same composite eroded at a lower impact velocity (45m/sec), higher stand-off distance (240mm) and higher impingement angle (90^0), it can be seen that in the second case the breaking of glass fibers is more prominent (Figure 6.4). It appears that cracks have grown on the fibers giving rise to breaking of the fibers into small fragments. Further the cracks have been annihilated at the fiber matrix interface and seem not to have penetrated through the matrix. Change in impact angle from oblique to normal changes the topography of the damaged surface very significantly. Figure 6.4 shows the dominance of micro-chipping and micro-cracking phenomena. It can be seen that multiple cracks originate from the point of impact, intersect one another and form wear debris due to brittle fracture in the fiber body. After repetitive impacts, the debris in platelet form are removed and account for the measured wear loss. The occurrence of peak erosion rate at 60^0 impact is understandable. In this case, both abrasion and erosion processes play important roles. The sand particles after impacting, slide on the surface and abrade while dropping down. The wear and subsequently the damage are therefore more than that in the case of normal impact. Marks of micro-ploughing on the ductile polyester matrix region seen in Figure 6.3 support this argument.

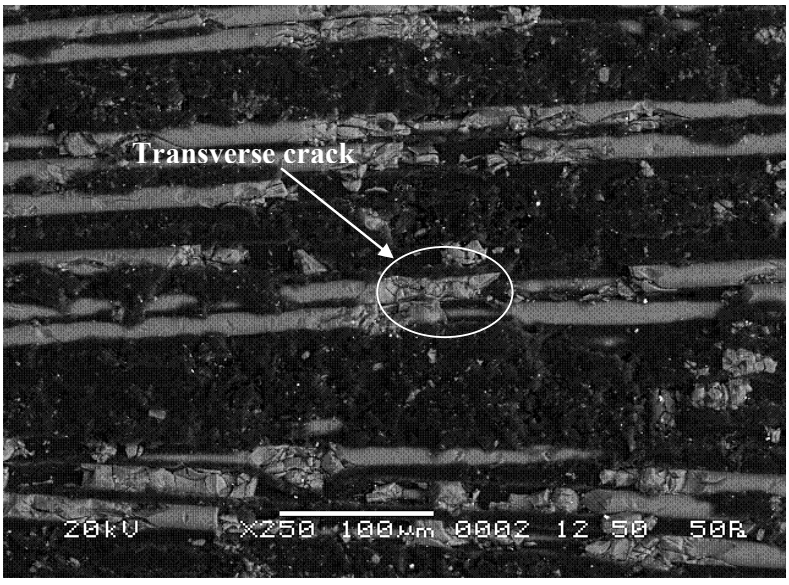

Figure 6.2.SEM micrograph of GF Polymer composite eroded surface (impact velocity 58m/sec, fiber loading 50 wt%, S.O.D 120mm, impingement angle 60^0 and erodent size 300µm).

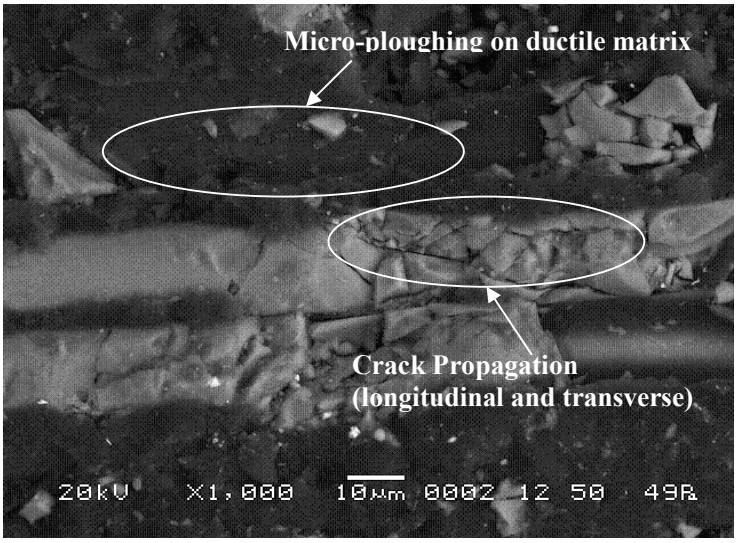

Figure 6.3. SEM micrograph of GF Polymer composite eroded surface (impact velocity 58m/sec, fiber loading 50%, S.O.D 120mm, impingement angle 60^0 and erodent size 300µm)

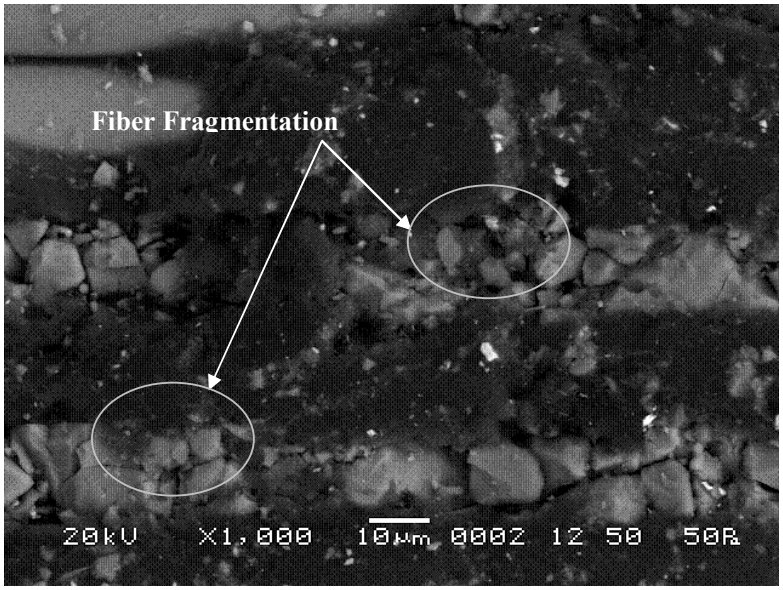

Figure 6.4. SEM micrograph of GF Polymer composite eroded surface (impact velocity 45m/sec, fiber loading 50%, S.O.D 240mm, impingement angle 90^0 and erodent size 300µm).

A possible reason for the semi-ductile erosion behaviour exhibited by the polyester based composites in the present investigation is that the glass fibers used as reinforcements for polyester matrix are a typical brittle material. Their erosion is caused mostly by damage mechanism such as micro-cracking. Such damage is supposed to increase with the increase of kinetic energy loss of the impinging sand

particles. According to Hutchings et al. [257], kinetic energy loss is a maximum at normal impact, where erosion rates are highest for brittle materials. In the present study also, the peak erosion rate shifts to a larger value of impingement angle (60^0) and it is clearly due to the brittle nature of glass fibers. So although polyester is a ductile material , the presence of fibers makes the composite relatively more sensitive to impact energy which increases when the impact mode pattern changes from tangential ($\alpha = 0^0$) to normal ($\alpha = 90^0$) . This explains the semi-ductile nature of the glass-polyester composites with respect to solid particle erosion.

From Table 6.1, the overall mean for the S/N ratio of the erosion rate is found to be **-** 48.97 db. Figure 6.5 shows graphically the effect of the six control factors on erosion rate. The analysis was made using the popular software specifically used for design of experiment applications known as MINITAB 14. Before any attempt is made to use this simple model as a predictor for the measures of performance, the possible interactions between the control factors must be considered. Thus factorial design incorporates a simple means of testing for the presence of the interaction effects. Analysis of the result leads to the conclusion that factor combination of A_1(A= impact velocity 32 m/sec), B_2 (B = Fiber content 40%), C_1 (C = Stand-off Distance 120mm), D_1 (D=Impingement angle 30^0)and E_2 (E = Erodent size 500 μm) gives minimum erosion rate is shown in Figure 6.5.

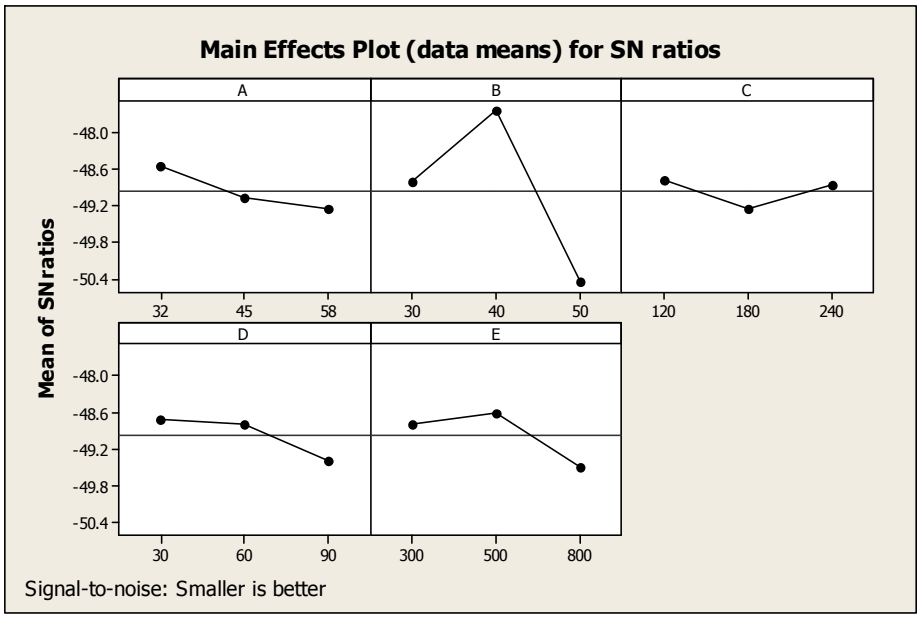

Figure 6.5. Effect of control factors on erosion rate (for unfilled glass polyester composites)

In the main effect of control factors on erosion rate plot if the line for a particular factor is near horizontal, then the factor has no significant effect. On the other hand, a factor for which the line has the highest inclination will have the most significant effect. It is very much clear from the Figure 6.5 that factor B (Fiber loading), factor E (Erodent size) and factor D (impingement angle) are the most significant factor while factor A (impact velocity) and factor C (stand-off distance) have relatively less significant influence. As far as the interaction graphs are concerned, estimating an interaction means determining the non-parallelism of factor effects. Thus, if the lines on the interaction graphs are non-parallel, interaction occurs and if the lines cross, strong interaction occurs between factors.

Table 6.1. Experimental design using L_{27} orthogonal array (for unfilled glass polyester composites)

Sl. No	Impact Velocity(A) (m/sec)	Fiber loading(B) (%)	Stand-off Distance(C) (mm)	Impingement angle(D) (Degree)	Erodent size (E) (μm)	Erosion rate (Er) mg/kg	S/N Ratio (db)
1	32	30	120	30	300	309.83	-49.8225
2	32	30	180	60	500	315.25	-49.9731
3	32	30	240	90	800	305.19	-49.6914
4	32	40	120	60	500	186.07	-45.3936
5	32	40	180	90	800	272.79	-48.7166
6	32	40	240	30	300	230.96	-47.2707
7	32	50	120	90	800	287.69	-49.1785
8	32	50	180	30	300	279.85	-48.9385
9	32	50	240	60	500	255.25	-48.1393
10	45	30	120	60	800	288.86	-49.2137
11	45	30	180	90	300	249.80	-47.9518
12	45	30	240	30	500	255.25	-48.1393
13	45	40	120	90	300	239.76	-47.5955
14	45	40	180	30	500	249.18	-47.9304
15	45	40	240	60	800	298.23	-49.4910
16	45	50	120	30	500	261.17	-48.3385
17	45	50	180	60	800	364.31	-51.2294
18	45	50	240	90	300	389.94	-51.8201
19	58	30	120	90	500	315.10	-49.9690
20	58	30	180	30	800	245.19	-47.7901
21	58	30	240	60	300	219.89	-46.8441
22	58	40	120	30	800	261.27	-48.3418
23	58	40	180	60	300	239.76	-47.5955
24	58	40	240	90	500	210.66	-46.4716
25	58	50	120	60	300	369.47	-51.3516
26	58	50	180	90	500	452.81	-53.1183
27	58	50	240	30	800	391.45	-51.8535

From Fig. 6.6, it can be seen that there is strong interaction between the parameters A and B while there is moderate interaction between the parameters A and C, and between B and C as shown in Figures 6.7 and 6.8. Thus from the present analysis it is clear that B (fiber content) and E (erodent size) are the most influencing factors for wear characteristics of glass fiber reinforced polyester composites.

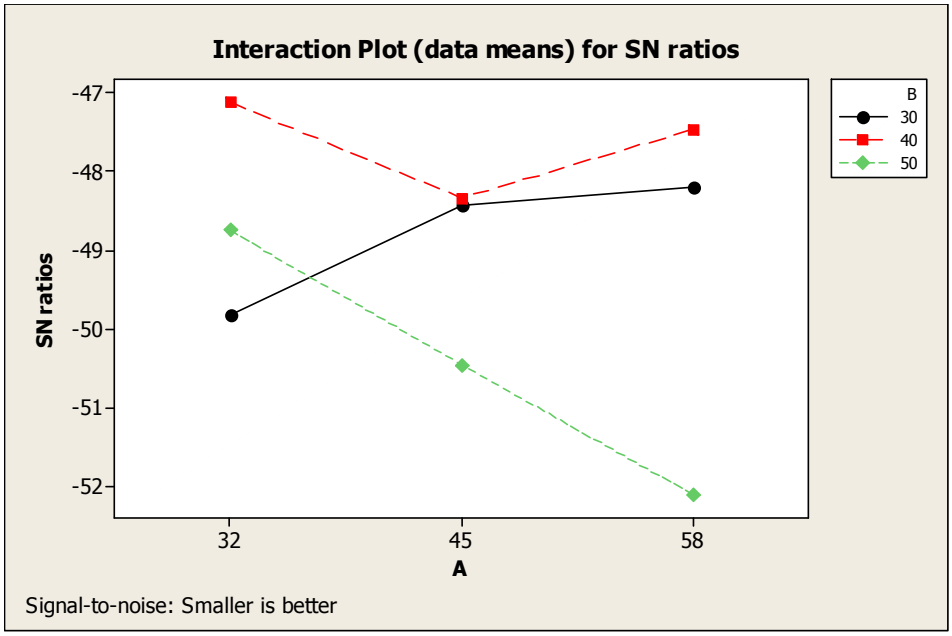

Figure 6.6. Interaction graph between A×B for erosion rate (for unfilled glass polyester composites)

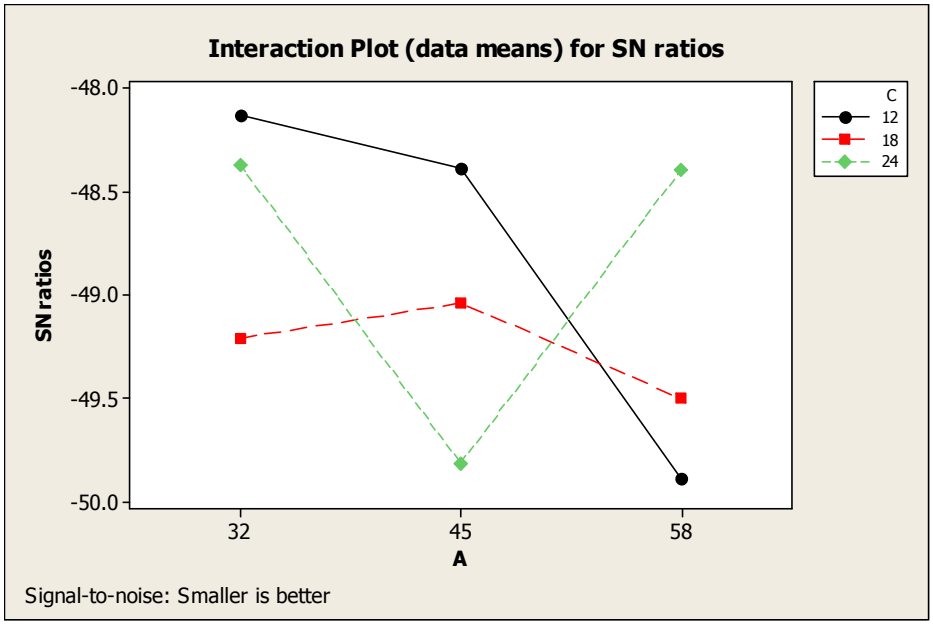

Figure 6.7. Interaction graph between A×C for erosion rate (for unfilled glass polyester composites)

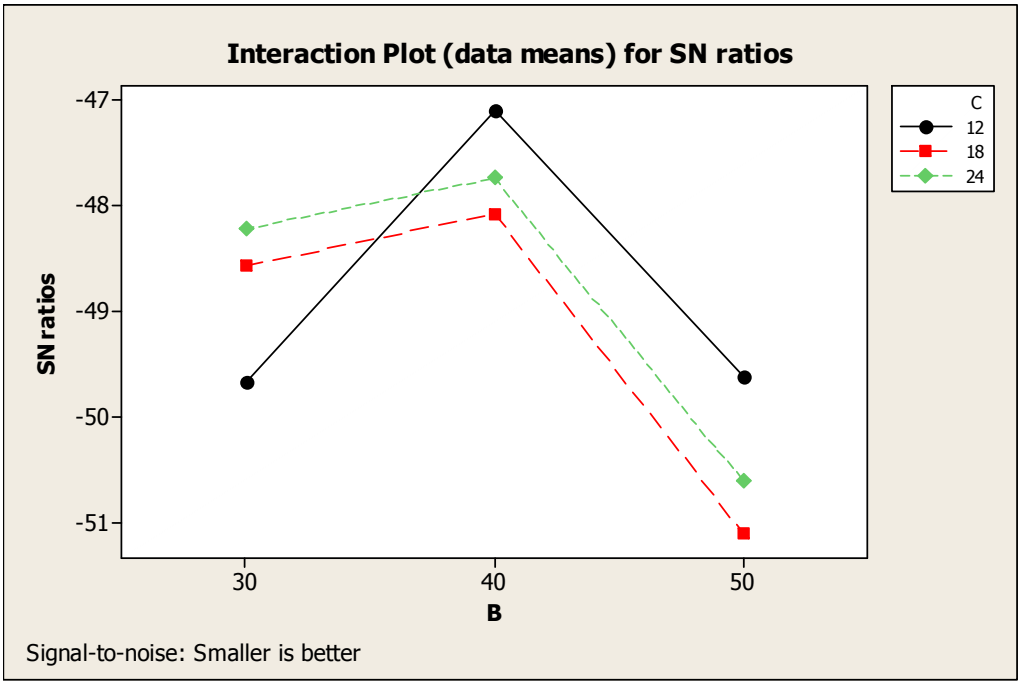

Figure 6.8. Interaction graph between B × C for erosion rate (for unfilled glass polyester composites)

Similar observation is made in the surface plots of erosion rate with significant control factors [Figures 6.9a, 6.9b, and 6.9c]. From this analysis it is concluded that among all the factors, stand-off distance is most insignificant while impact velocity has relatively less significance compared to the other remaining factors. Figure (6.9a) shows the significant interaction between impact velocity and fiber loading for minimization of erosion rate. The main effects plot for S/N ratio for erosion rate indicates the selection of medium fiber loading (40%), lower impact velocity (32m/sec) and lower stand-off distance (120mm) results in the best combination to get minimum erosion rate, within the selected range of experiment. Using Figure 6.5 for S/N ratio, the optimum combination of significant control factors is A_1 (A= impact velocity 32 m/sec), B_2 (B = Fiber content 40%) and C_1 (C = Stand-off Distance 120mm). Surface response plot Figure 6.9d indicates that minimum erosion rate can be achieved in composite with medium fiber loading eroded at smaller impact velocity region.

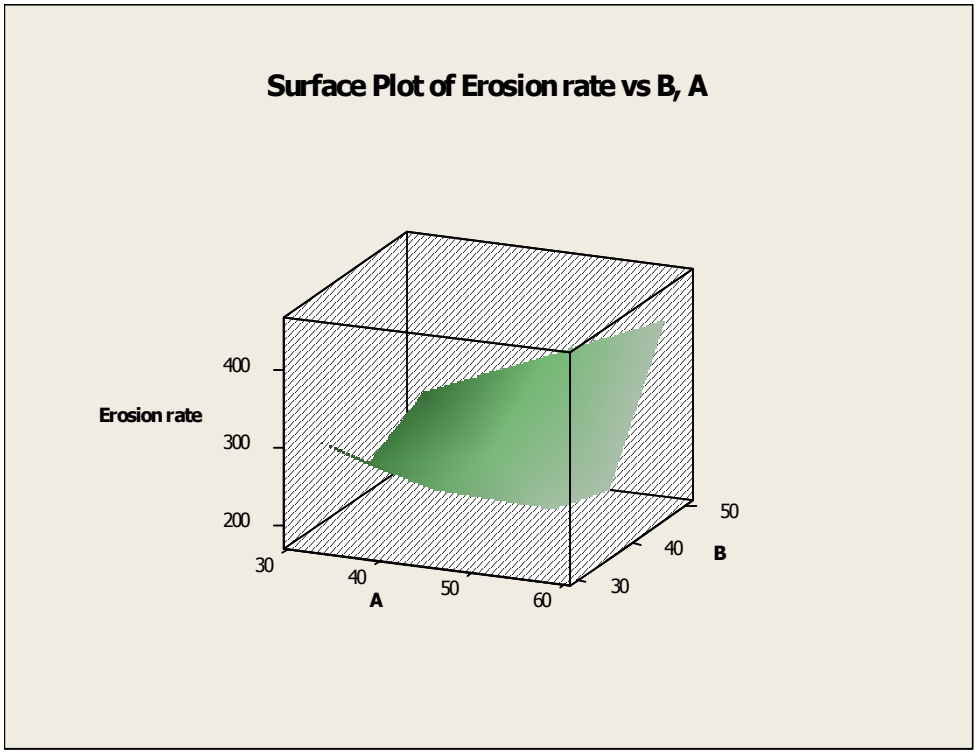

Figure 6.9a. Surface plot of erosion rate vs. A×B interaction (for unfilled glass polyester composites)

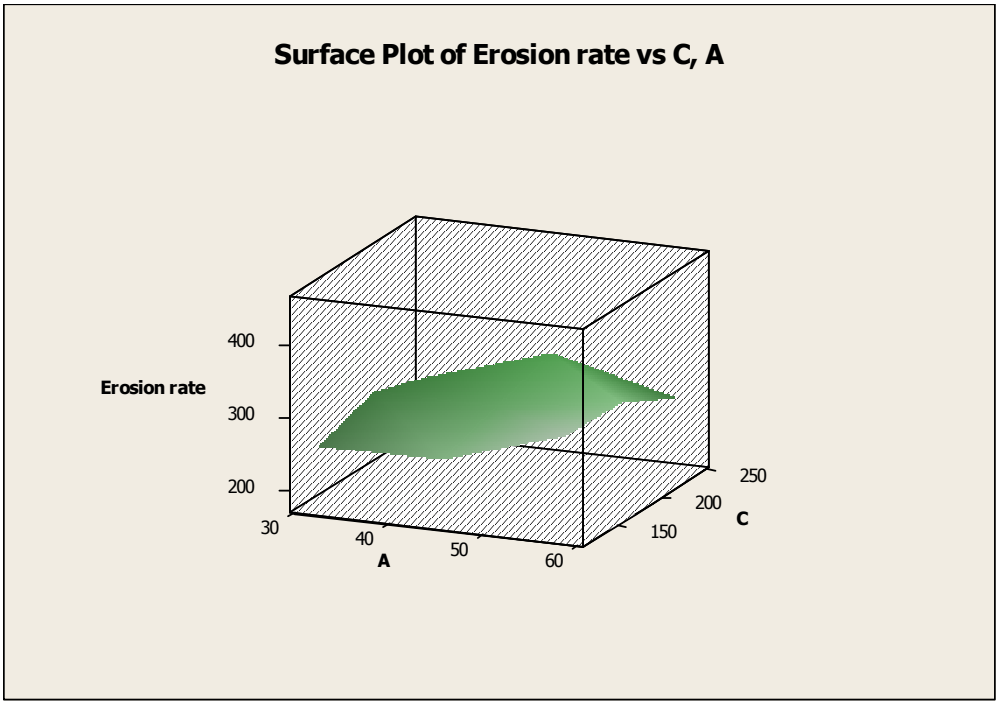

Figure 6.9b. Surface plot of erosion rate vs. A×C interaction (for unfilled glass polyester composites)

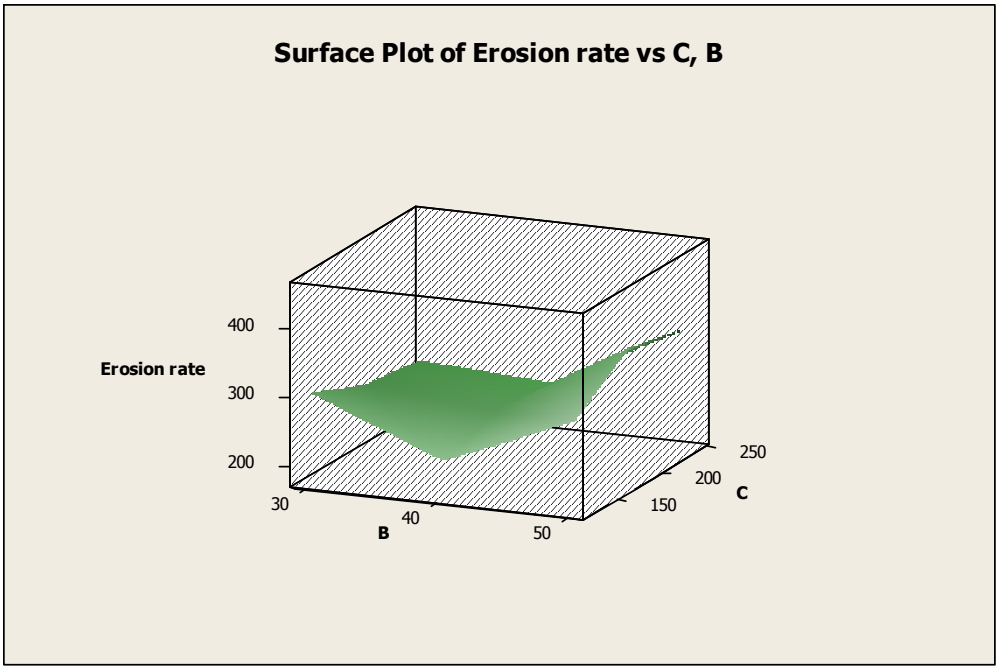

Figure 6.9c. Surface plot of erosion rate vs. B × C interaction (for unfilled glass polyester composites)

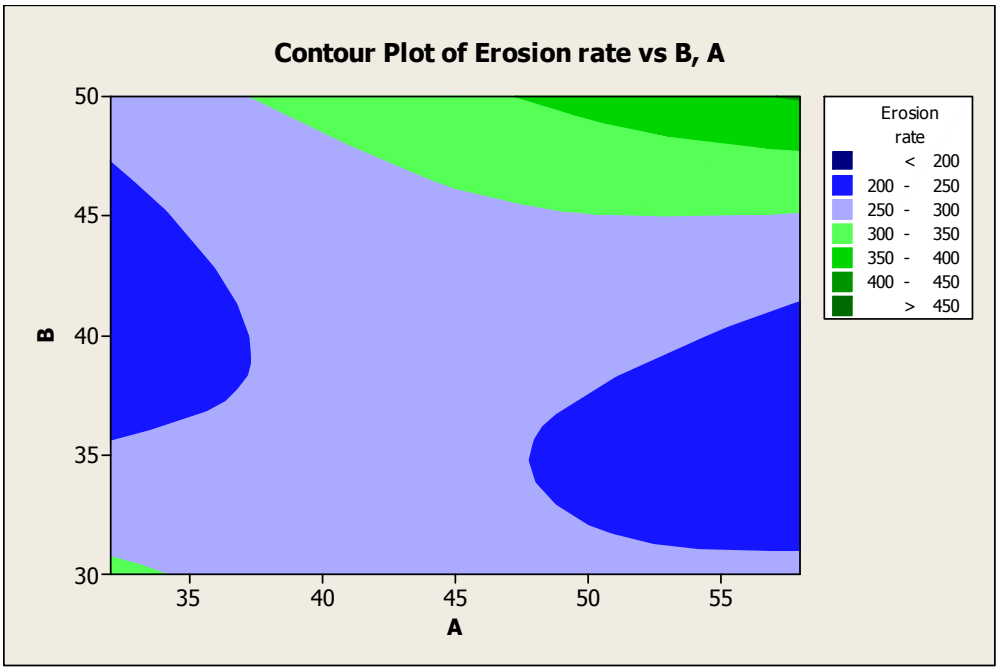

Figure 6.9d. Surface response plot for fiber loading × impact velocity interaction

6.3 Erosion efficiency

The hardness alone is unable to provide sufficient correlation with erosion rate, largely because it determines only the volume displaced by each impact and not

really the volume eroded. Thus a parameter which will reflect the efficiency with which the volume that is displaced is removed should be combined with hardness to obtain a better correlation. The erosion efficiency is obviously one such parameter. In the case of a stream of particles impacting a surface normally (i.e. at $\alpha=90^0$), erosion efficiency (η_{normal}) defined by Sundararajan et. al. [254] is given as

$$\eta_{normal} = \frac{2ErHv}{\rho V^2} \tag{6.1}$$

But considering impact of erodent at any angle α to the surface, the actual erosion efficiency (η) can be obtained by modifying Eq. (6.1) as

$$\eta = \frac{2ErHv}{\rho V^2 Sin^2\alpha} \tag{6.2}$$

where E_r the erosion rate (kg/kg), H_v the hardness of target material (Pa), ρ the density of the erodent (kg/m^3) and V the impact velocity (m/sec).

The values of erosion efficiencies of these composites (A_1, B_1 and C_1) calculated using Eq. (6.2) are summarized in Table 6.2 along with their hardness values and operating conditions. It clearly shows that erosion efficiency is not exclusively a material property; but also depends on other operational variables such as impingement angle and impact velocity. The erosion efficiencies (Table 6.2) of these composites under normal impact (η_{normal}) vary from 3 to 6%, 6-9% and 9-12% for impact velocities 58m/sec, 45m/sec and 32m/sec respectively. The value of η for a particular impact velocity under oblique impact can be obtained simply by multiplying a factor $1/Sin^2\alpha$ with $\eta_{normal.}$ Similar observation on velocity dependence of erosion efficiency has previously been reported by few investigators [108].

Table 6.2. Erosion efficiency of GF-reinforced polyester resin

Sl. No.	Impact Velocity (V) m/sec	Density of eroding material (ρ) kg/m^3	Hardness of eroding material (Hv) MPa	Erosion rate (Er) mg/kg	Erosion efficiency (η)
1	32	1738	32	309.83	43.70689
2	32	1738	32	315.25	12.83002
3	32	1738	32	305.19	10.76308
4	32	1874	34	186.07	7.462040
5	32	1874	34	272.79	9.479905
6	32	1874	34	230.96	32.10497
7	32	1932	39	287.69	11.12368
8	32	1932	39	279.85	43.28217
9	32	1932	39	255.25	11.38925
10	45	1738	32	288.86	5.944763
11	45	1738	32	249.80	4.454857
12	45	1738	32	255.25	18.20820
13	45	1874	34	239.76	4.213340
14	45	1874	34	249.18	17.51554
15	45	1874	34	298.23	6.047942
16	45	1932	39	261.17	20.42593
17	45	1932	39	364.31	8.220070
18	45	1932	39	389.94	7.624237
19	58	1738	32	315.10	3.382663
20	58	1738	32	245.19	10.52866
21	58	1738	32	219.89	2.724091
22	58	1874	34	261.27	11.05526
23	58	1874	34	239.76	2.926861
24	58	1874	34	210.66	2.228443
25	58	1932	39	369.47	5.018254
26	58	1932	39	452.81	5.329466
27	58	1932	39	391.45	18.42909

The theoretical erosion wear rates (E_{rth}) of the polyester-GF composites are calculated using Eq. 5.7. These values are compared with those obtained from experiments (E_{rexpt}) conducted under similar operating conditions. Usually seventy five percent data (patterns) is used for training and twenty five percent for testing. The parameters of three layer architecture of ANN model are set as input node = 5, output node = 1, hidden node = 12, learning rate = 0.01, momentum parameter = 0.03, number of epochs = 20, 0000 and a set of predicted output (E_{rANN}) is obtained. Table 6.3 presents a comparison among the theoretical, experimental and the ANN predicted results. The errors calculated with respect to the theoretical results are also given. It is observed that maximum error between theoretical and experimental wear rate is 0-10%, whereas same between ANN prediction and experimental wear rate is 0-14%. The error in case of ANN model can further be reduced if number of test patterns is increased. However, present study demonstrates application of ANN for prediction of wear rate in a complex process of solid particle erosion of polymer composites.

The magnitude of η can be used to characterize the nature and mechanism of erosion. For example, ideal microploughing involving just the displacement of the material from the crater without any fracture (and hence no erosion) will results in η=0. In contrast, if the material removal is by ideal micro-cutting, η=1.0 or 100%. If erosion occurs by lip or platelet formation and their fracture by repeated impact, as is usually the case in the case of ductile materials, the magnitude of η will be very low, i.e $\eta \leq 100\%$. In the case of brittle materials, erosion occurs usually by spalling and removal of large chunks of materials resulting from the interlinking of lateral or radial cracks and thus η can be expected to be even greater than 100% [249]. The erosion efficiencies of the composites under the present study indicate that at low impact speed the erosion response is semi-ductile (η=10-100%). On the other hand at relatively higher impact velocity the composites exhibit ductile ($\eta < 10\%$) erosion behavior [108].

Table 6.3. Comparison of theoretical, experimental and ANN results (for unfilled glass polyester composites)

Expt. No.	E_{rth} (mg/kg)	$E_{rexpt.}$ (mg/kg)	E_{rANN} (mg/kg)	Error (%) $\frac{E_{rth}-E_{r\exp t}}{E_{rth}}\times 100$	Error (%) $\frac{E_{rth}-E_{rANN}}{E_{rth}}\times 100$
1	314.84	309.83	340.33	1.5912	8.0945
2	321.69	315.25	308.95	2.0019	3.9601
3	304.17	305.19	291.93	0.3353	4.0226
4	201.98	186.07	176.31	7.8765	12.711
5	271.78	272.79	295.34	0.3716	8.6687
6	238.45	230.96	269.54	3.1411	13.038
7	286.69	287.69	251.33	0.3488	12.332
8	296.75	279.85	258.51	5.6950	12.886
9	276.81	255.25	292.07	7.7887	5.5125
10	309.29	288.86	289.53	6.6054	6.3882
11	248.76	249.80	267.10	0.4180	7.3727
12	266.73	255.25	238.76	4.3039	10.485
13	238.76	239.76	233.65	0.4188	2.1385
14	257.34	249.18	251.49	3.1693	2.2722
15	319.46	298.23	321.04	6.6455	0.4947
16	289.38	261.17	293.27	9.7484	1.3438
17	378.38	364.31	327.33	3.7184	13.491
18	387.95	389.94	351.06	0.5155	9.5067
19	314.14	315.10	272.29	0.3056	13.321
20	259.21	245.19	248.82	5.4087	4.0069
21	227.76	219.89	206.00	3.4553	9.5529
22	281.37	261.27	318.62	7.1436	13.239
23	248.75	239.76	277.37	3.6140	12.312
24	209.66	210.66	229.48	0.4769	9.4519
25	387.34	369.47	349.40	4.6135	9.7947
26	451.81	452.81	391.23	0.2213	13.408
27	405.27	391.45	363.25	3.4101	10.369

6.4 ANOVA and the effects of factors

In order to understand a concrete visualization of impact of various factors and their interactions, it is desirable to develop analysis of variance (ANOVA) table to find out the order of significant factors as well as interactions. Table 6.4 shows the results of the ANOVA with the erosion rate. This analysis was undertaken for a level of confidence of significance of 5 %. The last column of the table indicates that the main effects are highly significant (all have very small p-values).

Table 6.4. ANOVA table for erosion rate (without particulate fillers)

Source	DF	Seq SS	Adj SS	Adj MS	F	P
A	2	2.3056	2.3056	1.1528	1.88	0.265
B	2	35.4646	35.4646	17.7323	28.95	0.004
C	2	1.0737	1.0737	0.5369	0.88	0.483
D	2	2.4297	2.4297	1.2149	1.98	0.252
E	2	3.9765	3.9765	1.9882	3.25	0.145
A*B	4	21.5781	21.5781	5.3945	8.81	0.029
A*C	4	7.5740	7.5740	1.8935	3.09	0.150
B*C	4	7.1630	7.1630	1.7908	2.92	0.162
Error	4	2.4498	2.4498	0.6125		
Total	26	84.0150				

From Table 6.4, one can observe that the fiber loading (p=0.004), erodent size (p=0.145), impingement angle (p=0.252) and impact velocity (p=0.265) have great influence on erosion rate. The interaction of impact velocity $\times$ fiber loading (p=0.029) shows significance of contribution on the erosion rate and the factor stand-off distance (p=0.493) and impact velocity $\times$ stand-off distance (p=0.150), fiber loading $\times$ stand-off distance (p=0.162) present less significance of contribution on erosion rate.

6.5 Confirmation experiment

The confirmation experiment is the final test in the design of experiment process. The purpose of the confirmation experiment is to validate the conclusions drawn during the analysis phase. The confirmation experiment is performed by conducting a new set of factor settings $A_2B_3D_2E_3$ to predict the erosion rate. The estimated S/N ratio for erosion rate can be calculated with the help of following prediction equation:

$$\hat{\eta}_1 = \overline{T} + (\overline{A}_2 - \overline{T}) + (\overline{B}_3 - \overline{T}) + [(\overline{A}_2\overline{B}_3 - \overline{T}) - (\overline{A}_2 - \overline{T}) - (\overline{B}_3 - \overline{T})] + \left(\overline{D}_2 - \overline{T}\right) + (\overline{E}_3 - \overline{T}) \quad (6.3)$$

$\overline{\eta}_1$ Predicted average

$\overline{T}$ Overall experimental average

$\overline{A}_2, \overline{B}_3, \overline{D}_2 \; and \; \overline{E}_3$ Mean response for factors and interactions at designated levels.

By combining like terms, the equation reduces to

$$\overline{\eta}_1 = \overline{A}_2\overline{B}_3 + \overline{D}_2 + \overline{E}_3 - 2\overline{T} \quad (6.4)$$

A new combination of factor levels A_2, B_3, D_2 and E_3 is used to predict deposition rate through prediction equation and it is found to be $\overline{\eta}_1 = -50.8283\, dB.$ For each performance measure, an experiment was conducted for a different factors combination and compared with the result obtained from the predictive equation as shown in Table 6.5.

Table 6.5. Results of the confirmation experiments for erosion rate (without particulate fillers)

	Optimal control parameters	
	Prediction	Experimental
Level	$A_2B_3D_2E_3$	$A_2B_3D_2E_3$
S/N ratio for Erosion rate (db)	-50.8283	-49.5677

The resulting model seems to be capable of predicting erosion rate to a reasonable accuracy. An error of 2.48 % for the S/N ratio of erosion rate is observed. However, the error can be further reduced if the number of measurements is increased. This validates the development of the mathematical model for predicting the measures of performance based on knowledge of the input parameters.

6.6 Factor settings for minimum erosion rate

In this study, an attempt is made to derive optimal settings of the control factors for minimization of erosion rate. The single-objective optimization requires quantitative determination of the relationship between erosion rates with combination of control factors. In order to express, erosion rate in terms of mathematical model in the following form is suggested.

$$Er = K_0 + K_1 \times A + K_2 \times B + K_3 \times D + K_4 \times E + K_5 \times A \times B \quad (6.5)$$

Here, E_r is the performance output terms and K_i (i = 0, 1……..5) are the model constants. The constant are calculated using non-linear regression analysis with the help of **SYSTAT 7.0** software and the following relations are obtained.

$$E_r = 1.521 - 1.633A - 1.387B + 0.088D + 0.078E + 1.221AB$$

r^2=0.98 (6.6)

The correctness of the calculated constants is confirmed as high correlation coefficients (r^2) in the tune of 0.98 are obtained for Eq. (6.6) and therefore, the models are quite suitable to use for further analysis. Here, the resultant objective function to be maximized is given as:

Maximize Z = 1/ f (6.7)

f Normalized function for erosion rate

Subjected to constraints:

$A_{min} \leq A \leq A_{max}$ (6.8)

$B_{min} \leq B \leq B_{max}$ (6.9)

$D_{min} \leq D \leq D_{max}$ (6.10)

$E_{min} \leq E \leq E_{max}$ (6.11)

the min. and max. in Eqs.6.8-6.11 shows the lowest and highest control factors settings (control factors) used in this study (Table 3.4).

Genetic algorithm (GA) is used to obtain the optimum value for single-objective outputs to optimize the single-objective function. The computational algorithm is implemented in Turbo C^{++} and run on an IBM Pentium IV machine. Genetic algorithms (GAs) are mathematical optimization techniques that simulate a natural evolution process. They are based on the Darwinian Theory, in which the fittest species survives and propagate while the less successful tend to disappear. Genetic algorithm mainly depends on three types of operator's viz., reproduction, crossover and mutation. Reproduction is accomplished by copying the best individuals from one generation to the next, what is often called an elitist strategy. The best solution is monotonically improving from one generation to the next. The selected parents are submitted to the crossover operator to produce one or two children. The crossover is carried out with an assigned probability, which is generally rather high. If a number randomly sampled is inferior to the probability, the crossover is performed. The

genetic mutation introduces diversity in the population by an occasional random replacement of the individuals. The mutation is performed based on an assigned probability. A random number is used to determine if a new individual will be produced to substitute the one generated by crossover. The mutation procedure consists of replacing one of the decision variable values of an individual while keeping the remaining variables unchanged. The replaced variable is randomly chosen and its new value is calculated by randomly sampling within its specific range. In genetic optimization, population size, probability of crossover and mutation are set at 50, 75 %, and 5 % respectively for all the cases. Number of generation is varied till the output is converted.

Table 6.6. Optimum conditions for performance output (without particulate fillers)

Control factors and Performance characteristics	Optimum conditions
A: Impact velocity (m/sec)	33.15
B: Fiber loading (%)	41.02
D: Impingement angle (degree)	59.45
E: Erodent size (μm)	500.0
Erosion rate (mg/kg)	364.72

Table 6.6 shows the optimum conditions of the control factors with optimum performance out put gives a better combination of set of input control factors. The pattern of convergence of performance output with number of generations is shown in Figure 6.10.

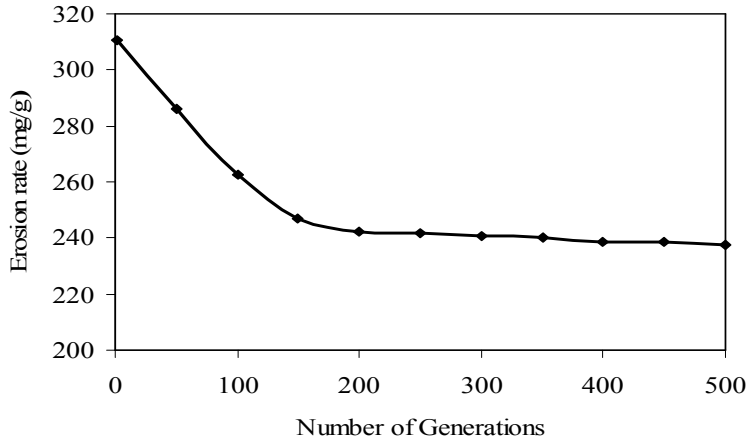

Figure 6.10. Convergence graph (for unfilled glass polyester composites)

Chapter summary:

This chapter has provided:

- The analytical and experimental investigation into the erosion behavior of glass fiber reinforced polyester composites leading to the following major conclusions:

1. Solid particle erosion characteristics of these composites can be successfully analyzed using Taguchi experimental design scheme.
2. The results indicate that erodent size, fiber loading, impingement angle and impact velocity are the significant factors in a declining sequence affecting the erosion wear rate.
3. The composites exhibit semi-ductile erosion characteristics with the peak erosion wear occurring at 60^0 impingement angle.
4. The erosion efficiency (η) values obtained experimentally also suggest that the glass fiber reinforced polyester composites exhibit semi-ductile erosion response (η =10-60%) for low impact velocities. However, for relatively high impact velocity, they present a ductile erosion response (η < 10%).

The next chapter presents a detailed study on the erosion wear characteristics of a series of particulate filled glass polyester composites.

****

Chapter 7

Study on Erosion Wear Characteristics of Particulate Filled Glass-Fiber Polyester Composites

Chapter 7

STUDY ON EROSION WEAR CHARACTERISTICS OF PARTICULATE FILLED GLASS-FIBER POLYESTER COMPOSITES

Introduction

This chapter reports a detailed study on the effect of particulate fillers on the solid particle erosion characteristics of glass-polyester composites. The test results of erosion trials carried out on the glass-polyester hybrid composites (C_1-C_9) are presented and compared with the calculated values obtained from the theoretical model proposed in chapter-5. Besides, the critical analysis of the experimental results using Taguchi model and the artificial neural network (ANN) is also presented followed by the determination of optimal factor settings using genetic algorithm (GA). The relative performance of non-conventional fillers (industrial wastes such as: flyash and cement by-pass dust) against the conventional ceramic (alumina and silicon carbide) fillers is discussed.

7.1 Steady state erosion

The variation of erosion wear rate of the composites with angle of impingement is studied keeping all other parameters at fixed levels. Figure 7.1 presents this variation for composites C_2 (Polyester +50wt% glass fiber + 10wt% flyash), C_4 (Polyester +50wt% glass fiber +10wt% Alumina), C_6 (Polyester +50wt% glass fiber +10wt% SiC) and C_8 (Polyester +50wt% glass fiber +10wt% CBPD) with filler content 10 wt% and compares with that of the unfilled composite C_1(Polyester +50wt% glass fiber). Similarly, the dependence of erosion rate on angle of impact for composites C_3 (Polyester +50wt% glass fiber +20wt% flyash), C_5 (Polyester +50wt% glass fiber +20wt% Alumina), C_7 (Polyester +50wt% glass fiber +20wt% SiC) and C_9 (Polyester +50wt% glass fiber +20wt% CBPD) with filler content 20 wt% are shown in Figure 7.2.

It is clear from these figures that in solid particle erosion, the rate of material loss of glass polyester composites reduces significantly with the addition of hard particulate fillers into the matrix. This improvement in the wear resistance depends on the type and content of filler. The composites with alumina filling show better erosion resistance than the composites filled with other three fillers.

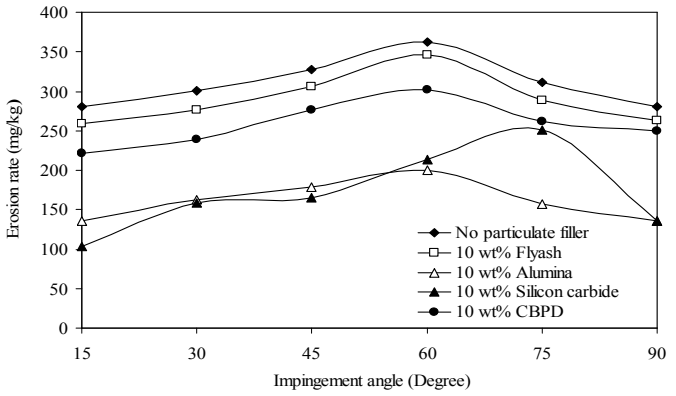

Figure 7.1. Erosion rate vs. angle of impingement for different fillers.

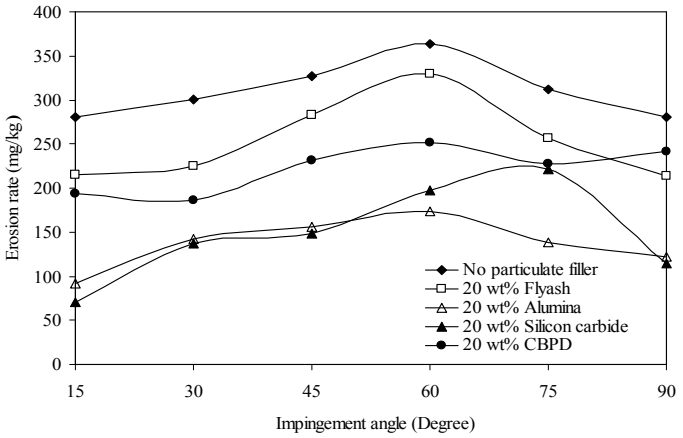

Figure 7.2. Erosion rate vs. angle of impingement for different fillers.

The reduction in material loss in these particle filled composites can be attributed to two reasons. One is the improvement in the bulk hardness of the composite with addition of these hard ceramic particles. Secondly, during the erosion process, the filler particles absorb a good part of the kinetic energy associated with the erodent. This results in less amount of energy being available to be absorbed by the matrix body and the reinforcing glass fiber phase. These two factors together lead to enhancement of erosion wear resistance of the composites.

The behaviour of ductile materials like polymers is characterized by maximum erosion rate at low impingement angles (15^0 to 30^0). Brittle materials, on the other show maximum erosion under normal impingement angle (90^0). Reinforced composites have been shown, however, to exhibit a semi-ductile behaviour with maximum erosion occurring in the angular range 45^0- 60^0 [258]. In the present work

also, the erosion results presented in Figures 7.1 and 7.2 show the peak erosion taking place at an impact angle of 60^0 for all the composites except for C_6 and C_7. For these two composites with SiC fillers, the maximum erosion has been recorded at an impact angle of 75^0. Thus, the composites under this study clearly exhibit semi-ductile erosion behaviour. The loss of ductility may be attributed partly to the presence of fillers and largely to the reinforcement of brittle glass fibers in all these composites. This can further be explained as follows: the erosion of fibers is mainly caused by damage mechanisms as micro-cracking or plastic deformation due to the impact of silica sand. Such damage is supposed to increase with the increase of kinetic energy loss. According to Hutchings et al. [257], kinetic energy loss is maximum at normal impact (90^0), where erosion rates are maximum for brittle materials. Hence, although the polymer matrix itself is ductile, the composites show semi-ductile or often semi-brittle erosion behaviour. Similar observations for polyphenylenesulphide (PPS) composites have been reported by Tamer et al. [259].

The variation of erosion wear loss confirms that the angle at which the stream of solid particles impinges the composite surface significantly influences the rate at which the material is removed. It further suggests that, this dependency is also influenced by the nature of the filler material. In fact, the angle of impact determines the relative magnitude of the two components of the impact velocity namely, the component normal to the surface and parallel to the surface. The normal component will determine how long the impact will last (i.e. contact time) and the load. The product of this contact time and the tangential (parallel) velocity component determines the amount of sliding that takes place. The tangential velocity component also provides a shear loading to the surface, which is in addition to the normal load that the normal velocity component causes. Hence as this angle changes the amount of sliding that takes place also changes the nature and magnitude of the stress system. Both of these aspects influence the way a composite wears out. This study therefore implies that composites with fillers of different type and content would exhibit different angular dependency.

7.2 Surface morphology

Erosion wear behaviour can be grouped as ductile and brittle categories although this grouping is not definitive. However, there is a dispute about this failure

classification as the erosive wear behaviour depends strongly on the experimental conditions and the composition of the target material [256]. To characterize the morphology of as-received and eroded surfaces and to identify the mode of material removal, the eroded samples are observed under scanning electron microscope. Figure 7.3a shows the surface of the flyash filled composite C_2 eroded at an impact angle of 60^0. The erodent particle size, stand-off distance and the impact velocity are set at 300 μm, 240 mm and 58 m/sec respectively. In this micrograph, the crack formation and propagation are clearly visible along with groove formation, which implies the removal of bulk mass of materials from the surface. Figure 7.3b presents the micrograph of the same composite surface when eroded with bigger erodent (500 μm), lower stand-off distance (180 mm) and at lower impact velocity (32 m/sec). Here, a relatively small fraction of the material is seen to be removed from the surface although formation of large amount of grooves is visible. However, crack formation and propagation is not seen. This may be due to either large erodent size which do not help in crack formation or lower impact velocity that has not favoured the crack propagation.

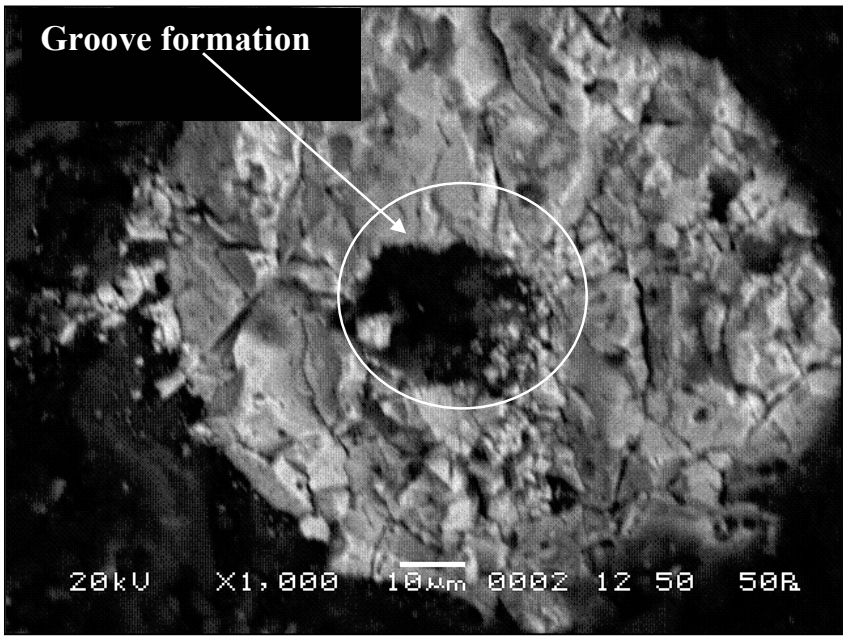

Figure 7.3a. Scanning electron micrograph of eroded composite surface (impact velocity 58m/sec, flyash content 20 %, S.O.D 240mm, impingement angle 60^0 and erodent size 300μm).

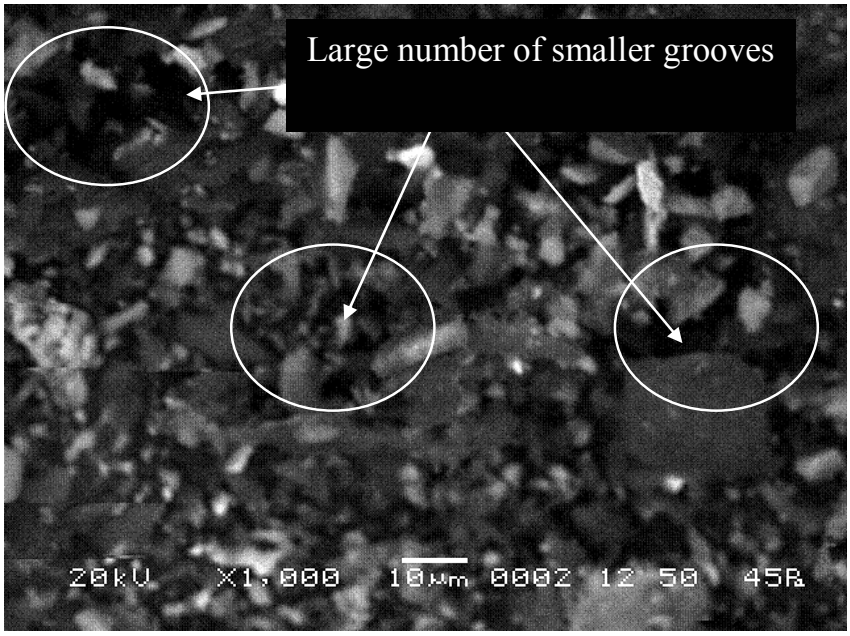

Figure 7.3b. Scanning electron micrograph of eroded composite surface (impact velocity 45m/sec, flyash content 10 %, S.O.D 180mm, impingement angle 30^0 and erodent size 500µm).

Figure 7.4a shows a portion of the alumina filled composite C_5 surface before erosion occurred. Scattered alumina particles are observed on the upper surface. As seen in the micrograph, the distribution of alumina particles is reasonably uniform although at places, these are seen to have formed small and big clusters. Figure 7.4b shows the micrograph of surface eroded at an impingement angle of 60^0 and an impact velocity of 45 m/sec. A small portion of a fiber exposed during the sand erosion is noticed. The matrix covering the fiber seems to be chipped off and the crater thus formed shows the fiber body which is almost intact. Repeated impact of the erodent has caused roughening of the surface. Erosion along the fibers and clean removal of the matrix at the interface is observed in the magnified image given alongside. Figure 7.4c clearly shows the crater formation due to penetration of hard silica sand particles onto the surface and cause material removal mostly from the matrix regime. Small cracks and multiple fractures are also distinctly shown in this micrograph.

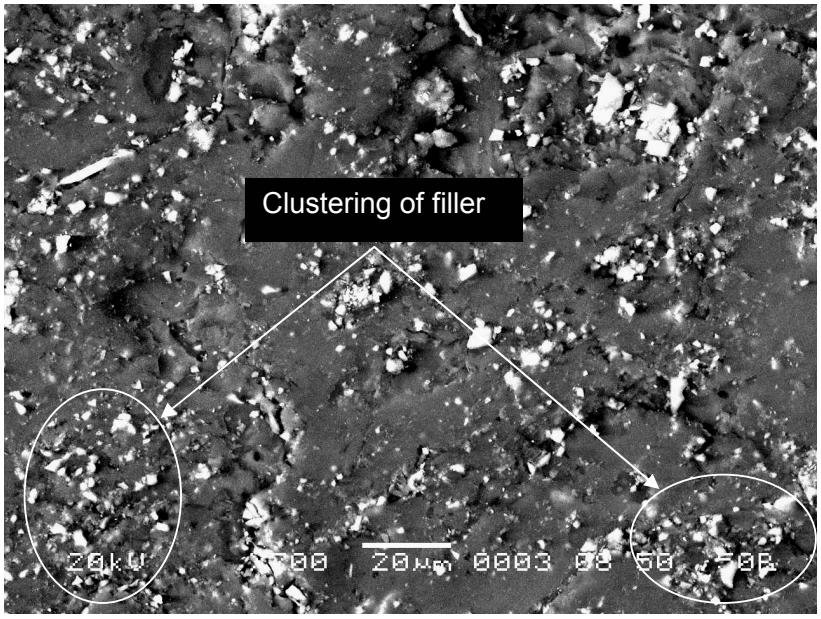

Figure 7.4a. Scanning electron micrograph of uneroded composite surface (Alumina content 20 %).

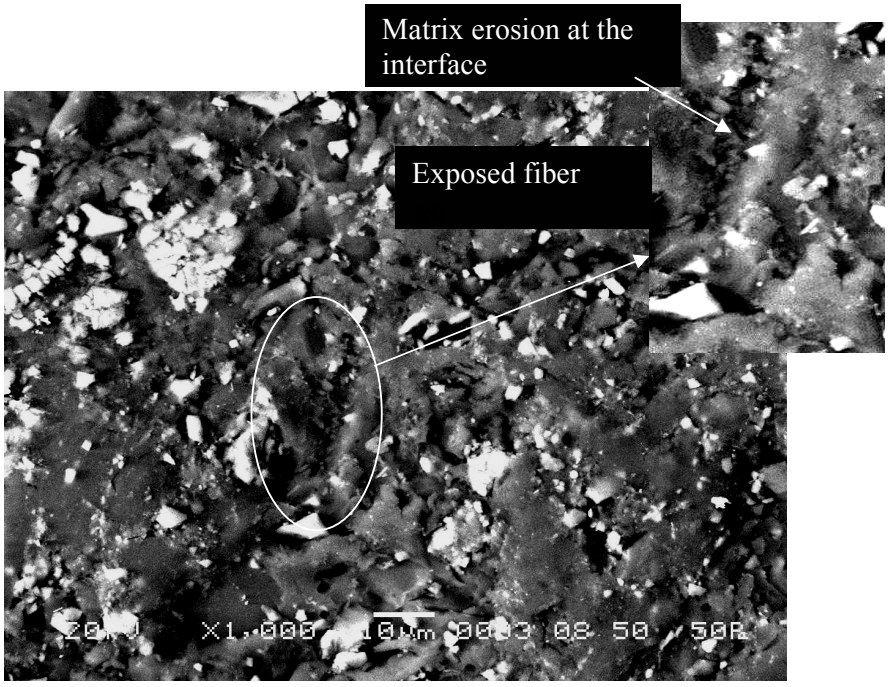

Figure 7.4b. Scanning electron micrograph of eroded composite surface (impact velocity 45m/sec, alumina content 20 %, S.O.D 180 mm, impingement angle 60^0 and erodent size 800μm).

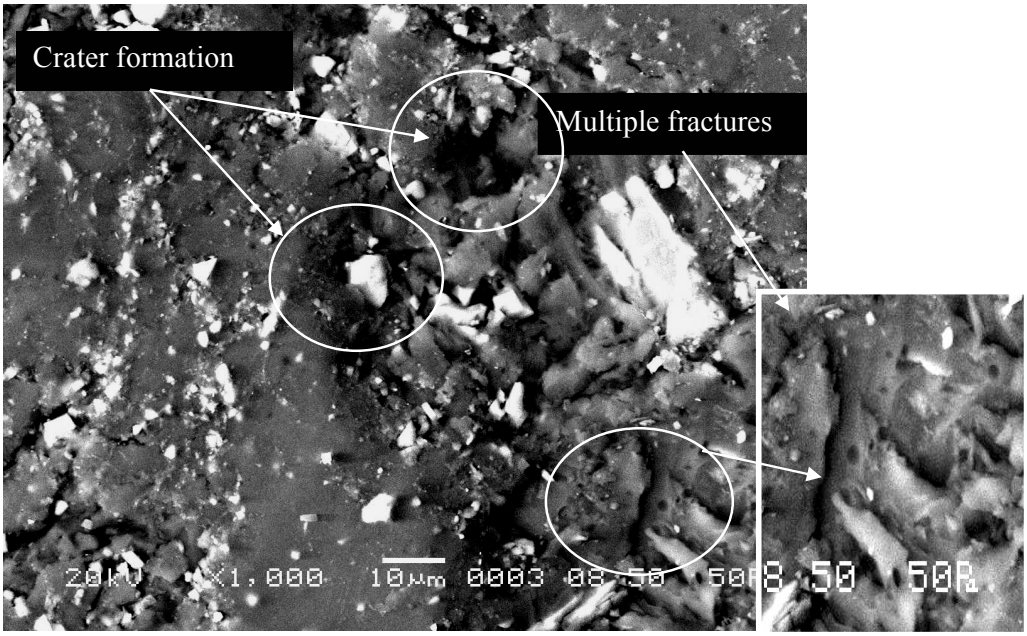

Figure 7.4c**.** Scanning electron micrograph of eroded composite surface (impact velocity 58 m/sec, alumina content 20 %, S.O.D 180 mm, impingement angle 60^0 and erodent size 800µm).

From SEM observations of the eroded surfaces of SiC filled glass polyester composites it appears that the composites exhibit several stages of erosion and material removal process. Figure 7.5a shows the plastic flow of matrix material along the erosion direction for the composite eroded at lower impact angle ($\alpha = 30^0$). When impacting at such low angle, the hard erodent particles penetrate the surface and cause material removal mostly by micro-ploughing. It is possible to investigate the particle flow direction easily from the wear trace on the matrix body which is indicated by an arrow in this micrograph. The higher impact speed of 58 m/sec (Figure 7.5b) makes the sample surface remarkably rougher compared to that in case of lower impact speed of 32 m/sec (Figure 7.5a). Subsequently the material removal becomes faster. The wear trace is distinctly visible and the protrusion of fibers beneath the matrix layer is seen. Figure 7.5c shows a portion of the composite surface eroded at an impact angle of 75^0. This is the case of maximum material loss due to impact erosion in case of SiC filling. The matrix covering the fiber seems to be chipped off due to repeated impact of hard silica sand particles. A crater thus formed shows an array of almost intact fibers. After the local removal of matrix this array of fibers is exposed to erosive environment. Figure 7.5d shows fragments of SiC particles and the fibers which are result of continued sand impact. The broken

fiber and carbide filler fragments are mixed with the matrix micro-flake debris and the damage of the composite is characterized by separation and detachment of this debris.

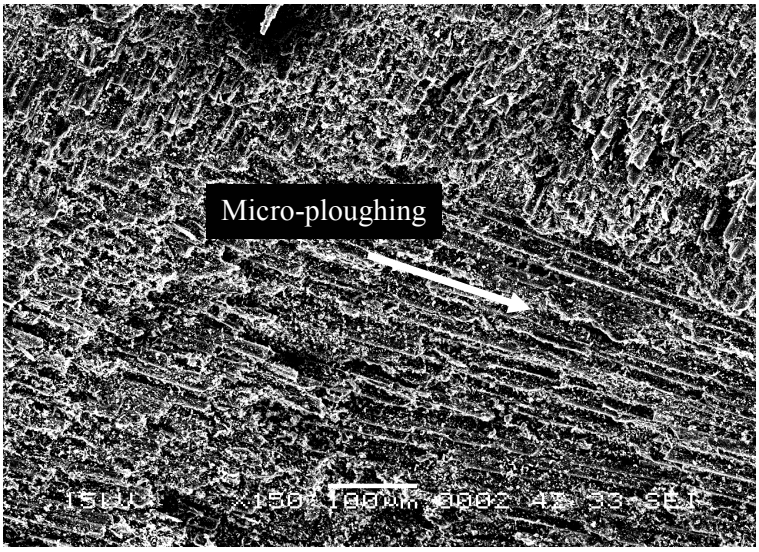

Figure 7.5a. Scanning electron micrograph of the composite (with 20wt% SiC) eroded at 30^0 impingement angle and 32m/sec impact velocity

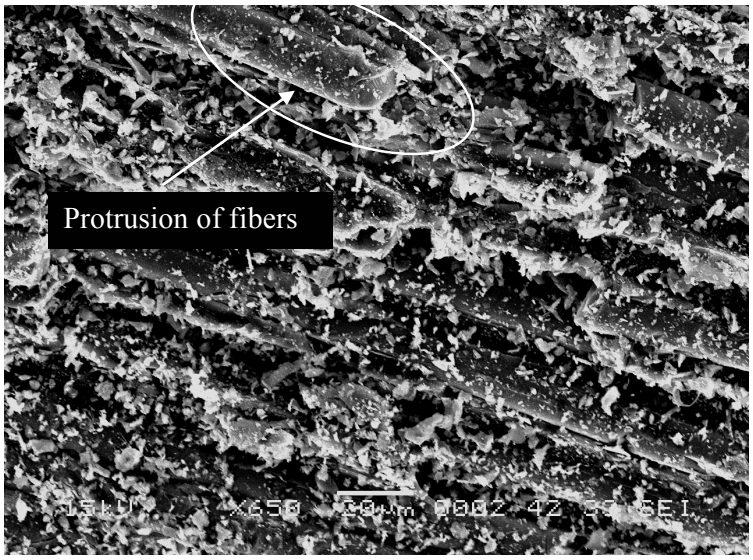

Figure 7.5b. Scanning electron micrograph of the composite (with 20wt% SiC) eroded at 30^0 impingement angle and 58 m /sec impact velocity.

Figure 7.5c. Scanning electron micrograph of the composite (with 20wt% SiC) eroded at 75^0 impingement angle and 58m/sec impact velocity

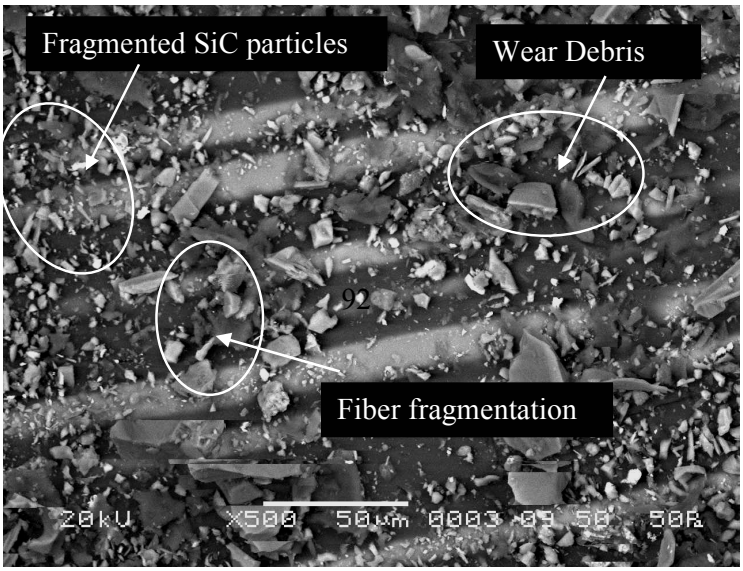

Figure 7.5d.Magnified scanning electron micrograph of the same composite showing fiber and filler fragmentation.

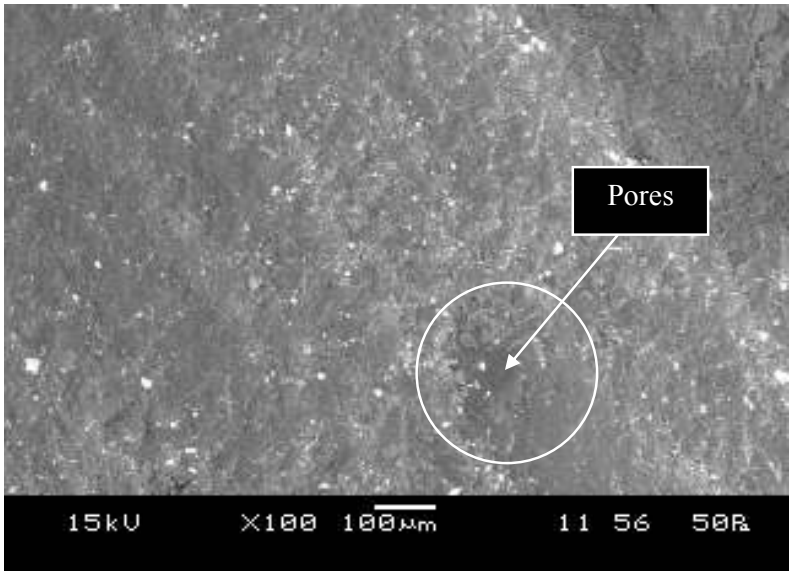

Figure 7.6a.Scanning electron micrograph of the uneroded composite C_8 (10wt% CBPD)

Figure 7.6a presents an SEM image of the uneroded surface of CBPD filled glass polyester composite. The presence of cement by-pass dust particles in the matrix body can be clearly seen in this micro-graph. The morphology appears to be indicating uniform distribution of filler materials although some small pores and voids can be seen.

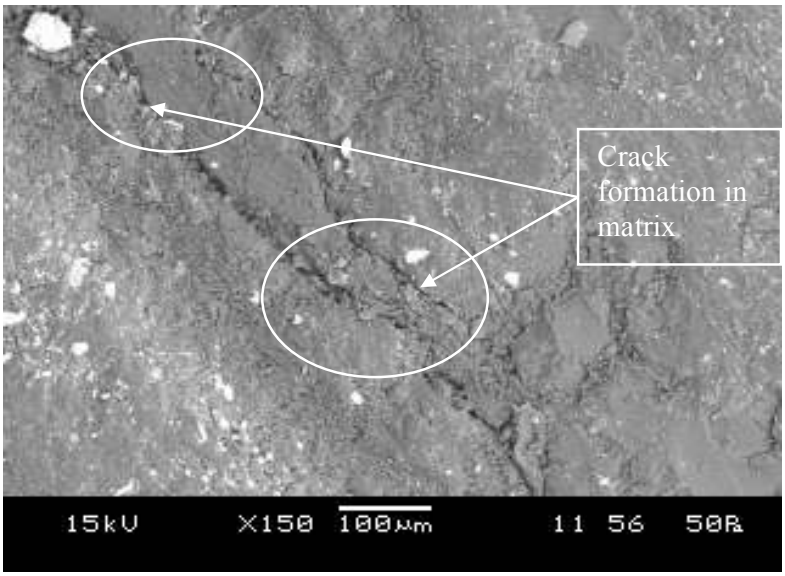

Figure 7.6b Scanning electron micrograph of the composite C_8 (10 wt% CBPD) eroded at eroded at 60^0 impingement angle and 32 m/sec impact velocity

Scanning electron micrograph of the surface of composite C_8 eroded at impingement angle of 60^0 in the steady-state wear regime is given in Figure 7.6b. The plastic flow of matrix material along the erosion direction is visible. The micro-graph also shows formation of crack in the matrix instead of matrix debris (fiber breakage and removal of fiber). This may be due to the low velocity of impact (32 m/sec) of the erodent particles. The crack propagation is clearly seen and weak bonding between the fibre, filler and the resin can possibly be the cause for these long and deep cracks on the worn surface. The same composite when eroded at a relatively larger impact velocity (58 m/sec), the micro-graph, Figure 7.6c looks entirely different. Here, the extent of surface damage is higher as more fibres are detached from the matrix and the matrix is peeled seriously forming craters on the upper surface. This image also gives a clear indication of occurrence of plastic deformation of CBPD filled polyester matrix.

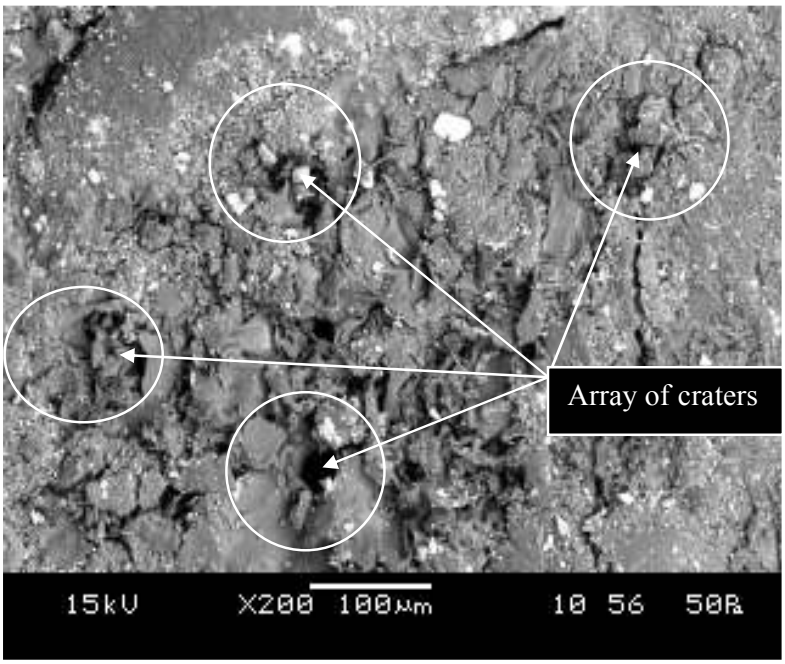

Figure 7.6c. Scanning electron micrograph of the composite C_8 (10 wt% CBPD) eroded at eroded at 60^0 impingement angle and 58 m/sec impact velocity

Figure 7.6d illustrates the SEM image of the eroded surface of the composite C_9. The plastic flow of CBPD filled matrix is seen to have taken place as in the case of composite C_8 (Figure 7.5b) but with less amount of surface cracks. With the increase of CBPD content (20 wt%), this composite exhibits better erosion resistance (Figure 7.2) but shows poorer tensile strength (Figure 4.6). A possible reason for this may be that the CBPD particles present in the matrix body carry most of the impact load imparted by the hard silica sand particles and prevent the rubbing-off of matrix

surface, resulting in the reduction of wear of the composite. But at the same time the load stress might not be effectively transmitted from the matrix to fibers, which reduces the load-carrying capability (tensile strength) of the composite.

Particle impingement produces a rise in temperature of the composite surface which makes the matrix deformation easy because the high temperature known to occur in solid particle erosion invariably soften the matrix [260]. On impact, the erodent particle kinetic energy is transferred to the composite body that leads to crater formation and subsequently material loss. The presence of hard fillers in the matrix helps in absorbing a good fraction of this kinetic energy and therefore energy available for the plastic deformation of polyester becomes less.

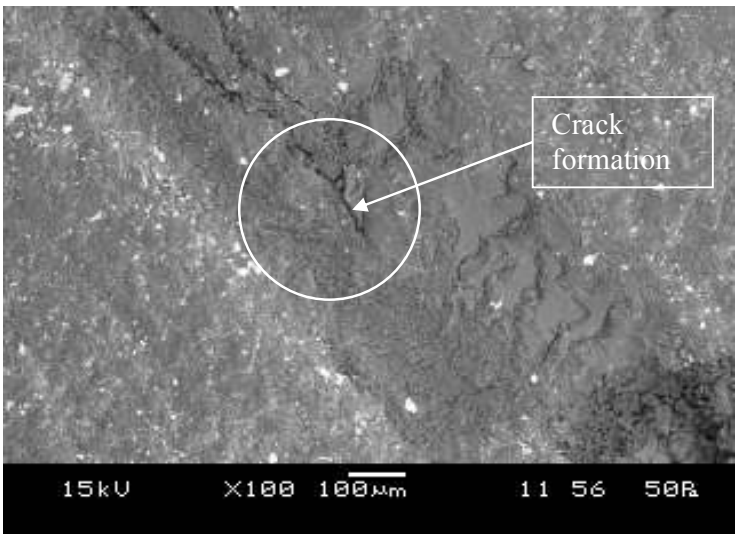

Figure 7.6d. Scanning electron micrograph of the composite C_8 (20 wt% CBPD) eroded at eroded at 60^0 impingement angle and 58 m/sec impact velocity

The presence of particulate fillers in these composites improves their erosion wear resistance and this improvement depends on the type and content of the fillers. Among the four different fillers taken in this work, Al_2O_3 is found to be the best one as far as the improvement in the wear performance of the composites is concerned. This also delays the initiation of fiber exposure as compared to the composite without any filler. All these factors combined together result in exhibition of better erosion response by the particulate filled composites than that of unfilled glass-polyester composite.

7.3 X-Ray diffraction study

The X-ray diffraction patterns recorded for raw flyash particles and for the eroded composite C_3 (20 wt% of fly ash) are shown in Figures 7.7a and 7.7b respectively.

The XRD of the raw flyash exhibits distinct peaks which are assignable to various metal oxide phases such as quartz (SiO_2), anatase (TiO_2), corundum (Al_2O_3) and hematite (Fe_2O_3) present in it (Figure 7.7a). It is seen in Figure 7.7b that most of these phases are retained even after erosion of the flyash filled composite.

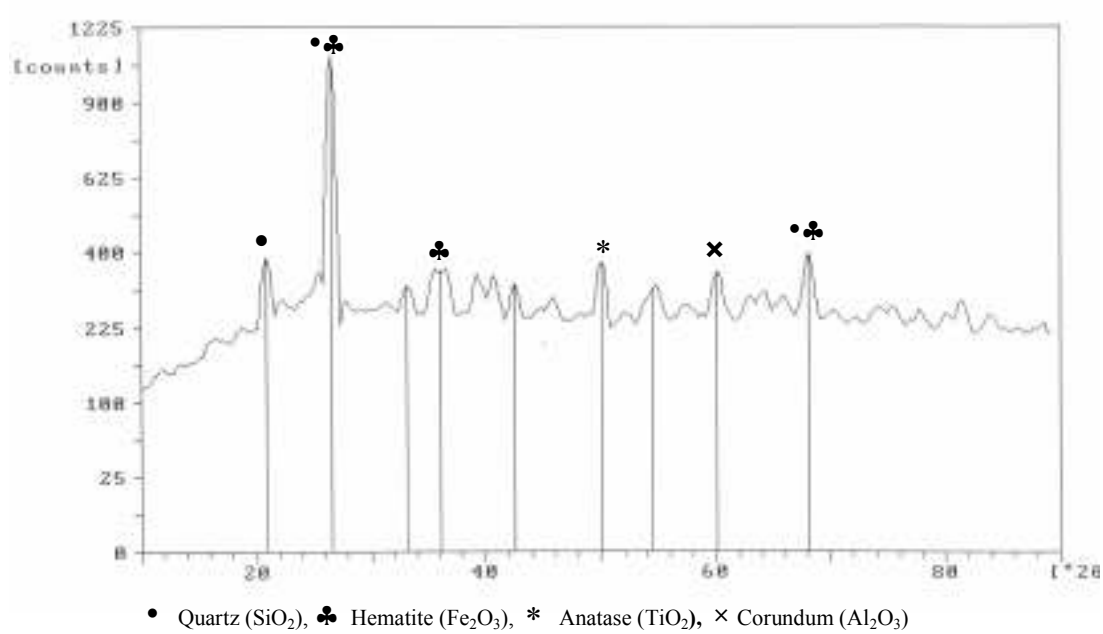

• Quartz (SiO_2), ♣ Hematite (Fe_2O_3), * Anatase (TiO_2), × Corundum (Al_2O_3)

Figure 7.7a. X-ray diffractogram of the raw flyash.

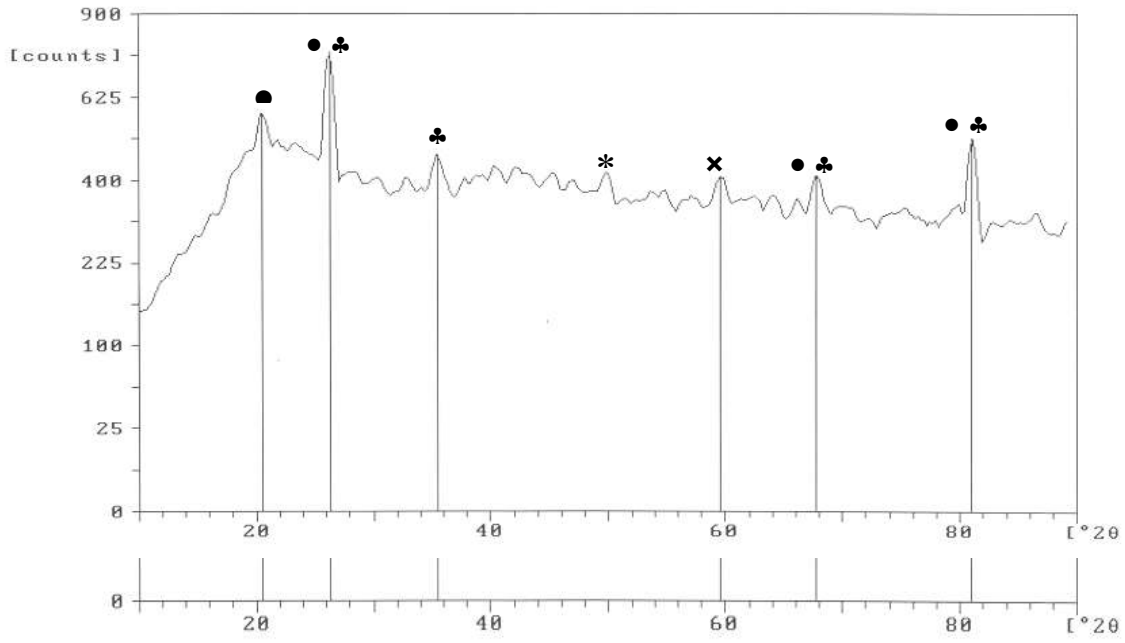

● Quartz (SiO_2), ♣ Hematite (Fe_2O_3), * Anatase (TiO_2), × Corundum (Al_2O_3)

Figure 7.7b. X-ray diffractogram of the eroded composite (20 wt% of fly ash).

Similarly, Figures 7.7c and 7.7d present the XRDs for the raw CBPD particles and the eroded composite C_9 (20wt% of CBPD) respectively.

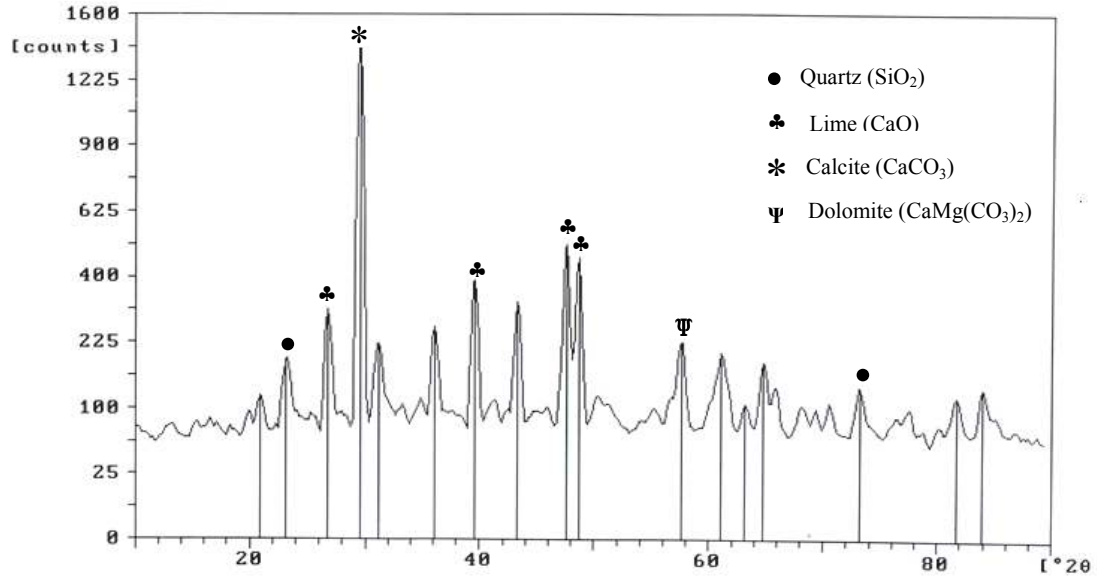

Figure 7.7c. X-ray diffractogram of the raw CBPD.

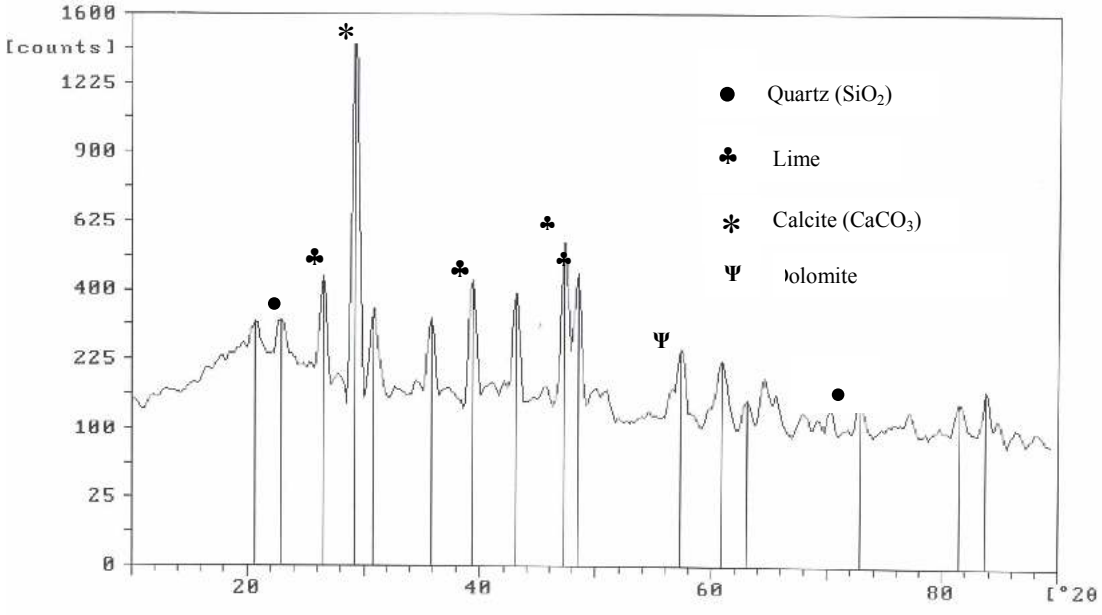

Figure 7.7d. X-ray diffractogram of the eroded composite (20 wt% of CBPD).

The diffractogram (Figure 7.7c) indicates calcite ($CaCO_3$) as the predominant phase in the cement by-pass dust. The presence of small amount of dolomite ($CaMg(CO_3)_2$)

apart from lime (CaO) and quartz (SiO_2) is also evident. Again in this case, most of these phases are seen to be retained even after erosion of the CBPD filled composite. Careful analysis of all these diffractograms suggests that the composites exhibit semi-crystalline behaviour.

7.4 Taguchi analysis

In Tables 7.1a and 7.1b the erosion rates of different composites for all 27 test runs and their corresponding S/N ratios are given. Each value is in fact the average of two replications. The overall mean for the S/N ratios of composites reinforced with flyash, alumina, SiC and CBPD are found to be -48.88db, -46.33db, -48.45db and -48.31 db respectively. The analyses are made using the popular software specifically used for design of experiment applications known as MINITAB 14. Before any attempt is made to use this simple model as a predictor for the measure of performance, the possible interactions between the control factors must be considered. Thus, factorial design incorporates a simple means of testing for the presence of the interaction effects. Where A, B, C, D and E are the input parameters such as A: impact velocity, B: filler content, C: stand off-distance, D: impingement angle and E: erodent size.

The effects of control factors on erosion rate of composites with the four different fillers are shown in Figures 7.8a, b, c and d respectively.

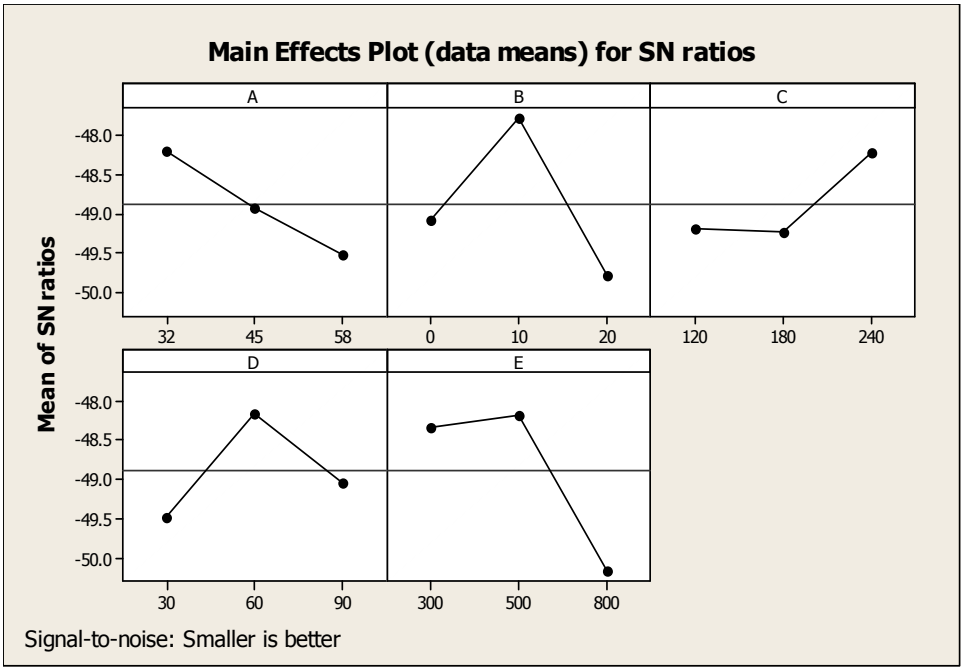

Figure 7.8a. Effect of control factors on erosion rate (for flyash filled composites)

Table7.1a. Experimental design using L_{27} orthogonal array (for conventional fillers)

Expt. No.	A	B	C	D	E	$Er_{alumina}$ mg/kg	S/N ratio(db)	Er_{SiC} mg/kg	S/N ratio(db)
1	32	0	120	30	300	309.83	-49.8225	309.83	-49.8225
2	32	0	180	60	500	235.25	-47.4306	235.25	-47.4306
3	32	0	240	90	800	315.19	-49.9714	315.19	-49.9714
4	32	10	120	60	500	173.77	-44.7995	232.05	-47.3116
5	32	10	180	90	800	264.94	-48.4630	269.67	-48.6167
6	32	10	240	30	300	139.96	-42.9201	189.80	-45.5659
7	32	20	120	90	800	289.48	-49.2324	253.40	-48.0761
8	32	20	180	30	300	227.49	-47.1392	299.70	-49.5337
9	32	20	240	60	500	197.88	-45.9280	173.28	-44.7750
10	45	0	120	60	800	318.86	-50.0720	318.86	-50.0720
11	45	0	180	90	300	349.80	-50.8764	349.80	-50.8764
12	45	0	240	30	500	235.25	-47.4306	235.25	-47.4306
13	45	10	120	90	300	174.94	-44.8578	247.93	-47.8866
14	45	10	180	30	500	133.18	-42.4888	132.71	-42.4581
15	45	10	240	60	800	172.78	-44.7499	212.63	-46.5525
16	45	20	120	30	500	183.96	-45.2945	197.82	-45.9254
17	45	20	180	60	800	287.83	-49.1827	288.68	-49.2083
18	45	20	240	90	300	311.76	-49.8764	353.83	-50.9759
19	58	0	120	90	500	395.10	-51.9341	395.10	-51.9341
20	58	0	180	30	800	215.19	-46.6564	215.19	-46.6564
21	58	0	240	60	300	239.89	-47.6002	239.89	-47.6002
22	58	10	120	30	800	207.34	-46.7428	279.38	-48.9239
23	58	10	180	60	300	259.79	-48.2924	293.76	-49.3599
24	58	10	240	90	500	184.44	-45.3171	277.38	-48.8615
25	58	20	120	60	300	282.68	-49.0259	299.80	-49.5366
26	58	20	180	90	500	318.96	-50.0747	495.92	-53.9082
27	58	20	240	30	800	305.88	-49.7110	280.63	-48.9627

Table 7.1b. Experimental design using L_{27} orthogonal array (for non-conventional fillers)

Expt. No.	A	B	C	D	E	Er_{flyash} mg/kg	S/N ratio(db)	Er_{CBPD} mg/kg	S/N ratio(db)
1	32	0	120	30	300	309.830	-49.8225	309.830	-49.8225
2	32	0	180	60	500	235.250	-47.4306	235.250	-47.4306
3	32	0	240	90	800	315.190	-49.9714	315.190	-49.9714
4	32	10	120	60	500	186.071	-45.3936	179.921	-45.1016
5	32	10	180	90	800	272.790	-48.7166	228.865	-47.1916
6	32	10	240	30	300	249.960	-47.9574	194.960	-45.7989
7	32	20	120	90	800	387.980	-51.7762	338.730	-50.5971
8	32	20	180	30	300	269.945	-48.6255	248.718	-47.9141
9	32	20	240	60	500	161.479	-44.1623	179.680	-45.0900
10	45	0	120	60	800	318.860	-50.0720	318.860	-50.0720
11	45	0	180	90	300	349.800	-50.8764	349.800	-50.8764
12	45	0	240	30	500	235.250	-47.4306	235.250	-47.4306
13	45	10	120	90	300	239.760	-47.5955	207.350	-46.3341
14	45	10	180	30	500	249.184	-47.9304	191.182	-45.6289
15	45	10	240	60	800	238.230	-47.5399	205.505	-46.2564
16	45	20	120	30	500	222.960	-46.9645	203.460	-46.1696
17	45	20	180	60	800	330.380	-50.3803	309.105	-49.8021
18	45	20	240	90	300	379.780	-51.5906	345.770	-50.7757
19	58	0	120	90	500	395.100	-51.9341	395.100	-51.9341
20	58	0	180	30	800	215.190	-46.6564	215.190	-46.6564
21	58	0	240	60	300	239.890	-47.6002	239.890	-47.6002
22	58	10	120	30	800	261.270	-48.3418	234.305	-47.3956
23	58	10	180	60	300	319.760	-50.0965	289.775	-49.2412
24	58	10	240	90	500	210.660	-46.4716	237.550	-47.5151
25	58	20	120	60	300	349.640	-50.8724	316.160	-49.9981
26	58	20	180	90	500	419.690	-52.4586	369.325	-51.3482
27	58	20	240	30	800	368.010	-51.3172	336.945	-50.5512

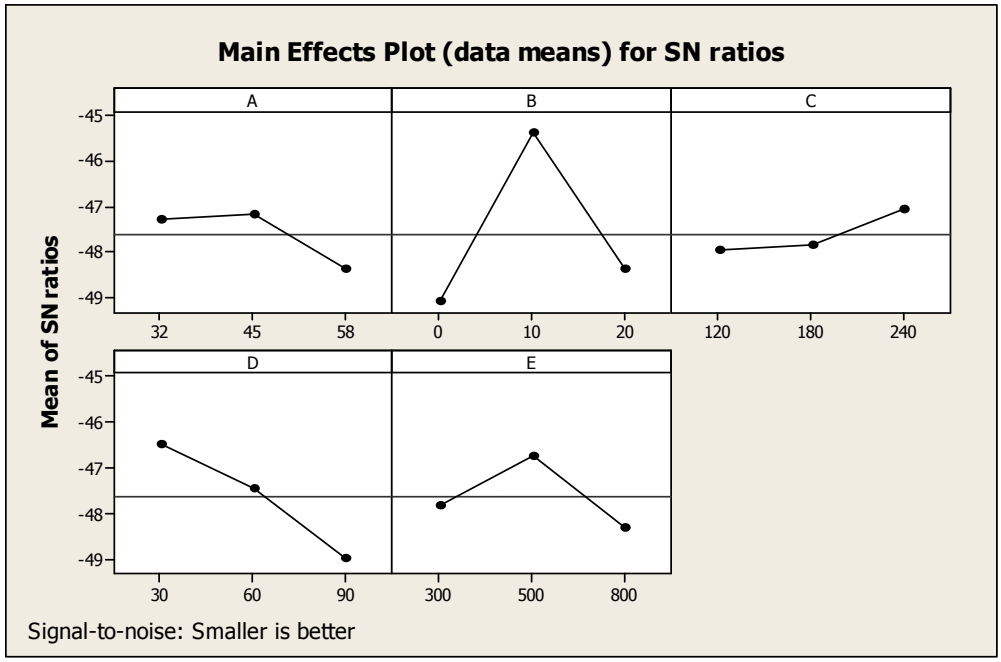

Figure 7.8b. Effect of control factors on erosion rate (for Al_2O_3 filled composites)

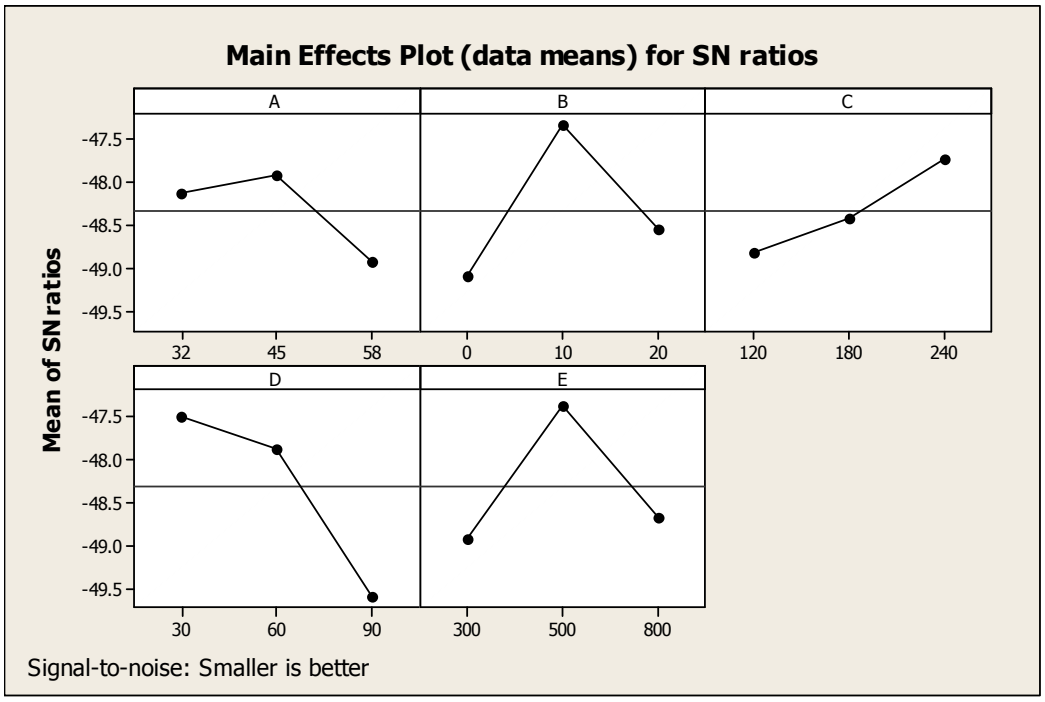

Figure 7.8c. Effect of control factors on erosion rate (for SiC filled composites)

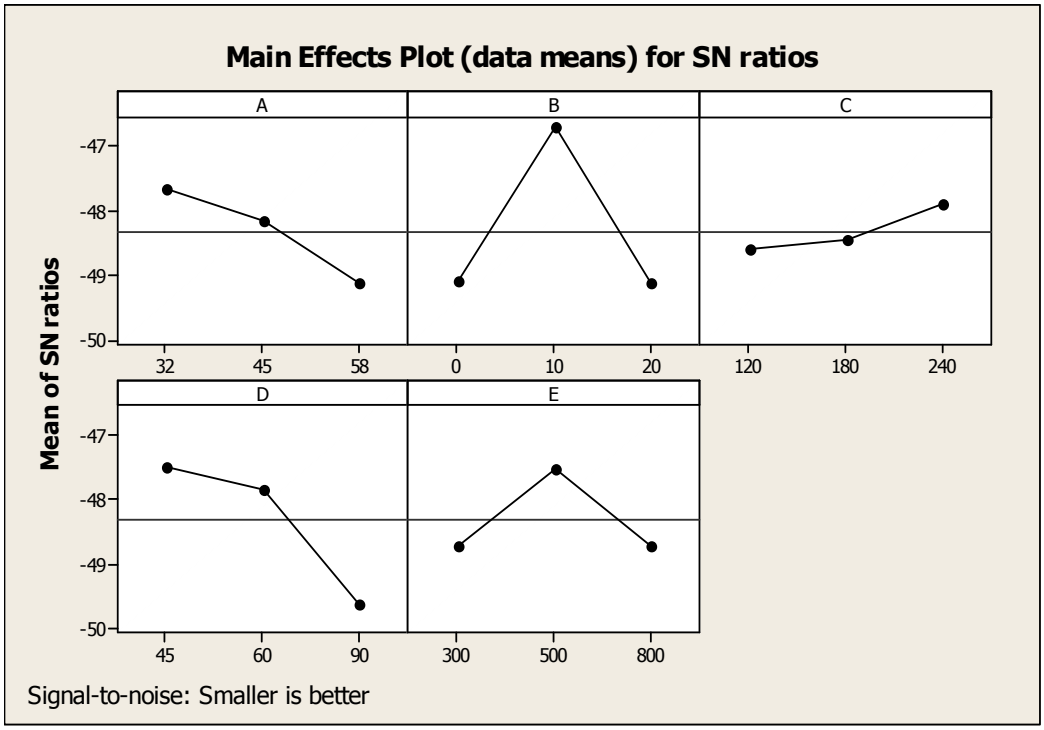

Figure 7.8d. Effect of control factors on erosion rate (for CBPD filled composites)

The analysis of the result gives the combination of factors producing minimum wear rate of the composites. These combinations are found to be different for different filler materials. For flyash the factor combination of A_1(impact velocity 32 m/sec), B_2 (flyash content 10%), C_3 (stand off-distance 240mm), D_2 (impingement angle 60^0) and E_2(erodent size 500μm)gives minimum erosion rate while in case of alumina this is A_1(impact velocity 32 m/sec), B_2 (alumina content 10%), C_3 (stand off-distance 240mm), D_1(impingement angle 30^0) and E_2 (erodent size 500μm). Similarly, while the combination A_2 (impact velocity 45 m/sec), B_2 (SiC content 10%), C_3 (stand off-distance 240), D_1(impingement angle 30^0) and E_2(erodent size 500 μm)gives minimum erosion rate for SiC filler, for CBPD filler the combination is found to be A_1(impact velocity 32m/sec),B_2 (CBPD content 10%),C_3 (stand off-distance 240mm), D_1 (impingement angle 30^0) and E_2 (erodent size 500μm). As far as minimization of erosion rate is concerned, factors A, B, D and E have significant effects on all the three different composites, whereas factor C has the least effect. It is observed from Figures 7.9a, b, c and d that the interactions between A×B show most significant effect on erosion rate whereas it can be considered from Figures 7.8a, b, c and d that interaction between A×C is less significant. Thus this analysis suggests that few

of the factors have individual effect and similarly, some of the interactions have combined effect on erosion rate. Although, these plots are indicators of the relative significance of various control factors and their interactions, this can be confirmed only after performing the analysis of variance (ANOVA).

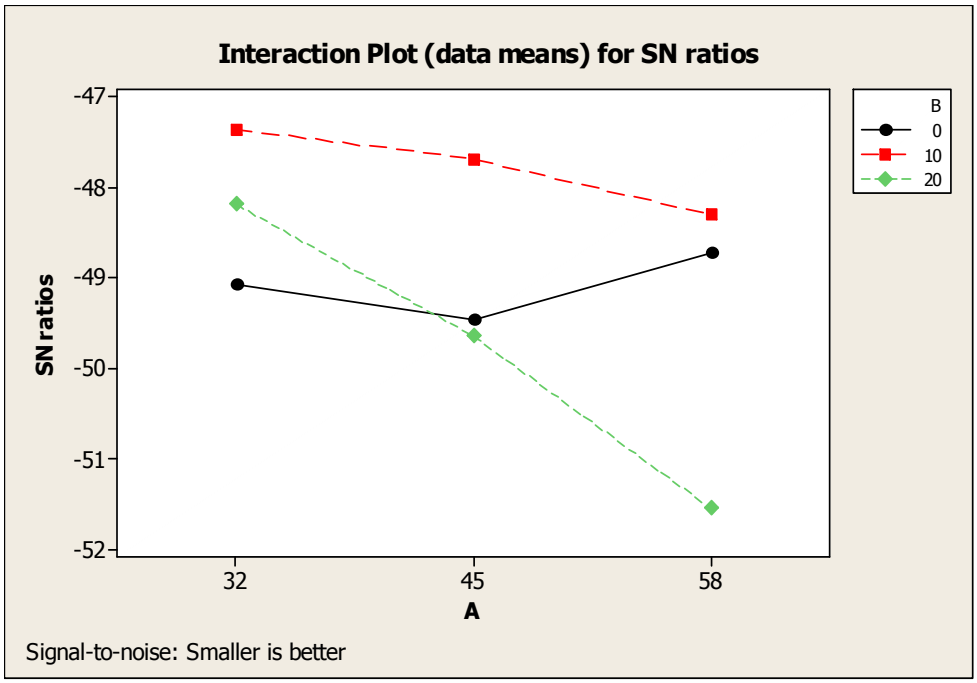

Figure 7.9a. Interaction graph between A×B for erosion rate (for flyash filler)

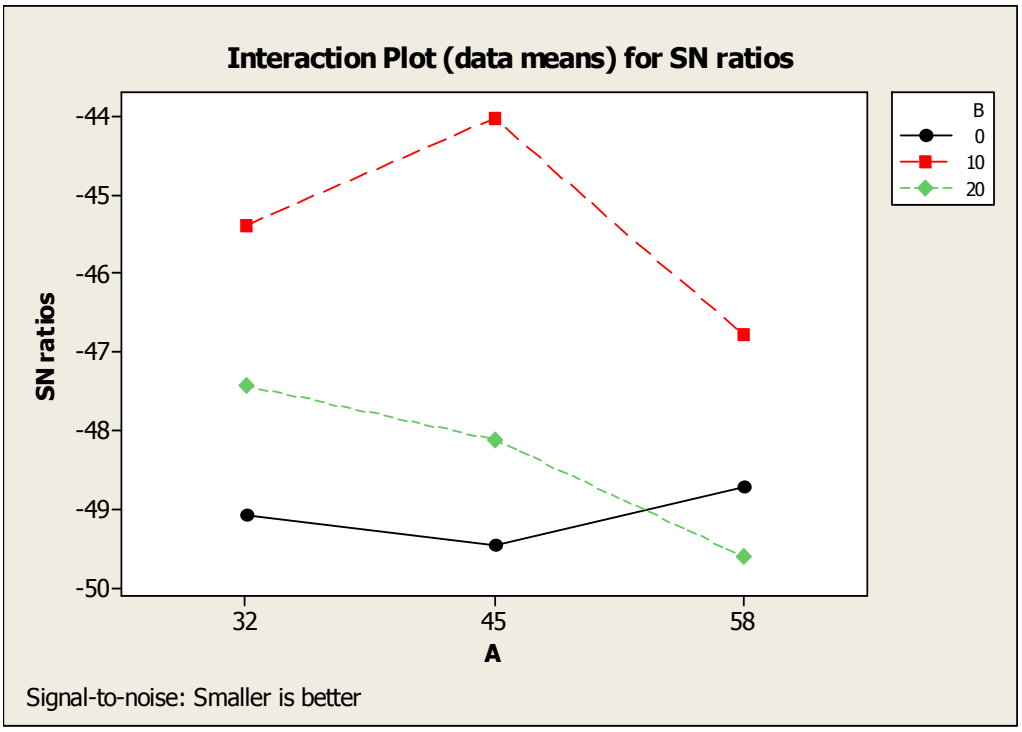

Figure 7.9b. Interaction graph between A×B for erosion rate (for Al_2O_3 filler)

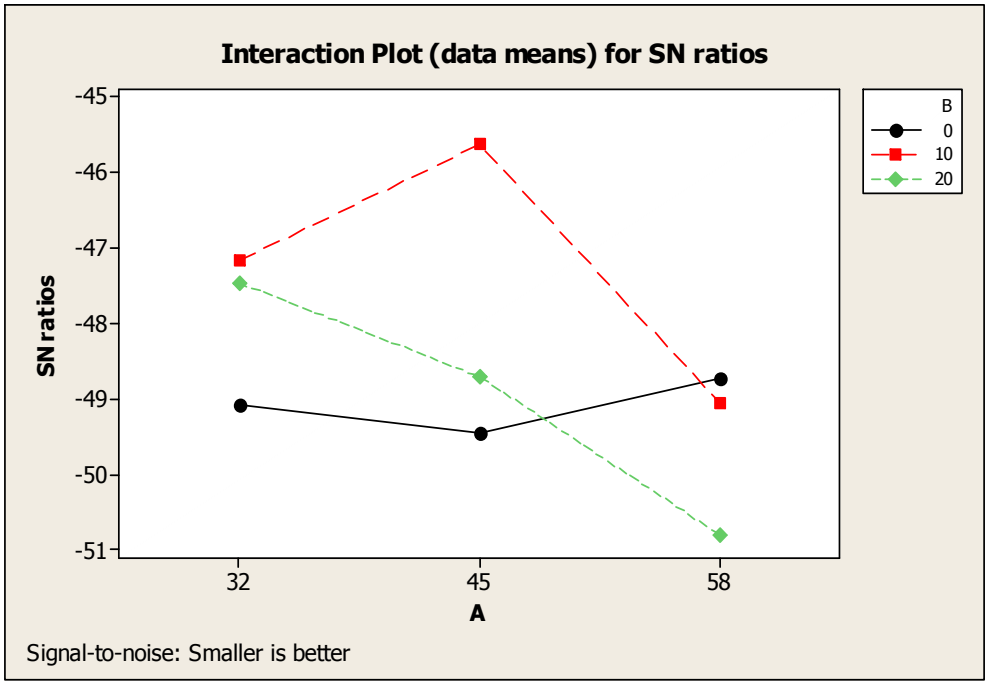

Figure 7.9c. Interaction graph between A×B for erosion rate (for SiC filler).

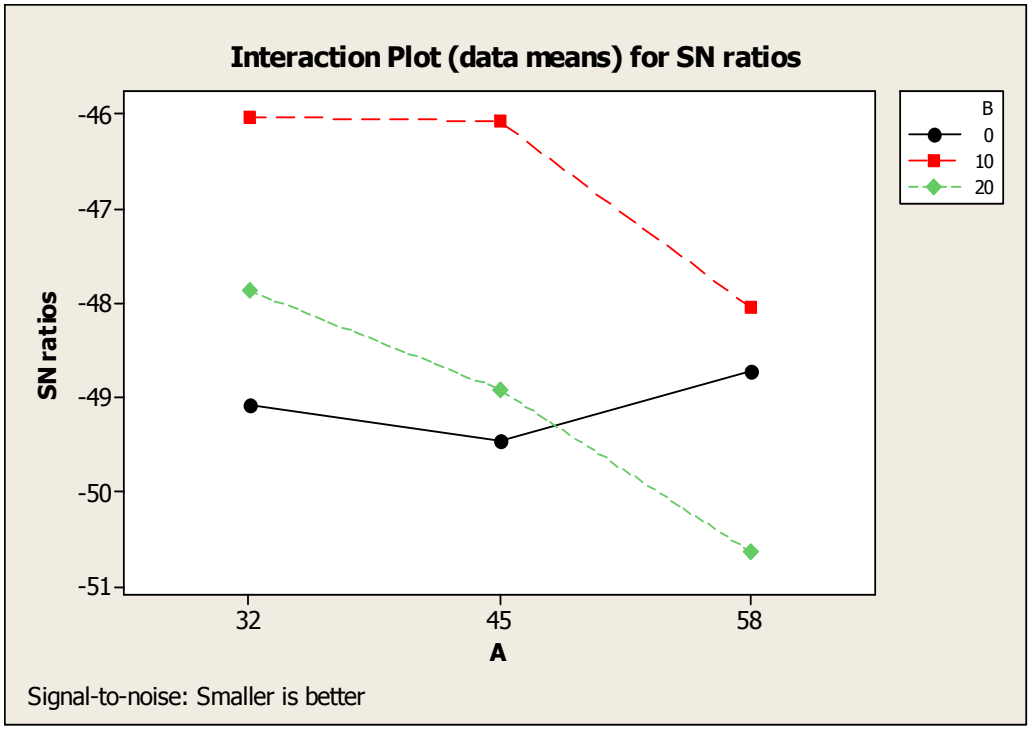

Figure 7.9d. Interaction graph between A×B for erosion rate (for CBPD filler)

7.5 Erosion efficiency

The hardness alone is unable to provide sufficient correlation with erosion rate, largely because it determines only the volume displaced by each impact and not really the volume eroded. Thus a parameter which will reflect the efficiency with which the volume that is displaced is removed should be combined with hardness to obtain a better correlation. The erosion efficiency is obviously one such parameter. In case of a stream of particles impacting a surface normally (i.e. at $\alpha=90^0$), the erosion efficiency (η_{normal}) defined by Sundararajan et. al [254] is given as

$$\eta_{normal} = \frac{2ErHv}{\rho V^2} \tag{7.1}$$

But considering impact of erodent at any angle α to the surface, the actual erosion efficiency can be obtained by modifying Eq. (7.1) as

$$\eta = \frac{2ErHv}{\rho V^2 Sin^2\alpha} \tag{7.2}$$

According to the theoretical erosion wear model presented in chapter-5, the non-dimensional erosion wear rate of a composite material is given by

$$E_{rth} = \frac{\rho_C . \eta . V^2 . Sin^2\alpha}{2Hv} \tag{7.3}$$

where

α	angle of impingement (degree)
V	impact velocity (m/sec)
Hv	hardness (N/m^2)
ρ_c	density of composite (kg/m^3)
ρ	density of erodent (kg/m^3)
η	erosion efficiency
E_r	actual erosion wear rate (kg/kg)
E_{rth}	theoretical erosion wear rate (kg/kg)

The values of erosion efficiencies of composites under this study are calculated using Eq. (7.2) and are given in Table 7.2a, b along with their hardness values and operating conditions. It clearly shows that erosion efficiency is not exclusively a material property; but also depends on other operational variables such as impingement angle and impact velocity. The erosion efficiencies of these composites

under normal impact (η_{normal}) vary from 3 to 6%, 6-9% and 9-12% for impact velocities 58m/sec, 45m/sec and 32m/sec respectively. The value of η for a particular impact velocity under oblique impact can be obtained simply by multiplying a factor $1/Sin^2\alpha$ with $\eta_{normal.}$ Similar observation on velocity dependence of erosion efficiency has previously been reported by few investigators [108].

Table 7.2a. Erosion efficiency (η) of composites with different filler content and impact velocity (for conventional fillers).

Expt. No.	Filler content (wt %)	Impact velocity (m/sec)	η Al_2O_3 filling (%)	η SiC filling (%)
1	0	32	47.91894	47.9189
2	0	32	10.49685	10.4968
3	0	32	12.18698	12.1869
4	10	32	8.26962	12.5889
5	10	32	10.92578	12.6774
6	10	32	23.08708	35.6908
7	20	32	11.69854	13.1181
8	20	32	36.77353	62.0599
9	20	32	9.228278	10.3518
10	0	45	7.194564	7.19456
11	0	45	6.839407	6.83940
12	0	45	18.39875	18.3987
13	10	45	3.648120	5.89392
14	10	45	11.10910	12.6194
15	10	45	4.157950	5.83318
16	20	45	15.03735	20.7142
17	20	45	6.787811	8.72091
18	20	45	6.371010	9.26262
19	0	58	4.650233	4.65023
20	0	58	10.13094	10.1309
21	0	58	3.258259	3.25825
22	10	58	10.41099	15.9918
23	10	58	3.763373	4.85113
24	10	58	2.315284	3.96935
25	20	58	4.012895	5.45187
26	20	58	3.923676	7.81484
27	20	58	15.05109	17.6889

Table 7.2b. Erosion efficiency (η) of composites with different filler content and impact velocity (for non-conventional fillers).

Expt. No.	Filler content (wt %)	Impact velocity (m/sec)	η flyash filling (%)	η CBPD filling (%)
1	0	32	47.9189	47.91894
2	0	32	12.1281	10.49685
3	0	32	8.3204	12.18698
4	10	32	12.0136	9.563229
5	10	32	13.2095	10.54135
6	10	32	48.4160	35.91885
7	20	32	16.0798	13.78987
8	20	32	44.7514	40.50175
9	20	32	08.9233	8.441354
10	0	45	08.3126	7.194564
11	0	45	06.8394	6.839407
12	0	45	18.3987	18.39875
13	10	45	05.8709	4.82943
14	10	45	24.4069	17.81143
15	10	45	07.7780	5.523572
16	20	45	18.6911	16.75408
17	20	45	09.2321	7.343335
18	20	45	07.9594	7.118178
19	0	58	04.6502	4.650233
20	0	58	10.1301	10.13094
21	0	58	03.7646	3.258259
22	10	58	15.4046	13.14021
23	10	58	06.2844	4.688432
24	10	58	03.1052	3.33055
25	20	58	05.8813	4.5213
26	20	58	05.2947	4.576772
27	20	58	18.5710	16.70204

The theoretical erosion wear rates (E_{rth}) of all the nine composites are calculated using Eq. 7.3. These values are compared with those obtained from experiments (E_r) conducted under similar operating conditions. Tables 7.3a, b present a comparison between the theoretical and experimental results for the composites with different fillers. The errors in experimental results with respect to the theoretical ones lie in the range 0-10%. The magnitude of η can be used to characterize the nature and mechanism of erosion. For example, ideal micro-ploughing involving just the displacement of the material from the crater without any fracture (and hence no erosion) will result in η=0. In contrast, if the material removal is by ideal micro-cutting, η=1.0 or 100%. If erosion occurs by lip or platelet formation and their fracture by repeated impact, as is usually in the case of ductile materials, the magnitude of η will be very low, i.e $\eta \leq 100\%$. In the case of brittle materials, erosion occurs usually by spalling and removal of large chunks of materials resulting from the interlinking of lateral or radial cracks and thus η can be expected to be even greater than 100% [249]. The erosion efficiencies of the composites under the present study indicate that at low impact speed the erosion response is semi-ductile (η=10-100%). On the other hand at relatively higher impact velocity the composites exhibit ductile ($\eta < 10\%$) erosion behaviour [108].

Table 7.3a. Comparison of theoretical and experimental erosion results (for conventional fillers).

Expt. No.	Ertheo (alumina) mg/kg	Erexpt. (alumina) mg/kg	Error (alumina) (%)	Ertheo (SiC) mg/kg	Erexpt. (SiC) mg/kg	Error (SiC) (%)
1	290.42	309.83	6.68342	290.42	309.83	6.68342
2	245.45	235.25	4.15563	245.45	235.25	4.15563
3	314.49	315.19	0.22258	330.00	315.19	4.48787
4	179.18	173.77	3.01931	252.00	232.05	7.91666
5	269.46	264.94	1.67742	272.54	269.67	1.05305
6	136.59	139.96	2.46724	186.37	189.80	1.84042
7	288.48	289.48	0.34664	252.47	253.40	0.36836
8	246.52	227.49	7.71945	307.18	299.70	2.43505
9	206.34	197.88	4.10002	168.00	173.28	3.14286
10	325.61	318.86	2.07303	325.61	318.86	2.07303
11	356.87	349.80	1.98111	356.87	349.80	1.98111
12	245.43	235.25	4.14782	258.00	235.25	8.81782
13	182.16	174.94	3.96354	246.26	247.93	0.67815
14	138.24	133.18	3.66030	136.56	132.71	2.81927
15	186.37	172.78	7.29194	224.16	212.63	5.14364
16	193.68	183.96	5.01858	206.49	197.82	4.19875
17	298.47	287.83	3.56484	297.43	288.68	2.94186
18	310.49	311.76	0.40903	352.74	353.83	0.30901
19	407.11	395.10	2.95006	413.00	395.10	4.33414
20	228.26	215.19	5.72592	228.26	215.19	5.72592
21	246.19	239.89	2.55899	246.19	239.89	2.55899
22	214.68	207.34	3.41904	288.76	279.38	3.24837
23	276.82	259.79	6.15201	314.25	293.76	6.52028
24	182.64	184.44	0.98555	275.89	277.38	0.54007
25	296.46	282.68	4.64818	312.58	299.80	4.08855
26	319.48	318.96	0.16276	494.39	495.92	0.30947
27	307.91	305.88	0.65928	283.14	280.63	0.88648

Table 7.3b. Comparison of theoretical and experimental erosion results (for non-conventional fillers).

Expt. No.	Ertheo (flyash) mg/kg	Erexpt. (flyash) mg/kg	Error (flyash) (%)	Ertheo (CBPD) mg/kg	Erexpt. (CBPD) mg/kg	Error (CBPD) (%)
1	290.43	309.830	6.67975	293.83	309.83	5.44533
2	245.45	235.250	4.15563	223.609	235.25	5.20606
3	226.34	215.190	4.92622	295.19	315.19	6.77532
4	195.71	186.071	4.92514	168.834	179.921	6.56712
5	282.84	272.790	3.55325	239.257	228.865	4.34340
6	264.94	249.960	5.65411	206.368	194.960	5.52794
7	394.12	387.980	1.55790	342.543	338.730	1.11320
8	281.42	269.945	4.07754	263.266	248.718	5.52604
9	178.58	161.479	9.57610	167.609	179.680	7.20162
10	325.61	318.860	2.07303	299.500	318.860	6.46411
11	356.88	349.800	1.98386	339.800	349.800	2.94291
12	245.43	235.250	4.14782	225.250	235.250	4.43951
13	249.45	239.760	3.88455	211.483	207.350	1.95420
14	258.83	249.184	3.72677	202.369	191.182	5.52792
15	242.16	238.230	1.62289	198.272	205.505	3.64797
16	234.75	222.960	5.02236	215.361	203.460	5.52602
17	339.37	330.380	2.64903	287.179	309.105	7.63496
18	378.19	379.780	0.42040	355.995	345.770	2.87223
19	407.20	395.100	2.97151	375.100	395.100	5.33191
20	228.26	215.190	5.72593	205.190	215.190	4.87353
21	246.19	239.890	2.55899	224.625	239.890	6.79587
22	268.49	261.270	2.68911	243.015	234.305	3.58418
23	332.80	319.760	3.91827	269.476	289.775	7.53297
24	208.56	210.660	1.00690	241.450	237.550	1.61524
25	352.17	349.640	0.71840	293.642	316.160	7.66845
26	420.58	419.690	0.21161	376.928	369.325	2.01707
27	369.54	368.010	6.67975	356.654	336.945	5.52603

For revalidation of the theoretical formulation for predictive purpose another prediction model based on ANN is employed and the results of both are compared. The neural network is constructed taking the experimental database generated during the erosion trials on the composites. Seventy five percent of data is used for training whereas twenty five percent data is used for testing. The parameters of three layer architecture of ANN model are set as: input nodes = 5, output node = 1, hidden nodes = 12, learning rate = 0.01, momentum parameter = 0.03, number of epochs = 20, 0000 and a set of predicted output (E_{rANN}) is obtained. Table 7.4a, b present a comparison between the theoretical and the ANN predicted results for both conventional and non-conventional fillers. The errors associated with each of the ANN predicted results with respect to the theoretical results are also given. It is observed that errors between theoretical and experimental wear rates lie in the range of 0-10%, whereas the same between ANN prediction and theoretical wear rate lie in the range of 0-14%. The error in case of ANN model can further be reduced if number of test patterns is increased. The present study thus, demonstrates successful application of ANN for prediction of wear rate in a complex process like solid particle erosion of polymer composites.

Table 7.4a. Comparison of theoretical and ANN results (for conventional filler)

Expt. No.	E_{rth} (mg/kg) Alumina	$E_{ANN.}$ (mg/kg) Alumina	Error (%) Alumina	E_{rth} (mg/kg) SiC	$E_{ANN.}$ (mg/kg) SiC	Error (%) SiC
1	290.42	280.58	3.38819	290.42	261.85	9.83747
2	245.45	235.89	3.89488	245.45	263.41	7.31717
3	314.49	293.57	6.65204	330.00	299.44	9.26060
4	179.18	156.94	12.41210	252.00	262.44	4.14286
5	269.46	280.78	4.20099	272.54	294.55	8.07588
6	136.59	143.28	4.89780	186.37	165.12	11.40205
7	288.48	257.66	10.68358	252.47	234.14	7.26026
8	246.52	236.48	4.07269	307.18	281.13	8.48037
9	206.34	209.46	1.51207	168.00	147.02	12.4881
10	325.61	283.62	12.89580	325.61	318.22	2.26958
11	356.87	326.27	8.57455	356.87	350.24	1.85781
12	245.43	229.61	6.44583	258.00	243.16	5.75193
13	182.16	201.05	10.37000	246.26	275.84	12.01170
14	138.24	144.53	4.55006	136.56	146.57	7.33011
15	186.37	210.54	12.96880	224.16	241.52	7.74447
16	193.68	214.48	10.73940	206.49	221.31	7.17710
17	298.47	267.77	10.28579	297.43	291.04	2.14840
18	310.49	273.75	11.83291	352.74	325.09	7.83863
19	407.11	364.55	10.45418	413.00	366.99	11.14040
20	228.26	209.07	8.40708	228.26	255.90	12.10900
21	246.19	220.12	10.58938	246.19	269.68	9.54141
22	214.68	232.78	8.43115	288.76	279.11	3.34187
23	276.82	254.57	8.03770	314.25	307.13	2.26571
24	182.64	179.20	1.88348	275.89	289.32	4.86788
25	296.46	297.85	0.46887	312.58	352.38	12.73270
26	319.48	319.99	0.15963	494.39	468.29	5.27923
27	307.91	299.90	2.60141	283.14	247.94	12.43200

Table 7.4b. Comparison of theoretical and ANN results (for non-conventional filler)

Expt. No.	E_{rth} (mg/kg) flyash	$E_{ANN.}$ (mg/kg) flyash	Error (%) flyash	E_{rth} (mg/kg) CBPD	$E_{ANN.}$ (mg/kg) CBPD	Error (%) CBPD
1	290.43	256.74	11.6000	293.830	259.295	11.75330
2	245.45	266.20	8.45386	223.609	249.805	11.71510
3	226.34	237.41	4.89087	295.190	268.425	9.06704
4	195.71	198.62	1.48689	168.834	185.530	9.88900
5	282.84	279.91	1.03592	239.257	272.230	13.78140
6	264.94	247.48	6.59017	206.368	206.300	0.03295
7	394.12	387.38	1.71013	342.543	310.760	9.27854
8	281.42	284.13	0.96297	263.266	282.630	7.35530
9	178.58	169.57	5.04535	167.609	158.295	5.55698
10	325.61	321.57	1.24074	299.500	319.895	6.80968
11	356.88	347.94	2.50504	339.800	349.090	2.733960
12	245.43	241.66	1.53608	225.250	242.410	7.61820
13	249.45	240.52	3.57987	211.483	238.180	12.62370
14	258.83	239.72	7.38322	202.369	193.145	4.55801
15	242.16	229.88	5.07102	198.272	225.700	13.83350
16	234.75	248.80	5.98509	215.361	235.055	9.14465
17	339.37	322.70	4.91204	287.179	306.870	6.85670
18	378.19	364.88	3.51939	355.995	344.985	3.09274
19	407.20	385.10	5.42731	375.100	376.045	0.25193
20	228.26	225.78	1.08648	205.190	230.840	12.50060
21	246.19	238.63	3.07079	224.625	254.155	13.14640
22	268.49	255.94	4.67429	243.015	267.525	10.08580
23	332.80	289.02	13.15505	269.476	298.075	10.61280
24	208.56	228.69	9.65190	241.450	259.005	7.27066
25	352.17	332.50	5.58537	293.642	332.440	13.21270
26	420.58	365.25	13.15564	376.928	416.770	10.57020
27	369.54	333.68	9.70395	356.654	310.810	12.85391

7.6 ANOVA and the effects of factors

In order to find out statistical significance of various factors like impact velocity (A), filler content (B), stand-off distance (C), impingement angle (D) and erodent size (E) and their interactions on erosion rate, analysis of variance (ANOVA) is performed on experimental data. Tables 7.5a, b, c and d show the results of the ANOVA with the erosion rate. This analysis is undertaken for a level of confidence of significance of 5%. The last column of each table indicates p-value for the individual control factors and their possible interactions. It is known that smaller is the p-value, greater is the significance of the factor/interaction corresponding to it [261].

The ANOVA results for flyash filled glass fiber polyester composites (Table 7.5a), indicate that, the flyash content (p=0.083), impingement angle (p= 0.091), erodent size (p=0.274) and impact velocity (p=0.367), in this order, are significant control factors affecting the erosion rate. It means, the filler content is the most significant factor and the stand-off distance with a p-value of 0.518 has negligible influence on the performance output. Between the two possible interactions, the interaction of impact velocity×flyash content (p=0.608) has greater contribution on the erosion rate compared to the interaction of impact velocity×stand-off distance (p=0.678).

Similarly, in case of alumina filled glass-polyester composites (Table 7.5b), alumina content (p=0.002), impingement angle (p= 0.025), erodent size (p=0.146) and impact velocity (p=0.256) have greater influence on erosion rate while between the interactions, the impact velocity×alumina content (p=0.354) shows significant contribution. Again in Table 7.5c, for the SiC filled glass-polyester composites, the following factors show significant effect on erosion rate. Erodent size (p=0.146), SiC content (p=0.131), impact velocity (p=0.171) and impingement angle (p= 0.409). The interaction of impact velocity× SiC content (p=0.354) also shows remarkable contribution on the erosion rate. From Table 7.5d, for CBPD filled composites, it is noted that, the CBPD content (p=0.015), impingement angle (p=0.039), erodent size (p = 0.174) and impact velocity (p=0.219), in this sequence, significantly influence the erosion rate. The interaction of impact velocity× CBPD content (p=0.419) is found to have relatively more significant contribution on the erosion rate compared to the remaining factor and interaction. It is interesting to note that, all the particulate fillers (with the exception of SiC) show similar trend in regard to the order of

significant control factors affecting their erosion rate. Moreover, for all the composites, including even the SiC filled ones, the stand-off-distance and its interaction with impact velocity are found to be the factor and interaction respectively, with the least significance as far as solid particle erosion of these hybrid composites are concerned.

Table 7.5a. ANOVA table for erosion rate (for flyash filled composites)

Source	DF	Seq SS	Adj SS	Adj MS	F	p
A	2	8510	8510	4255	1.14	0.367
B	2	24589	24589	12294	3.29	0.083
C	2	5336	5336	2668	0.71	0.518
D	2	25800	25800	12900	3.45	0.091
E	2	11411	11411	5705	1.53	0.274
A*B	4	10599	10599	2650	0.71	0.608
A*C	4	8846	8846	2212	0.59	0.678
Error	8	29881	29881	3735		
Total	26	124973				

DF: degree of freedom; Seq.SS: sequential sum of squares; AdjSS: extra sum of squares; Adj MS: extra mean squares; p: level of significance

Table 7.5b. ANOVA table for erosion rate (for Al_2O_3 filled composites)

Source	DF	Seq SS	Adj SS	Adj MS	F	p
A	2	7.580	7.580	3.790	1.62	0.256
B	2	68.885	68.885	34.442	14.75	0.002
C	2	4.455	4.455	2.228	0.95	0.425
D	2	28.269	28.269	14.134	6.05	0.025
E	2	11.548	11.548	5.774	2.47	0.146
A*B	4	11.968	11.968	2.992	1.28	0.354
A*C	4	5.705	5.705	1.426	0.61	0.667
Error	8	18.685	18.685	2.336		
Total	26	157.095				

DF: degree of freedom; Seq.SS: sequential sum of squares; AdjSS: extra sum of squares; Adj MS: extra mean squares; p: level of significance

Table 7.5c. ANOVA table for erosion rate (for SiC filled composites)

Source	DF	Seq SS	Adj SS	Adj MS	F	p
A	2	15.576	15.576	7.788	2.22	0.171
B	2	18.563	18.563	9.282	2.65	0.131
C	2	4.943	4.943	2.471	0.70	0.523
D	2	40.043	40.043	20.022	5.71	0.029
E	2	7.027	7.027	3.514	1.00	0.409
A*B	4	19.899	19.899	4.975	1.42	0.312
A*C	4	6.819	6.819	1.705	0.49	0.747
Error	8	28.073	28.073	3.509		
Total	26	140.942				

DF: degree of freedom; Seq.SS: sequential sum of squares; AdjSS: extra sum of squares; Adj MS: extra mean squares; p: level of significance

Table 7.5d. ANOVA table for erosion rate (for CBPD filled composites)

Source	DF	Seq SS	Adj SS	Adj MS	F	p
A	2	8.607	8.607	4.304	1.85	0.219
B	2	34.433	34.433	17.216	7.38	0.015
C	2	2.563	2.563	1.282	0.55	0.598
D	2	23.428	23.428	11.714	5.02	0.039
E	2	10.230	10.230	5.115	2.19	0.174
A*B	4	10.256	10.256	2.564	1.10	0.419
A*C	4	5.722	5.722	1.431	0.61	0.665
Error	8	18.660	18.660	2.332		
Total	26	113.899				

DF: degree of freedom; Seq.SS: sequential sum of squares; AdjSS: extra sum of squares; Adj MS: extra mean squares; p: level of significance

7.7 Confirmation experiment

The optimal combination of control factors has been determined in the previous analysis. However, the final step in any design of experiment approach is to predict and verify improvements in observed values through the use of the optimal combination level of control factors. The confirmation experiment is performed by taking an arbitrary set of factor combination $A_2B_3D_1E_3$ for flyash filling, $A_1B_3D_2E_3$ for alumina filling, $A_1B_3D_2E_3$ for SiC filling and $A_2B_3D_2E_1$ for CBPD filling, but the factor C

has been intentionally omitted for all the cases because factor C and interaction A×C have the least effect on erosion rate as evident from Table 7.5a, b, c and d. The estimated S/N ratios for the composites with the three different fillers, the erosion rates can be calculated with the help of following prediction equations:

$$\hat{\eta}_{flyash} = \overline{T} + (\overline{A}_2 - \overline{T}) + (\overline{B}_3 - \overline{T}) + [(\overline{A}_2\overline{B}_3 - \overline{T}) - (\overline{A}_2 - \overline{T}) - (\overline{B}_3 - \overline{T})] + (\overline{D}_1 - \overline{T}) + (\overline{E}_3 - \overline{T}) \quad (7.4)$$

$$\hat{\eta}_{alu\min a} = \overline{T} + (\overline{A}_1 - \overline{T}) + (\overline{B}_3 - \overline{T}) + [(\overline{A}_1\overline{B}_3 - \overline{T}) - (\overline{A}_1 - \overline{T}) - (\overline{B}_3 - \overline{T})] + (\overline{D}_2 - \overline{T}) + (\overline{E}_3 - \overline{T}) \quad (7.5)$$

$$\hat{\eta}_{SiC} = \overline{T} + (\overline{A}_1 - \overline{T}) + (\overline{B}_3 - \overline{T}) + [(\overline{A}_1\overline{B}_3 - \overline{T}) - (\overline{A}_1 - \overline{T}) - (\overline{B}_3 - \overline{T})] + (\overline{D}_2 - \overline{T}) + (\overline{E}_3 - \overline{T}) \quad (7.6)$$

$$\hat{\eta}_{CBPD} = \overline{T} + (\overline{A}_2 - \overline{T}) + (\overline{B}_3 - \overline{T}) + [(\overline{A}_2\overline{B}_3 - \overline{T}) - (\overline{A}_2 - \overline{T}) - (\overline{B}_3 - \overline{T})] + (\overline{D}_2 - \overline{T}) + (\overline{E}_1 - \overline{T}) \quad (7.7)$$

where,

$\hat{\eta}_{flyash}, \hat{\eta}_{alu\min a}, \hat{\eta}_{SiC}$ *and* $\hat{\eta}_{CBPD}$ Predicted average

$\overline{T}$ Overall experimental average

$\overline{A}_1, \overline{A}_2, \overline{B}_3, \overline{D}_1, \overline{D}_2, \overline{E}_1$ *and* $\overline{E}_3$ Mean response for factors and interactions at designated levels.

The calculated predicted average values are compared with the experimental results for all the four test cases and the error associated with each set is determined, as shown in Table 7.6.The percentage errors are within the tolerance limit and therefore the model is considered to be capable of predicting erosion rate to a reasonable accuracy. However, the error can be further reduced if the number of measurements is increased. This validates the development of the mathematical model for predicting the measures of performance based on knowledge of the input parameters.

Table 7.6. Results of the confirmation experiments for erosion rate of the composites (with particulate fillers)

Type of filler	Optimal control factor settings	S/N ratio Predictive values (dB)	S/N ratio Experimental values (dB)	Error (%)
1. Flyash	$A_2B_3D_1E_3$	-51.4966	-48.4788	5.86
2. Alumina	$A_1B_3D_2E_3$	-47.9446	-45.6864	4.71
3. Silicon Carbide	$A_1B_3D_2E_3$	-47.0984	-48.4788	2.84
4. CBPD	$A_2B_3D_2E_1$	-48.8363	-47.0586	3.63

7.8 Factor settings for minimum erosion rate

In this study, an attempt is made to derive optimal settings of the control factors for minimization of erosion rate. The single-objective optimization requires quantitative determination of the relationship between erosion rates with combination of control factors. In order to express, erosion rate in terms of mathematical model in the following form is suggested.

$$Er = K_0 + K_1 \times A + K_2 \times B + K_3 \times D + K_4 \times E + K_5 \times A \times B \quad (7.8)$$

Here, E_r is the performance output terms and K_i (i = 0, 1……..5) are the model constants. The constant are calculated using non-linear regression analysis with the help of **SYSTAT 7.0** software and the following relations are obtained for all the three composites.

$$Er_{flyash} = 0.522 - 0.060 \times A - 0.378 \times B + 0.234 \times D + 0.022 \times E + 0.581 \times A \times B \quad r^2=0.96$$

$$Er_{alumina} = 0.467 - 0.031 \times A - 0.355 \times B + 0.273 \times D + 0.053 \times E + 0.382 \times A \times B \quad r^2=0.95$$

$$Er_{SiC} = 0.413 - 0.021 \times A - 0.412 \times B + 0.275 \times D - 0.047 \times E + 0.540 \times A \times B \quad r^2=0.96$$

$$Er_{CBPD} = 0.520 + 0.003 \times A - 0.404 \times B + 0.279 \times D + 0.018 \times E + 0.534 \times A \times B \quad r^2=0.97$$

The correctness of the calculated constants is confirmed as high correlation coefficients (r^2) in the range of 0.95 to 0.97 are obtained for Eq. (7.8) and therefore, the models are quite suitable to use for further analysis. Here, the resultant objective function to be maximized is given as:

Maximize Z =1/ f (7.9)

f Normalized function for erosion rate

Subjected to constraints:

$$A_{min} \leq A \leq A_{max} \quad (7.10)$$

$$B_{min} \leq B \leq B_{max} \quad (7.11)$$

$$D_{min} \leq D \leq D_{max} \quad (7.12)$$

$$E_{min} \leq E \leq E_{max} \quad (7.13)$$

The min and max in Eqs.7.10-7.13 shows the lowest and highest control factors settings (control factors) used in this study (Table 3.4). Genetic algorithm (GA) is used to obtain the optimum value for single-objective outputs to optimize the single-objective function. The computational algorithm is implemented in Turbo C^{++} and run on an IBM Pentium IV machine. Genetic algorithms (GAs) are mathematical optimization techniques that simulate a natural evolution process. They are based on the Darwinian Theory, in which the fittest species survives and propagate while the less successful tend to disappear. Genetic algorithm mainly depends on three types of operator's viz., reproduction, crossover and mutation. Reproduction is accomplished by copying the best individuals from one generation to the next, what is often called an elitist strategy. The best solution is monotonically improving from one generation to the next. The selected parents are submitted to the crossover operator to produce one or two children. The crossover is carried out with an assigned probability, which is generally rather high. If a number randomly sampled is inferior to the probability, the crossover is performed. The genetic mutation introduces diversity in the population by an occasional random replacement of the individuals. The mutation is performed based on an assigned probability. A random number is used to determine if a new individual will be produced to substitute the one generated by crossover. The mutation procedure consists of replacing one of the decision variable values of an individual while keeping the remaining variables unchanged. The replaced variable is randomly chosen and its new value is calculated by randomly sampling within its specific range. In genetic optimization, population size, probability of crossover and mutation are set at 50, 75 %, and 5 % respectively for all the cases. Number of generation is varied till the output is converted. Table 7.6 shows the optimum conditions of the control factors with the optimum performance output i.e. the minimum erosion rate for composites with different filler materials. The pattern of convergence of performance output with number of generations is shown in Figures 7.10a, b, c and d.

Table 7.7. Optimum conditions for performance output of the composites (with fillers)

Type of filler	Optimum conditions				
	Impact velocity A (m/sec)	Filler content B (wt %)	Impingement angle D (degree)	Erodent size E (μm)	Erosion rate Er (mg/kg)
1. Flyash	32.31	19.90	47.16	518.40	239.84
2. Alumina	56.89	11.82	61.56	788.00	271.83
3. Silicon Carbide	57.07	18.26	88.11	444.80	368.96
4. CBPD	44.23	19.01	56.28	618.00	263.47

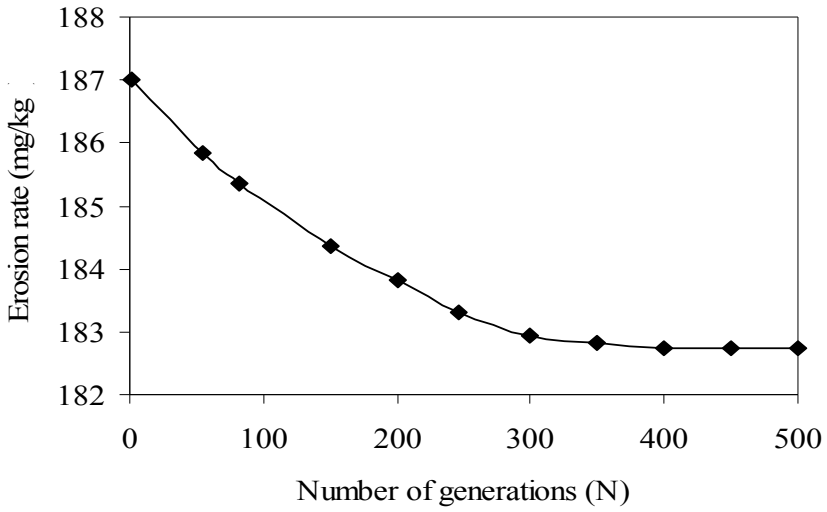

Figure 7.10a. Convergence Curve (for flyash filled composites)

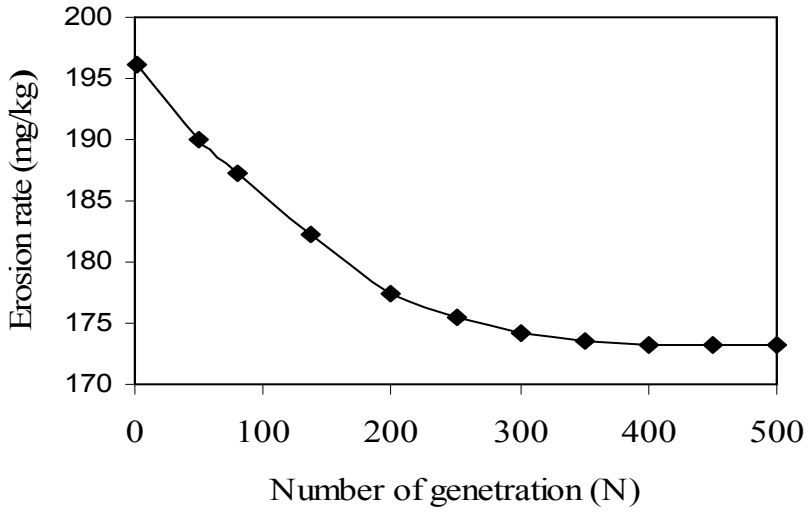

Figure 7.10b. Convergence Curve (for Al_2O_3 filled composites)

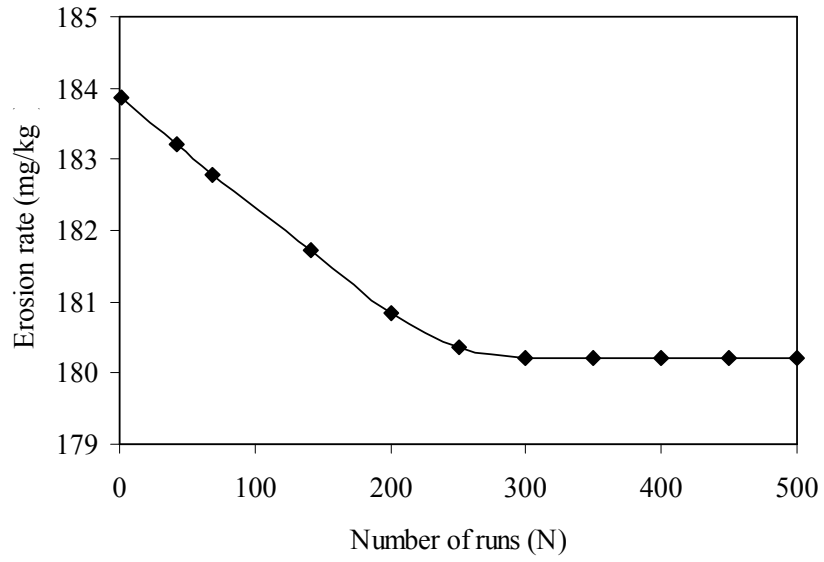

Figure 7.10c. Convergence Curve (for SiC filled composites)

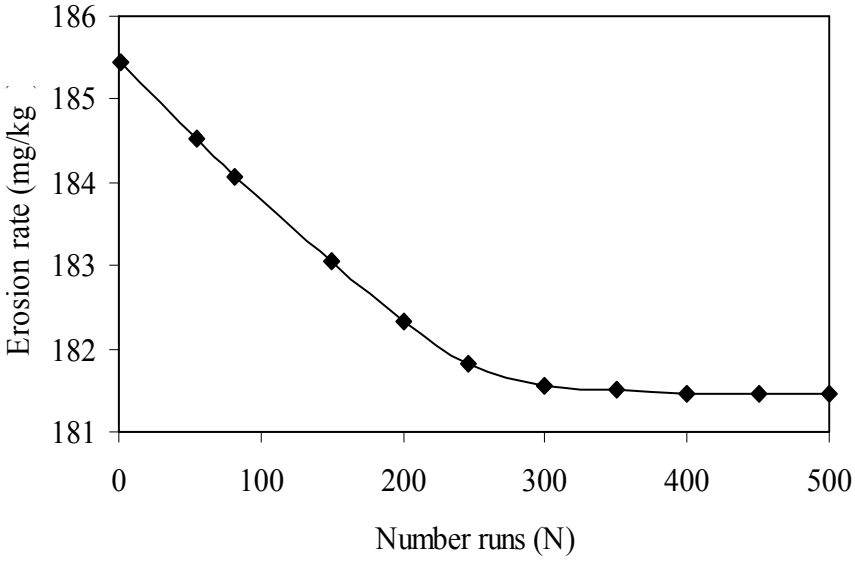

Figure 7.10d. Convergence Curve (for CBPD filled composites)

Chapter summary:

Based on the research presented in this chapter the following conclusions are drawn:

1. Multi-component hybrid composites consisting of isophthalic polyester reinforced with glass fiber and filled with particulate fillers such as flyash, Al_2O_3, SiC and CBPD possess fairly good potential for application in erosive environment.

2. Erosion characteristics of these composites can be successfully analyzed using Taguchi experimental design scheme.
3. The erosion wear performance of glass polyester composites improves with the incorporation of particulate fillers. Among all the materials chosen for this study, Al_2O_3 is found to be the filler imparting the maximum enhancement in the erosion resistance of the composite. The wear rates in case of flyash, SiC and CBPD filled composites are relatively higher than their alumina filled counterpart under similar test conditions.
4. The erosion efficiency (η), in general, characterizes the wear mechanism of composites. All these particulate filled composites exhibit semi-ductile erosion response (η =10-60%) for low impact velocities and ductile erosion response (η < 10%) for relatively high impact velocity. A study on the dependence of erosion wear on impingement angle also reveals their semi-ductile nature as the peak erosion rate is found to be occurring at 60^0 impingement angle for all the composites except the SiC filled ones where it has shifted to an angle of 75^0.
5. Factors like filler content, impingement angle, erodent size and impact velocity are found out to be the significant control factors affecting the erosion rate. The stand-off distance is identified as the least significant parameter as far as the wear of such composites is concerned.

The next chapter presents the executive summary and conclusions along with recommendations for future work.

****

Chapter 8

Executive Summary And Conclusions

Chapter 8

EXECUTIVE SUMMARY AND CONCLUSIONS

Introduction

The research reported in this thesis consists of two parts: the first part has provided the description of the experimental program and has presented the mechanical characteristics of the hybrid composites under this study and the second part has reported the effect of different ceramic fillers on the solid particle erosion characteristics of these glass-polyester composites. Two industrial wastes (flyash and cement by-pass dust), rich in metal oxides and two conventional ceramic powders (Al_2O_3 and SiC) have been used as the filler materials.

8.1 Summary of findings

By incorporating these particulate fillers into the glass-fiber reinforced polyester, synergistic effects, as expected were achieved in the form of modified mechanical properties and improved erosion wear resistance. Inclusion of glass fiber in neat polyester improved the load bearing capacity (tensile strength) and the ability to withstand bending (flexural strength) of the composites. But with the incorporation of particulate fillers, the tensile strengths of the composites were found to be less. There can be two reasons for this decline in tensile strength of these particulate filled composites compared to the unfilled one. One possibility is that the chemical reaction at the interface between the filler particles and the matrix may be too weak to transfer the tensile stress; the other is that the corner points of the irregular shaped particulates result in stress concentration in the polyester matrix.

Hardness values have been found to have marginally improved for most of the particulate filled composites. The reduction in tensile strength and the improvement in hardness with the incorporation of fillers can be explained as follows: under the action of a tensile force the filler-matrix interface is vulnerable to debonding depending on interfacial bond strength and this may lead to a break in the composite. But in case of hardness test, a compression or pressing stress is in action. So the polymeric matrix phase and the solid filler phase would be pressed together and touch each other more tightly. Thus, the interface can transfer pressure

more effectively although the interfacial bond may be poor. This might have resulted in an enhancement of hardness.

High strain rates or impact loads may be expected in many engineering applications of composite materials. The suitability of a composite for such applications should therefore be determined not only by usual design parameters, but by its impact or energy absorbing properties. Thus it is important to have a good understanding of the impact behavior of composites for both safe and efficient design of structures and to develop new composites having good impact properties. The results of impact tests in the present study reveal that the addition of the ceramic fillers has enhanced the impact strength of all the composite samples and the maximum improvement was recorded for the composites with cement by-pass dust (CBPD) filling. This establishes CBPD as a promising filler material.

The presence of pores and voids in the composite structure significantly affect some of the mechanical properties and even the performance of the composites. Higher void contents usually mean lower fatigue resistance, greater susceptibility to water penetration and weathering. However, presence of void is unavoidable in composite making particularly through hand-lay-up route. In the present investigation, it was noticed that the composites with particulate fillers have higher void fraction compared to the unfilled glass polyester composites. Among the particulate filled composites, least values of void content are recorded for composites with cement by-pass dust filling and this finding further supports the candidature of CBPD as potential filler in future hybrid composites.

The possible wear mechanism during solid particle erosion of glass-fibre reinforced polyester composites, as evident from test results and scanning electron microscopy, can be characterized as follows.

- First, there is local removal of resin material from the impacted surface which results in exposure of the fibres to the erosive environment.
- Sand particles impact on the fibres and cause fibres to break because of the formation of cracks perpendicular to their length. These cracks are presumably caused by fibre-bending stresses due to the impact of erodent particles on the unsupported fibers.

- Further damage results when the interfaces between the broken fibers and the matrix resin are degraded until the fibers are removed by subsequent impacts.

The erosion wear rates of particulate filled glass-polyester composites are found to be lower than those of the unfilled glass-polyester composites under similar test conditions. This has led to the conclusion that the presence of ceramic fillers improves the erosion wear resistance of fiber reinforced polyester. The reduction in material loss in these particulate filled composites can be attributed to two reasons. One is the improvement in the bulk hardness of the composite with addition of these hard ceramic particles. Secondly, during the erosion process, the filler particles absorb a good part of the kinetic energy associated with the erodent. This results in less amount of energy being available to be absorbed by the matrix body and the reinforcing glass fiber phase. These two factors together lead to the enhancement of erosion wear resistance of the composites. This study thus, shows that the filler content in the composite is significant in combating erosive wear.

The erosion wear rates of the composites were found to be dependent on the impingement angle. The findings of this research further suggest that, this dependency is also influenced by the nature of the filler material. In fact, the angle of impact determines the relative magnitude of the two components of the impact velocity namely, the component normal to the surface and parallel to the surface. The normal component will determine how long the impact will last (i.e. contact time) and the load. The product of this contact time and the tangential (parallel) velocity component determines the amount of sliding that takes place. The tangential velocity component also provides a shear loading to the surface, which is in addition to the normal load that the normal velocity component causes. Hence, as this angle changes the amount of sliding that takes place also changes the nature and magnitude of the stress system. Both of these aspects influence the way a composite wears out. This study therefore implies that composites with fillers of different type and content would exhibit different angular dependency.

8.2 Contribution of the research work

This analytical and experimental investigation on glass-polyester composites (with and without particulate fillers) has led to the following specific conclusions:

1. Successful fabrication of multi-component hybrid glass-polyester composites with reinforcement of ceramic fillers such as Al_2O_3 and SiC is possible. Industrial wastes like flyash and cement by-pass dust (CBPD) can also be gainfully utilized as fillers.
2. Incorporation of these fillers modifies the tensile, flexural, impact and inter-laminar shear strengths of the glass polyester composites. The micro-hardness and density of the composites are also greatly influenced by the type and content of fillers. Hence, while fabricating a composite of specific requirements, there is a need for the choice of appropriate filler material and for optimizing its content in the composite system.
3. A theoretical model based on conservation of particle kinetic energy during multiple impact erosion process has been developed. To overcome the shortcomings of the existing theoretical models, an 'erosion efficiency' term has been introduced. It is demonstrated that if supported by an appropriate magnitude of erosion efficiency, the model can perform well for polymer based hybrid composites for normal as well as oblique impacts.
4. The unfilled glass polyester composite has a strength of 349.6 MPa in tension and it may be seen from Table 4.2 that this value drops to 304.5 MPa and 279.4 MPa with addition of 10 wt% and 20 wt% of flyash respectively. Among the four fillers taken in this study, the inclusion of alumina causes maximum reduction in the composite strength.
5. It is interesting to note that composites C_2 (Polyester +50wt% glass fiber + 10wt% flyash),C_4 (Polyester +50wt% glass fiber +10wt% Alumina) and C_8 (Polyester +50wt% glass fiber +10wt% CBPD) with addition of small amount (10 wt%) of fly ash, alumina and CBPD exhibited improved flexural strength compared to the unfilled glass-polyester composite C_1(Polyester +50wt% glass fiber) from 368 MPa to 463.34MPa. But for the composite samples (C_3,C_5 and C_9) with 20 wt% of these fillers lower values of the flexural strength are recorded. However, this trend is not found in the composites (C_6 and C_7) with silicon carbide particles, where the flexural strength of the glass-polyester system declines monotonically with filler content from 309.2MPa to 353.8MPa.
6. Significant control factors affecting the erosion rate have been identified through successful implementation of analysis of variance (ANOVA). Filler

content, impingement angle, erodent size and impact velocity in declining sequence are found to be significant for minimizing the erosion rate of all the particulate filled composites except the ones with SiC filling. In the SiC filled composite impingement angle emerged as the most significant control factor followed by filler content, impact velocity and erodent size.

7. The presence of particulate fillers in these composites improves their erosion wear resistance and this improvement depends on the type and content of the fillers. Among the four different fillers taken in this work, Al_2O_3 is found to be the best one as far as the improvement in the wear performance of the composites is concerned.
8. Significant control factors affecting the erosion rate have been identified through successful implementation of analysis of variance (ANOVA). Filler content, impingement angle, erodent size and impact velocity in declining sequence are found to be significant for minimizing the erosion rate of all the particulate filled composites except the ones with SiC filling. In the SiC filled composite impingement angle emerged as the most significant control factor followed by filler content, impact velocity and erodent size.
9. The erosion efficiency (η), in general, characterizes the wear mechanism of composites. All these particulate filled composites exhibit semi-ductile erosion response (η =10-60%) for low impact velocities and ductile erosion response (η < 10%) for relatively high impact velocity. A study on the dependence of erosion wear on impingement angle also reveals their semi-ductile nature as the peak erosion rate is found to be occurring at 60^0 impingement angle for all the composites except the SiC filled ones where it has shifted to an angle of 75^0.
10. It is demonstrated that two predictive models; one based on ANN and the other on Taguchi approach well reflect the effects of various factors on the erosion loss.
11. Optimal factor settings for minimum wear rate of any composite can be determined using an effective technique based on genetic algorithm. The rationale behind the use of genetic algorithm lies in the fact that it has the capability to find the global optimal parameter settings, whereas the traditional optimization techniques are normally stuck up at the local optimum values.

8.3 Recommendations

Composite materials show excellent performance, these days, starting from manufacturing point of view to sports goods. It is due to their light weight, high stiffness-to-weight and strength-to-weight ratios, and potentially high resistance to environmental degradation, resulting in lower life-cycle costs.

The particulate filled glass-fiber reinforced hybrid composites fabricated and experimented upon in this investigation are found to have adequate potential for a wide variety of applications particularly in erosive environment. When solid particle erosion is not the predominant degrading factor, only glass-fiber polyester composites without any particulate filler can be recommended. Manufacturing of light weight sports goods such as: cricket bat, tennis racquets etc. is one such example. Of course, the weight fraction of fiber in the composite is to be decided from the view point of required strength.

If the place of use is erosive in nature, then particulate filled glass-fiber reinforced composite is to be preferred due to their reasonably high erosion resistance. The present study has established that Al_2O_3 and SiC can be excellent candidates as particulate fillers in hybrid composites. Their use may be suggested in applications like engineering structures in dusty environment and low cost building materials in deserts. The type and content of fillers are to be decided judiciously keeping the strength and intensity of erosion attack in mind. However, when cost reduction is the prime consideration, industrial wastes like flyash and cement by-pass dust can effectively replace the conventional and relatively expensive materials like Al_2O_3 and SiC. Use of all these composites, in general, may also be recommended for applications like partition boards, false ceilings, pipe lines carrying coal dust, exhaust fan blades, nozzles and diffusers, light weight vehicles etc.

Scope for future work

The present work leaves a wide scope for future investigators to explore many other aspects of particulate filled FRP composites. Some recommendations for future research include:

- The response of these composites to other wear modes such as sliding and abrasion.
- Possible use of other ceramic/metallic fillers, polymeric resins other than polyester and natural fibers in the development of new hybrid composites.

References

References

1. Agarwal B.D and Broutman L. J, (1990). Analysis and performance of fiber composites, Second edition, John wiley & Sons, Inc, pp.2-16.
2. Tong L, Mouritz A.P and Bannister M.K, (2002). 3D Fibre Reinforced Polymer Composites, ELSEVIER SCIENCE Ltd, The Boulevard, Langford Lane, Kidlington, Oxford OX5 IGB, UK, 1-2.
3. Jang B. Z, (1994). Advanced Polymer composites: principles and applications. ASM International.
4. Kuljanin J, Vuckovic M, Comor M.I, Bibic N, Djokovic V and Nedeljkovic J.M. (2002). Influence of CdS-filler on the thermal properties of polystyrene, European Polymer Journal, 38(8):1659–1662.
5. Weidenfeller B, Höfer M, Schilling F. (2004). Thermal conductivity, thermal diffusivity, and specific heat capacity of particle filled polypropylene, *Composites Part A*: Applied Science and Manufacturing, 35 (4):423–429
6. Stolarski T.A, (1990). Tribology in Machine Design, Heiman Newnes, UK.
7. Päivi Kivikytö-Reponen, (2006). Correlation of Material Characteristics and Wear of Powder Metallurgical Metal Matrix Composites, Doctoral Theses in Materials and Earth Sciences, Helsinki University of Technology, Laboratory of Materials Science, Espoo, 1-2.
8. Halling, (1975). Principles of tribology, The McMillan Press Ltd, NY, USA
9. Budinski K.G, (1998). Surface Engg. for Wear Resistance, N.J, USA.
10. Robinowicz E, (1965). Friction and wear of materials, Willey, NY, USA.
11. Thomas H. Kosel, (1992). ASM Handbook: Friction, Lubrication, and Wear Technology, ASM International Handbook Committee. 18, 371-372.
12. Pool K.V, Dharan C.K.H, and Finnie I, (1986). Erosion wear of composite materials, wear, vol. 107, 1-12
13. Aglan H.A and Chenock T.A Jr., (1993). Erosion damage features of polyimide Thermoset composites, SAMPE Quartery, 41-47.
14. Rao P.V, (1995). Characterization of optical and surface parameters during particle impact damage, ASME/Fluids engineering publications, 23:87-96.
15. Tennyson, R.C, (1991). LDEF Mission update: composites in space, Advance materials & processes, 5:33-36.

16. Gregory Sawyer W, Freudenberg Kevin D, Bhimaraj Pravee and Schadler Linda S, (2003). A study on the friction and wear behavior of PTFE filled with alumina nanoparticles, Wear, 254:573–580.
17. Jung-il K., Kang P.H and Nho Y.C, (2004). Positive temperature coefficient behavior of polymer composites having a high melting temperature, J Appl Poly Sci., 92:394–401.
18. Nikkeshi S, Kudo M and Masuko, T, (1998). Dynamic viscoelastic properties and thermal properties of powder-epoxy resin composites, J Appl Poly Sci., 69:2593-8.
19. Zhu, K and Schmauder, S, (2003). Prediction of the failure properties of short fiber reinforced composites with metal and polymer matrix, Comput Mater Sci. 28:743–8.
20. Rusu M, Sofian N and Rusu D, (2001). Mechanical and thermal properties of zinc powder filled high density polyethylene composites, Polym Test, 20: 409–17.
21. Tavman I. H, (1997). Thermal and mechanical properties of copper powder filled poly (ethylene) composites, Powder Technol, 91: 63–7.
22. Rothon R.N, (1997). Mineral fillers in thermoplastics: filler manufacture, J Adhesion, 64:87–109.
23. Rothon R.N, (1999). Mineral fillers in thermoplastics: filler manufacture and characterization. Adv. Polym. Sci. 139: 67–107.
24. Bonner W.H, (1962). U.S. Patent 3,065,205.
25. Nielsen L.E and Landel R.F, (1994). Mechanical properties of polymers and composites. 2nd ed. New York: Marcel Deckker, pp.377–459.
26. Peters S.T, (1998). Handbook of composites. 2nd ed. London: Chapman and Hall, pp. 242–243.
27. Young R.J and Beaumont P.W.R, (1977). Failure of brittle polymers by slow crack growth Part 3 Effect of composition upon the fracture of silica particle-filled epoxy resin composites. J Mater Sci., 12(4): 684–92.
28. Kinoch A.J, Maxwell D.L and Young R.J, (1985).The fracture of hybrid particulate composites. J Mater Sci., 20:4169–84.
29. Young R, Maxwell D.L and Kinloch A.J, (1986). The deformation of hybrid particulate composites. J Mater Sci., 21:380–388.

30. Koh S.W, Kim J.K and Mai Y.W, (1993). Fracture toughness and failure mechanisms in silica-filled epoxy resin composites: effects of temperature and loading rate. Polymer, 34(16):3446–3455.
31. Cantwell W.J and Moloney A.C, (1994). Fractography and failure mechanisms of polymers and composites. Amsterdam: Elesvier, pp.233.
32. Imanaka M, Takeuchi Y, Nakamura Y, Nishimura A and Lida T, (2001).Fracture toughness of spherical silica-filled epoxy adhesives. Int J Adhesin Adhes., 21:389–396.
33. Wang H, Bai Y, Lui S, Wu J and Wong C.P, (2002). Combined effects of silica filler and its interface in epoxy resin. Acta Mater., 50:4369–4377.
34. Yamamoto I, Higashihara T and Kobayashi T, (2003). Effect of silica-particle characteristics on impact/usual fatigue properties and evaluation of mechanical characteristics of silica-particle epoxy resins. JSME Int J, 46(2):145–153.
35. Nakamura Y, Yamaguchi M, Kitayama A, Okubo M and Matsumoto T, (1991). Effect of particle size on fracture toughness of epoxy resin filled with angular-shaped silica. Polymer, 32(12):2221–2229.
36. Nakamura Y, Yamaguchi M, Okubo M and Matsumoto T, (1991). Effect of particle size on impact properties of epoxy resin filled with angular shaped silica particles. Polymer, 32(16):2976–2979.
37. Nakamura Y, Yamaguchi M, Okubo M and Matsumoto T, (1992). Effects of particle size on mechanical and impact properties of epoxy resin filled with spherical silica. J Appl Polym Sci, 45:1281–1289.
38. Moloney A.C, Kausch H.H and Stieger H.R, (1983). The fracture of particulate filled epoxide resins. J Mater Sci., 18:208–216.
39. Moloney A.C, Kausch H.H, Kaiser T and Beer H.R, (1987). Review parameters determining the strength and toughness of particulate filled epoxide resins. J Mater Sci., 22:381–393.
40. Moloney A.C, Cantwell W.J and Kausch H.H, (1987). Parameters determining the strength and toughness of particulate-filled epoxy resins. Polym Compos., 8(5):314–323.
41. Adachi T, Araki W, Nakahara T, Yamaji A and Gamou M, (2002). Fracture toughness of silica particulate-filled epoxy composite. J Appl Polym Sci., 86:2261–2265.

42. Yuan J.J, Zhou S.X, Gu G.G and Wu L.M, (2005). Effect of the particle size of nanosilica on the performance of epoxy/silica composite coatings. J Mater Sci., 40:3927–3932.
43. Ng C.B, Schadler L.S and Siegel R.W, (1999). Synthesis and mechanical properties of TiO2-epoxy nanocomposites. Nanostruct Mater., 12:507–510.
44. Karger-Kocsis J, (1995). Microstructural aspects of fracture in polypropylene and in its filled, chopped fiber and fiber mat reinforced composites. In: Karger-Kocsis J, editor. Polypropylene: Structure, blends and composites. London: Chapman & Hall; pp. 142–201.
45. Pukanszky B, (1995). Particulate filled polypropylene: structure and properties. In: Karger-Kocsis J, editor. Polypropylene: Structure, blends and composites. London: Chapman & Hall; pp. 1–70.
46. Karger-Kocsis J, (2000). Swirl mat- and long discontinuous fiber matreinforced polypropylene composites-status and future trends. Polym Compos., 21:514–22.
47. Stokes V.K, Inzinna L.P, Liang E.W, Trantina G.G and Woods J.T, (2000). A phenomenological study of the mechanical properties of long fiber filled injection-molded thermoplastic composites. Polym Compos., 21(5):696–710.
48. Srivastava V.K, Prakash R and Shembekar P.S, (1988). Fracture behaviour of fly ash filled FRP composites. Compos Struct., 10:271–9.
49. Srivastava V.K and Shembekar P.S, (1990). Tensile and fracture properties of epoxy resin filled with flyash particles. J Mater Sci., 25:3513–3516.
50. Baré W, Albano C, Reyes J and Domínguez N, (2002). Effect of irradiation on the mechanical properties of high-density polyethylene reinforced with metallic fibres, Surface and Coatings Technolog**y**, Volumes 158-159:404-407
51. Gracia R, Evans R.E and Palmer R.J, (1987). Toughened composites, STP 937, N.J.Johnson, Ed., ASTM. 397-412.
52. Gracia R, (1983). Nadc-83058-60, July.
53. Lin T.L and Jang B.Z, (1989). Ann. Tech. Conf. (ANTEC) (New York), May.
54. Liau J.Y, Jang B.Z, Hwang L.R and Wilcox R.C, (1988). Plast. Eng., Nov.
55. Bijwe J, Logani C.M and Tewari U.S, (1990). Influence of fillers and fiber reinforcement on abrasive wear resistance of some polymeric composites, Wear, 138:77–92.

56. Wang M, Gu B and Songhao Ge S, (2003). Investigation of the influence of MoS2 filler on the tribological properties of carbon fiber reinforced nylon 1010 composites, Wear, 255:774–779.
57. Sunkara, (2000). The Role of Particulate Inorganic Fillers on the Tribological Behavior of Polyphenylene Sulfide, MS thesis, Iowa State University, Ames,
58. Hanmin Z, Guoren H and Guicheng Y, (1987). Friction and wear of poly (phenylene sulfide) and its carbon fiber composites: I Unlubricated, Wear, 116: 59–68.
59. Bahadur S, Gong D and Anderegg J.W, (1993). Tribochemical studies by XPS analysis of transfer films of nylon 11 and its composites containing copper compounds, Wear, 165:205–212.
60. Bahadur S, Gong D and Anderegg J, (1996). Investigation of the influence of CaS, CaO, and CaF2 fillers on the transfer and wear of nylon by microscopy and XPS analysis, Wear, 197: 271–279.
61. Hollaway L, (1994). Handbook of Polymer Composites for Engineers, Woodhead Publishing Ltd., Cambridge, pp. 1.
62. Pritchard G, (1999). Reinforced Plastics Durability, Woodhead Publishing Ltd., Cambridge, pp. 1.
63. Mason J.S and Smith B.V, (1972). The erosion of bends by pneumatically conveyed suspensions of abrasive particles, Powder Technol., 6: 323–335.
64. Tsai W, Humphrey J.A.C, Cornet I and Levy A.V, (1981). Experimental measurement of accelerated erosion in a slurry pot tester, Wear, 68: 289–303.
65. Hojo H, Tsuda K and Yabu T, (1986). Erosion damage of polymeric material by slurry, Wear, 112: 17–28.
66. Kumar R, Verma A.P and Lal G.K, (1983). Nozzle wear during the flow of a gas–particle mixture, Wear, 91: 33–43.
67. Crowley M.S, (1969). Influence of particle size on erosion resistance of refractory concretes, Am. Ceram. Soc. Bull. 48: 707–710.
68. Wright I.G, (1979). Proc. Corrosion/Erosion of Coal Conversion Systems Materials Conf., Berkeley, 103–138.
69. Jansson S.A, (1982). Proc. Corrosion-Erosion-Wear of Materials in Emerging Fossil Energy Systems, Berkeley, 548–560.
70. Neilson J.H and Gilchrist A, (1968). An experimental investigation into aspects of erosion in rocket motor tail nozzles, Wear 11:123–143.

71. Hibbert W.A, (1965). Helicopter trials over sand and sea, J. Roy. Aeronaut. Soc. 69: 769–776.
72. Tilly G. P,(1969). Erosion caused by airborne particles, Wear, 14(1):63-79.
73. Zahavi J, Nadiv S and Schmitt Jr G. F, (1981). Indirect damage in composite materials due to raindrop impact, Wear, 72(3):305-313
74. Tilly G. P and Wendy Sage, (1970). The interaction of particle and material behaviour in erosion processes, Wear, 16(6):447-465.
75. Tsiang T.H,(1989).Sand erosion of fiber composites: Testing and evaluation in CC. Chamis (Ed.), Test methods for design allowables for fibrous composites, Vol. 2, American Society for Testing and Materials, (ASTM) STP I003, Philadelphia, pp. 55-74.
76. Mathias P-J., Wu W, Goretta K.C, Routbort L.J, Groppi D.P and Karasek K.R, (1989). Solid particle erosion of a graphite-fiber reinforced bismaleimide polymer composite, Wear, I35: 161-169.
77. Abdul-Latif and Ali ahmed. (1987) Geostatistical estimation of reserves in the Abu-Tartur phosphate deposits western desert, Egypt. Masters thesis, King Fahd University of Petroleum and Minerals.
78. Karasek K.R, Goretta K.C, Helberg D.A and Routbort J.L, (1992). J. Mater. Sci. Lett., II 1143.
79. Tilly G.P, (1969). Sand erosion of metals and plastics: A brief review, Wear, 14(4):241-248.
80. Finnie I, (1960). An experimental study of erosion, Proc. Sot. Exp. Stress Anal., 17:65 - 70.
81. Finnie I, (1960). Erosion of surface by solid particles, Wear, 3: 87 - 103.
82. Smeltzer C. E, Gulden M. E and Compton W. A, (1970). Mechanisms of material removal by impacting dust particles, J. Basic Eng., 92: 639 - 654.
83. Schmitt G. P, (1970). The erosion behavior of polymeric coatings and composites at subsonic velocities. In A. A. Fyall and R. B. King (eds.), Proc. 3rd Int. Conf. on Rain Erosion and Associated Phenomena, Royal Aircraft Establishment, Farnborough, pp. 107 - 128.
84. Zahavi J and Schmitt, Jr., G. F, (1981). Solid particle erosion of polymeric coatings, Wear, 71: 191- 210.
85. Zahavi J and Schmitt Jr. G. F, (1981). Solid particle erosion of reinforced composite materials, Wear, 71: 179 - 190.

86. Ruff A.W and Wiederhorn S.M. (1979). Erosion by solid particle impact. In: Preece CM, editor. Treatise on materials science and technology, vol. 16. New York: Academic Press., pp. 69–125.
87. Preece C.M and Macmillan N.H, (1977). EROSION, Annual Review of Materials Science, 7: 95-121.
88. Sundararajan G, (1983). The solid particle erosion of metals and alloys. *Trans. Indian Inst. Met.* 36(6):474–495.
89. Evans A.G and Wilshaw T.R, (1976), Quasi-static solid particle damage in brittle solids, I. Observations, analysis and implications, Acta Metal., 24:939-956.
90. Kleis I,(1969). Probleme der Bestimmung des Strahlverschleisses bei metallen
Wear, 13(3):199-215.
91. Abrahamson G.R, (1961). Permanent periodic surface deformations due to a travelling jet, J. Appl. Mech. E 83: 519-528.
92. Cousen A. K, Hutchings I. M, Field J. E and Comey N. S (eds.), (1983). Proc. 6th Int. CM on Erosion by Liquid and Solid Impact, Cavendish Laboratory, University of Cambridge, 1983, Cambridge, Paper 41.
93. Venugopal Reddy A and Sundararajan G, (1986). Erosion behaviour of ductile materials with a spherical non-friable erodent, Wear, 111(3):313-323.
94. Sheldon G.L and Finnie I, (1966). On the ductile behavior of nominally brittle materials during erosive cutting, Trans ASME J Eng Ind., 88:387–392.
95. Zum Gahr K. H, (1987). Microstructure and Wear of Materials, tribology Series, Vol. 10, Elsevier, Amsterdam.
96. Kruschov M.M. (1974). Principles of abrasive wear, Wear, 28:69–88.
97. Murray M. J, Watson J. D, Mutton P and Ludema K. C, (ed.), (1979). Proc. Int. Conf. on Wear of Materials, American Society of Mechanical Engineers, New York, pp. 257.
98. Richardson R. C. D, (1967). The maximum hardness of strained surfaces and the abrasive wear of metals and alloys, Wear, 10(5):353-382.
99. Ericson F, Johansson S and Schweitz, J.-Å. (1988). Hardness and fracture toughness of semiconducting materials studied by indentation and erosion techniques. Mater. Sci. Eng. A: 105/106:131-141.

100. Wiederhorn M and Hockey B. J, (1980). Effect of material parameters on the erosion resistance of brittle materials, J. Mater. Sci., 18:766-780.
101. Friedrich K and Ludema K. C, (ed.), (1987). Proc. Int. Conf. on wear of Materials, American Society of Mechanical Engineers, New York, pp. 833.
102. Lamy B, (1984). Effect of brittleness index and sliding speed on the morphology of surface scratching in abrasive or erosive processes, Tribol. Int., 17(1):35-38.
103. Briscoe, B, (1981). Wear of Polymers-An Essay on Fundamental-Aspects, Tribol Int, 14: 231 –243.
104. Häger A, Friedrich K, Dzenis Y and Paipetis S.A, (1995). Study of erosion wear of advanced polymer composites, in: K. Street, B. Whistler (Eds.), Proceedings of the ICCM-10, Canada, Wood-head Publishing Ltd., Cambridge, UK, 155–162.
105. Finnie I, (1972). Some observations on the erosion of ductile metals, wear, 19:81-90.
106. Miyazaki N and Takeda N, (1993). Solid particle erosion of fiber reinforced plastics, J. Compos. Mater., 27 (1): 21–31.
107. Miyazaki N and Hamao T, (1996). Effect of interfacial strength on erosion behavior of FRPs, J. Compos. Mater., 30: 35–50.
108. Roy M, Vishwanathan B and Sundararajan G, (1994). Solid particle erosion of polymer matrix composites, Wear, 171:149–161.
109. Miyazaki N and Hamao T, (1994). Solid particle erosion of thermoplastic resins reinforced by short fibers, J. Compos. Mater., 28 (9): 871–883.
110. Haraki N, Tsuda K and Hojo H, (1992). Sand erosion behaviour of composites reinforced with glass cloth laminates, Adv. Compos. Lett., 1 (1): 31–33.
111. Lhymn C and Lhymn Y.O, (1989). Erosive wear of fibrous PEEK composites, in: Proceedings of the 21st International SAMPE Technical Conference, Eric, PA, USA, 25–28 September, 720–729.
112. Hovis S.K, Talia J.E and Scattergood R.O, (1986). Erosion in multiphase systems, Wear, 108:139–155.
113. Ballout Y.A, Hovis S.K and Talia J.E, (1990). Erosion in glass–fiber reinforced epoxy composite, Scripta Metallurgicaet materialia, 24: 195–200.

114. El-Tayeb N.S.M and Yousif B.F, (2007). Evaluation of glass fibre reinforced polyester composite for multi-pass abrasive wear applications, Int. J. Wear, 262:1140–1151.
115. Zum Gahr K.-H, (1987). Microstructure and wear of materials, Tribology Series 10, Elsevier, Amsterdam.
116. Finnie I, (1995). Some reflections on the past and future of erosion, Wear, 186/187:1–10.
117. Finnie I, (1960). Erosion of surfaces by solid particles. Wear, 3:87–103. 192.
118. Kulkarni S.M and Kishore K, (2001). Influence of matrix modification on the solid particle erosion of glass/epoxy composites. Polym Polym Compos, 9:25–30.
119. Finnie I, Stevick G.R and Ridgely J.R, (1992). The influence of impingement angle on the erosion of ductile metals by angular abrasive particles, Wear 152: 91–98.
120. Chevallier P and Vannes A.B, (1995). Effect on a sheet surface of an erosive particle jet upon impact, Wear 184:87–91.
121. Tabakoff W, (1995). High-temperature erosion resistance of coatings for use in turbo machinery, Wear 186/187:224–229.
122. Lammarre L, (1990). EPRI J. October-November-31.
123. Tirupataiah Y, Venkataraman B and Sundararajan G, (1990). The nature of the elastic rebound of a hard ball impacting on ductile, metallic target materials, Materials Science and Engineering: A, 124(2):133-140.
124. Tabakoff W, (1991). Measurements of particles rebound characteristics on materials used in gas turbines, Journal of Propulsion and Power, 7(5): 805-813.
125. Metwally M, Tabakoff W and Hamed A, (1995). Blade Erosion in Auto-motive
Gas Turbine Engine, ASME J. Eng. Gas Turbines Power, 117:213–219.
126. Wahl H, Hartenstein F, Strahlverschleiss, Frankh'sche Verlagshandlung, Stuttgart, 1946.
127. Neilson J. H, Gilchrist A, (1968). Erosion by a stream of solid particles Wear, 11(2):111-122.
128. Hibbert, W.A. (1965). Helicopter trials over sand and sea, J. Roy. Aero. Soc., 69: 769-776.

129. Gandhi B.K, Singh S.N and Seshadri V, (1999). Study of the parametric dependence of erosion wear for the parallel flow of solid–liquid mixtures, Tribol. Int. 32: 275–282.
130. Raask E, (1969). Tube erosion by ash impaction, Wear, 13(4-5):301-315.
131. Preece C. M and Macmillan N. H, (1977). Erosion, Annual Review of Materials Science, 7: 95-121.
132. Engel P.A, (1976). Impact Wear of Materials, Amsterdam, Elsevier, Amsterdam.
133. Finnie I, Levy A and McFadden D.H, (1979). Fundamental Mechanisms of the Erosion Wear of ductile metals by solid particles, ASTM STP 664: 36.
134. Barkoula N. M., (2002). in Solid Particle Erosion Behaviour of Polymers and Polymeric Composites"(IVW-Schriftreihe 29, Kaiserslautern)
135. Sheldon G.L, Similarities and differences in the erosion behaviour of materials. Trans. ASME, J. Basic Eng., Ser. D 92 (1970), pp. 619–626.
136. Hockey B.J, Wirderhorn S.M and Johnson H, (1978). Fracture Mechanics of Ceramics, Vol. 3, Flaws and Testing, Plenum, New York.
137. Sheldon G.L and Finnie I, (1966). Trans. ASME J. Eng. Ind. 88: 387–392.
138. Ballout Y.A, (1998). Erosion Mechanisms in Composite Materials and Ripple Formation Mechanism in Erosion, PhD Dissertation, Wichita State Univ.
139. Ibrahim A.T, (1990). A Mechanisms for Solid Particle Erosion in Ductile and Brittle Materials, MS Thesis, Wichita State Univ.
140. Tilly G.P. (1979). Erosion caused by impact of solid particles. In: Scott D, editor. Treatise on materials science and technology, 13:28-7.
141. Arnold J.C and Hutchings I.M. (1990). The mechanisms of erosion of unfilled elastomers by solid particle impact. Wear, 138:33–46.
142. Arnold J.C and Hutchings I.M. (1989). Flux rate effects in the erosive wear of elastomers. J Mater Sci., 24:833–839.
143. Friedrich K, (1986). Erosive wear of polymer surfaces by steel ball blasting. J Mater Sci., 21:3317–3332.
144. Zahavi J. (1981). Solid particle erosion of polymeric coatings. Wear; 71:191–210.
145. Williams Jr. J.H and Lau KE. (1974). Solid particle erosion of graphite epoxy composites. Wear, 29:219–30.

146. Dhar S, Krajac T, Ciampini D and Papini M, (2005).Erosion mechanisms due to impact of single angular particles, Wear, 258(1–4):567–579.
147. Gomes Ferreira C, Ciampini D and Papini M, (2004). The effect of inter-particle collisions in erosive streams on the distribution of energy flux incident to a flat surface, Tribology International, 37:791–807.
148. Tilly G.P, (1973). A two stage mechanisms of ductile erosion. Wear, 23:87–96.
149. Wiederhorn S.M and Hockey B.J, (1983). Effect of material parameters on the erosion resistance of brittle materials. J Mater Sci., 18:766–780.
150. Scattergood R.O and Routbort J.L, (1981). Velocity and size dependence of the erosion rate in silicon. Wear, 67:227.
151. Thai C.M, Tsuda K and Hojo H, (1981). Erosion behaviour of polystyrene. J Test Eval, 9(6):359–365.
152. Karasek K.R, Goretta K.C, Helberg D.A and Rourbort J.L. (1992). Erosion in bismaleimide polymers and bismaleimide-polymer composites. J Mater Sci Lett; 11:1143–1144.
153. Rao P.V and Buckley D.H, (1985). Angular particle impingement studies of thermoplastic materials at normal incidence. ASLE Trans, 29(3):283–298.
154. John Rajesh J, Bijwe J, Tewri U.S and Venkataramanan B, (2001). Erosive wear of various polyamides. Wear, 249(8):702–714.
155. G.A. Sargent, P.K. Mehrotra and Conrad H, Erosion prevention and useful application, ASTM STP 664 (W.F. Adler ed.), America1 Society for Testing and Materials, 1979, p.77.
156. Humphrey J.A.C, (1990). Fundamentals of fluid motion in erosion by solid particle impact. Int J Heat Fluid Flow, 11(3):170–195.
157. Rochester M.C and Brunton J.H, (1974). Influences of physical properties of the liquid on the erosion of solids. Erosion, wear and interfaces with corrosion ASTM STP 567. American Society of Testing and Materials, pp. 128–151.
158. True M.E and Weiner P.D. (1976). A laboratory evaluation of sand erosion of oil and gas well production equipment. Annual API production division meeting. Los Angeles, CA, pp. I-1, I-27.

159. Glaeser W.A and Dow A, (1977). Mechanisms of erosion in slurry pipelines. In: Proceedings of the second international conference on slurry transportation. Las Vegas, NV: March 2–4, pp. 136–140.
160. Roco M.C, Nair P, Addie G.R and Dennis J, (1984). Erosion of concentrated slurries in turbulent flow. J Pipelines, 4: 213–21.
161. Venkatesh E.S, (1986). Erosion damage in oil and gas wells, SPE paper 15183. Rocky mountain regional meeting of the society of petroleum engineers. Billings, MT.
162. Shook C.A, Mckibben M and Small M, (1987). Experimental investigation of some hydrodynamics factors affecting slurry pipeline wall erosion. ASME paper no. 87-PVP-9.
163. Soderberg S, Hogmark S and Swahn H, (1982). Mechanisms of material removal during erosion of a stainless steel, Paper no. 82-AM-4A-1. 37th ASLE Annual Meeting, Cincinnati, May 10–13.
164. Soderberg S, Hogmark S, Engman U and Swahn H, (1981). Erosion classification of materials using a centrifugal erosion tester. Tribol Int.,333–344.
165. Hutchings I.M, (1983). Monograph on the erosion of materials by solid particle impact. Materials Technology Institute of Chemical Process Industries, Inc.; MTI publication no. 10.
166. Hutchings I.M, (1983). Introduction to the microscopy of erosion. J Microscopy, 130:331–338.
167. McLaury B.S, Wang J, Shirazi S.A, Shadley J.R and Rybicki E.F,(1997). Solid particle erosion in long radius elbows and straight pipes. Society of Petroleum Engineers, Paper no. SPE 38842, pp. 977–986.
168. Edwards J.K, McLaury B.S and Shirazi S.A. (2000). Evaluation of alternative pipe bend fittings in erosive service. Proceedings of 2000 ASME fluids engineering summer meeting, June 11–15, Boston, MA: Paper no. FEDSM2000-11245,
169. Blanchard D.J, Griffith P and Rabinowicz E, (1984). Erosion of a pipe bend by solid particle entrained in water. J Eng Indust., 106:213–217.
170. Rabinowicz E, (1979). The wear equation for erosion of metals by abrasive particles, Department of ME, MIT.

171. Finnie I, (1958). The mechanism of erosion of ductile metals. In: Proceedings of 3rd US national congress of applied mechanics. pp. 527–532.
172. Nesic S, (1991).Computation of localized erosion-corrosion in disturbed two-phase flow, PhD thesis, University of Saskatchewan, Saskatoon, Canada.
173. Bitter J.G.A, (1963). A study of erosion phenomena, Part I. Wear, 6:5–21.
174. Bitter J.G.A, (1963). A study of erosion phenomena, Part II. Wear, 6:169–190.
175. Glaeser W.A and Dow A, (1977). Mechanisms of erosion in slurry pipelines. In: Proceedings of the second international conference on slurry transportation. Las Vegas, NV: March 2–4, pp. 136–140.
176. Laitone J.A, (1979). Erosion prediction near a stagnation point resulting from aerodynamically entrained solid particles. J Aircraft, 16(12):809–814.
177. Salama M.M and Venkatesh E.S, (1983). Evaluation of erosion velocity limitations of offshore gas wells. 15th Annual OTC. Houston, TX: May 2–5, OTC no. 4485.
178. Bourgoyne A.T, (1989). Experimental study of erosion in diverter systems due to sand production, Presented at the SPE/IADC Drilling Conference, New Orleans, LA, SPE/IADC 18716, 807–816.
179. Chase D.P, Rybicki E.F and Shadley J.R, (1992). A model for the effect of velocity on erosion of N80 steel tubing due to the normal impingement of solid particles. Trans ASME J Energy Resour Technol., 114:54–64.
180. McLaury B.S, (1993). A model to predict solid particle erosion in oil field geometries. MS thesis, The University of Tulsa,
181. Svedeman S.J and Arnold K.E, (1993). Criteria for sizing Multiphase flow lines for erosive/corrosive services. Paper presented at the 1993 SPE conference, Houston SPE 265:69.
182. Jordan K, (1998). Erosion in multiphase production of oil and gas. Corrosion 98, Paper no. 58, NACE International Annual Conference, San Antonio.
183. Shirazi S.A and McLaury B.S, (2000). Erosion modeling of elbows in multiphase flow. In: Proceedings of 2000 ASME fluids engineering summer meeting, June 11–15, Boston, MA: Paper no. FEDSM2000-11251.
184. Wang J, Shirazi S.A, Shadley J.R and Rybicki E.F, (1996). Application of flow modeling and particle tracking to predict sand erosion rates in 90-

degree elbows. FED-vol. 236, ASME fluids engineering division conference, vol. 1, pp. 725–734.

185. Edwards J.K, McLaury B.S and Shirazi S.A, (2000). Evaluation of alternative pipe bends fittings in erosive service. Proceedings of 2000 ASME fluids engineering summer meeting, June 11–15, Boston, MA: Paper no. FEDSM2000-11245.
186. Ahlert K.R, (1994). Effects of particle impingement angle and surface wetting on solid particle erosion on ANSI 1018 steel, MS thesis, University of Tulsa, USA.
187. Gomes Ferreira C, Ciampini D and Papini M, (2004). The effect of inter-particle collisions in erosive streams on the distribution of energy flux incident to a flat surface. Tribology International, 37:791–807.
188. Papini M, Ciampini D, Krajac T and Spelt J.K, (2003). Computer modelling of interference effects in erosion testing: effect of plume shape. Wear, 255(1–6):85–97.
189. Gorham D.A and Kharaz A.H, (2000). The measurement of particle rebound characteristics. Powder Technology, 112:193–202.
190. Wu C, Li L and Thornton C, (2003). Rebound behaviour of spheres for plastic impacts. International Journal of Impact Engineering, 28:929–946.
191. Karaz A.H and Gorham D.A, (2000). A study of the restitution coefficient in elastic–plastic impact. Philosophical Magazine Letters, 80: 549–559.
192. Molinari J.F and Ortiz M, (2002). A study of solid-particle erosion of metallic targets. International Journal of Impact Engineering, 27: 347–358.
193. Kleis I and Hussainova I, (1998). Investigation of particle-wall impact process, Wear, 233–235:168–173.
194. Hutchings I.M, Winter R.E and Field J.E, (1976). Solid particle erosion of metals: the removal of surface material by spherical projectiles. Proceedings of the Royal Society of London A, 348:379.
195. Hutchings I.M, (1979). Mechanisms of the erosion of metals by solid particles. In: Adler WF, editor. Erosion: prevention and useful applications, ASTM STP664. Philadelphia: American Society for Testing and Materials, pp. 59–76.
196. Hutchings I. M, (1977). Deformation of metal surfaces by the oblique impact of square plates. International Journal of Mechanical Sciences, 19:45–52.

197. Rickerby D.G and MacMillan N.H, (1980). On the oblique impact of a rigid sphere against a rigid plastic solid. International Journal of Mechanical Sciences, 22:491–494.
198. Hutchings I.M, Macmillan N.H and Rickerby D. G, (1981). Further studies of the oblique impact of a hard sphere against a ductile solid. International Journal of Mechanical Sciences, 23(11):639–646.
199. Sundararajan G and Shewmon P.G, (1987). The oblique impact of a hard ball against ductile, semi-infinite, target materials—experiment and analysis. International Journal of Impact Engineering, 6(1): 3–22.
200. Tirupataiah Y, Venkataraman B and Sundararajan G, (1990). The nature of the elastic rebound of a hard ball impacting on ductile, metallic target materials. Materials Science and Engineering A, 24:133–140.
201. Sundararajan G, (1991). The depth of the plastic deformation beneath eroded surfaces: the influence of impact angle and velocity, particle shape and material properties. Wear, 149:129–153.
202. Papini M and Spelt J.K, (1998). The plowing erosion of organic coatings by spherical particles. Wear, 222:38–48.
203. Papini M, (1999). Organic coating removal by single particle impact. PhD thesis, Department of Mechanical and Industrial Engineering, University of Toronto, Toronto, Ont., Canada.
204. Papini M and Spelt J.K, (2000). Impact of rigid angular particles with fully plastic targets—Part I: Analysis. International Journal of Mechanical Sciences, 42(5):991–1006.
205. Papini M and Spelt J.K, (2000). Impact of rigid angular particles with fully plastic targets—Part II: Parametric study of erosion phenomena. International Journal of Mechanical Sciences, 42(5):1007–1025.
206. Dhar S, Krajac T, Ciampini D and Papini M, (2005). Erosion mechanisms due to impact of single angular particles. Wear, 258(1–4):567–579.
207. Hutchings I.M, (1981). A model for the erosion of metals by spherical particles at normal incidence, Wear, 70:269–281.
208. Brown R, Jun E and Edington J, (1982). Mechanisms of solid particle erosive wear for 90◦ impact on copper and iron, Wear, 74:143–156.
209. Gulden M.E, (1981). Solid particle erosion of Si3N4 materials, Wear 69:115–129.

210. Sundararajan G, (1983). The solid particle erosion of metals and alloys, Trans. Indian Inst. Metals 36:474–495.
211. Gachon Y, Vannes A.B and Farges G, (1998). Study of sand particle erosion of magnetron sputtered multilayer coatings, in: Proceedings of the International Conference on Erosive and Abrasive Wear (ICEAW); 9th International Conference on Erosion by Liquid and Solid Impact (ELSI IX), Cambridge, UK.
212. Shimizu K, Noguchi T and Seitoh H, (1998). FEM analysis of the dependency on impact angle during erosive wear, in: Proceedings of the International Conference on Erosive and Abrasive Wear (ICEAW); 9th International Conference on Erosion by Liquid and Solid Impact (ELSI IX), Cambridge, UK.
213. Schimizu K, Noguchi T and Matubara Y, (1999). FEM analysis of erosive wear, Int. J. Cast Metals Res. 11:515–520.
214. Tomassone M.S, Sokoloff J.B and Widom A, (1997). Dominance of phonon friction for a xenon film on a silver surface, Phys. Rev. Lett. 79: 4798–4801.
215. Gumbsch P and Cannon R.M, (2000). Atomic aspects of brittle fracture, MRS Bull. 25:15–20.
216. Zhong W and Tománek D, (1990). First-principles theory of atomic-scale friction, Phys. Rev. Lett. 64:3054–3057.
217. Li D.Y, Elalem K, Anderson M.J and Chiovelli S, (1999). A micro-scale dynamical model for wear simulation, Wear, 225: 380–386.
218. Elalem K and Li D.Y, (2001). Modelling abrasive wear of homogenous and heterogeneous materials, hydraulic failure analysis: fluids, components and system effects, ASTM, LISA.
219. Chen Q and Li D.Y, (2003). Computer simulation of solid particle erosion, Wear, 254:203–210.
220. Ratner S.N, Farberoua I.I, Radyukeuich O.V and Lure E.G, (1967). Correlation between wear resistance of plastics and other mechanical properties, in: D.I. James (Ed.), Abrasion of Rubber, MacLaren, London, pp.145–154.
221. Lancaster J.K, (1972). Friction and wear, in: A.D. Jenkins (Ed.), Polymer Science and Material Science Handbook, North Holland, London, (Chapter 14).

222. Friedrich K, (1986). Erosive wear of polymer surfaces by steel ball blasting, J. Mater. Sci. 21:3317–3332.
223. Velten K, Reinicke R and Friedrich K, (2000). Wear volume prediction with artificial neural networks, Tribol. Int. 33:731–736.
224. Zhang Z, Friedrich K and Velten K, (2002). Prediction on tribological properties of short fiber composites using artificial neural networks, Wear, 252:668–675.
225. Zhang Z and Friedrich K, (2003). Artificial neural networks applied to polymer composites: a review, Compos Sci Technol, 63:2029–2044.
226. Esteban Fernandez J, Ma del Rocio Fernandez M, Vijande Diaz R and Tucho Navarro R, (2003). Wear, 255:38–43.
227. Spuzic S, Zec M, Abhary K, Ghomashchi R and Reid I, (1997). Fractional design of experiments applied to a wear simulation, Wear, 212(1):131-139.
228. Prasad B. K, (2002). Abrasive wear characteristics of a zinc-based alloy and zinc-alloy/ SiC composite, Wear, 252(3-4):250-263.
229. Deuis R. L, Subramanian C and Yellup J. M, (1998). Three-body abrasive wear of composite coatings in dry and wet environments, Wear, 214(1):112-130.
230. Banerji A, Prasad S. V, Surappa M. K and Rohatgi P. K, (1982). Abrasive wear of cast aluminium alloy-zircon particle composites, Wear, 82(2):141-151.
231. Mondal D. P, Das S, Jha A. K and Yegneswaran A. H, (1998). Abrasive wear of Al alloy–Al_2O_3 particle composite: a study on the combined effect of load and size of abrasive, Wear, 223(1-2):131-138.
232. Taguchi G and Konishi S, (1987).Taguchi Methods: Orthogonal Arrays and Linear Graphs; Tools for Quality Engineering, American Supplier Institute Inc., Dearborn, MI.
233. Taguchi G, (1990). Introduction to Quality Engineering, Asian Productivity Organization, Tokyo,
234. Phadke M.S, (1989). Quality Engineering using Robost Design, Prentice-Hall, Englewood Cliffs, NJ.
235. Wu Y and Moore W.H, (1986). Quality Engineering: Product & Process Design Optimization, American Supplier Institute Inc., Dearborn, MI.
236. Logothetis N and Haigh A, (1987). Profession. Statist. 6:10–16.

237. Logothetis N and Haigh A, (1988). Qual. Reliab. Eng. Int. 4:159–169.
238. Shoemaker A.C and Kackar R.N, (1988). A methodology for planning experiments in robust product and process design, Qual. Reliab. Eng. Int. 4:95–103.
239. Phadke M.S and Dehnad K, (1988). Optimization of product and process design for quality and cost. Qual. Reliab. Eng. Int. 4:105–112.
240. Mahapatra S.S, Patnaik Amar and Khan M.S, (2006). Development and Analysis of Wear Resistance Model for Composites of Aluminium Reinforced with Red mud, The journal of Solid Waste Technology and Management, 32(1):28-35.
241. Mahapatra S.S and Patnaik Amar, (2006). Optimization of Parameter Combinations in Wire Electrical Discharge Machining using Taguchi method, Indian journal of engineering & material sciences, 13:493-502.
242. Mahapatra S.S and Patnaik Amar, (2006). Optimization of Wire Electrical Discharge Machining (WEDM) process Parameters using Taguchi Method, Int. J.Adv. Manuf. Technol. DOI.10.1007/s00170-006-0672-6.
243. Mahapatra, S.S and Patnaik Amar, (2007). Parametric Optimization of Wire Electrical Discharge Machining (WEDM) Process using Taguchi method, Journal of the Brazilian Society of Mechanical Sciences 28(4):423-430.
244. Mahapatra S.S and Patnaik Amar, (2006). Determination of Optimal Parameters Settings in Wire Electrical Discharge Machining (WEDM) Process using Taguchi method, The Institution of Engineering 87:16-24.
245. Mahapatra S.S and Patnaik Amar, (2006). Parametric Analysis and Optimization of Drilling of Metal Matrix Composites based on the Taguchi Method, The International Journal for Manufacturing Science and Technology 8(1):5-12.
246. Mahapatra S.S and Patnaik Amar, (2007). Optimization of Wire Electrical Discharge Machining (WEDM) Process Parameters using Taguchi method, The International Journal for Manufacturing Science and Technology 9(2):129-144.
247. Ruff A.W and Ives L.K, (1975). Measurement of solid particle velocity in erosive wear, Wear, 35 (1):195-199.
248. Srivastava V.K and Pawar A.G, (2006). Solid particle erosion of glass fiber reinforced flyash filled epoxy resin composites, Composite science and technology, 66 (15):3021-3028.

249. Suresh. A and Harsha A. P, (2006). Study of erosion efficiency of polymers and polymer composites, Polymer testing, 25 (2):188-196.
250. Al Emran Ismail*, Nor Azila Zamani Tensile and impact behavior of hybrid extruded glass/natural fiber reinforced polypropylene composites International Conference on Environmental Research and Technology (ICERT 2008), pp-793-796.
251. Simon Haykin, Neural Networks: A Comprehensive Foundation, Prentice Hall, 1999.
252. Zhou R, Lu D.H, JiangY.H and Li Q.N, (2005). Mechanical properties and erosion wear resistance of polyurethane matrix composites, Wear, 259 (1-6):676-683.
253. Mishra, P.K. (1997). Nonconventional machining. Narosa Publishing House, New Delhi.
254. Sundararajan G, Roy M and Venkataraman B, (1990). Erosion efficiency-a new parameter to characterize the dominant erosion micromechanism, Wear, 140: 369.
255. Stachowiak, G.W and Batchelor, A.W. (1993). Engineering tribology, Tribology Series 24, Elsever. Amsterdam. 588.
256. Barkoula N. M and Karger-Kocsis J, (2002). Effects of fibre content and relative fibre-orientation on the solid particle erosion of GF/PP composites, Wear, 252(1-2):80-87.
257. Hutchings I.M, Winter R.E and Field J.E, (1976). Solid particle erosion of metals: the removal of surface material by spherical projectiles, Proc Roy Soc Lond, Ser A 348:379-392.
258. Harsha A.P, Tewari U.S and Venkatraman B, (2003). Solid particle erosion behaviour of various polyaryletherketone composites, Wear, 254:693-712.
259. Tamer S and Taskiran I, (2007). Erosion Wear behaviour of polyphenylenesulphide (PPS) composites, Materials and Design, 28:2471-2477.
260. Tewari U.S, Harsha A.P, Hager A.M and Friedrich K, (2002). Solid particle erosion of unidirectional carbon fiber reinforced polyetheretherketone composites, Wear, 252 (11-12):992-1000.
261. Montgomery D.C, (2005). Design and Analysis of Experiments, fifth Ed. John wiley & Sons, Inc. 363-382.

Appendices

LIST OF PUBLICATIONS OUT OF THIS WORK

INTERNATIONAL CONFERENCES

1. **Amar Patnaik,** S.S. Mahapatra, Alok Satapathy and R.R.Dash "A Study on Erosion Behaviour of Glass--Fiber Reinforced Polyester" Fourth AIMS International Conference on Management (AIMS4) IIM-Indor-2006.
2. **Amar Patnaik,** S.S.Mahapatra,Alok Satapathy, S.N.Mahendra and R.R.Dash**,** **"**A Study on Erosion Behaviour of Glass-Fiber Reinforced Polyester composites using Taguchi Mehod" 2nd International Conference on Recent Advances in Composite Materials,BHU-Varanasi, Feb.-2007.
3. **Amar Patnaik,** S.S.Mahapatra, Alok Satapathy, S.N.Mahendra and R.R.Dash**,** "Implementation of Taguchi Method for Tribo-Performance of Hybrid Composites" Eighth International Conference on Operations and Quantitative Management (ICOQM-8), Assumption University, Bangkok, Thailand October 17-20, 2007.

INTERNATIONAL JOURNALS

1. **Amar Patnaik**, Alok Satapathy, S.S. Mahapatra and R.R.Dash., 2008, "Modeling and Prediction of Erosion Response of Glass Reinforced Polyester-Flyash Composites" Journal of Reinforced Plastics and Composites- DOI: 10.1177/0731684407085644.
2. **Amar Patnaik**, Alok Satapathy, S.S. Mahapatra and R.R.Dash., 2008,"A Taguchi Approach for Investigation of Erosion of Glass Fiber–Polyester Composites'' Journal of Reinforced Plastics and Composites, doi:10.1177/0731684407085728.
3. **Amar Patnaik**, Alok Satapathy, S.S. Mahapatra and R.R.Dash., 2008, "Parametric Optimization of Erosion Wear of Polyester-GF-Alumina Hybrid Composites using Taguchi Method'' Journal of Reinforced Plastics and Composites, doi:10.1177/0731684407086867
4. **Amar Patnaik**, Alok Satapathy, S.S. Mahapatra and R.R.Dash.,2008, "Implementation of Taguchi Design for Erosion of Fiber Reinforced

Polyester Composite Systems with SiC Filler'' Journal of Reinforced Plastics and Composites- doi: 10.1177/0731684407087688.

5. **Amar Patnaik**, Alok Satapathy, S.S. Mahapatra and R.R.Dash., 2008 "A Comparative Study on Different Ceramic Fillers affecting Mechanical Properties of Glass-Polyester Composites'' Journal of Reinforced Plastics and Composites, doi:10.1177/0731684407086589.
6. **Amar Patnaik**, Alok Satapathy, S.S. Mahapatra and R.R.Dash, 2008, "Erosive Wear Assesment of Glass Reinforced Polyester-Flyash Composites using Taguchi Method" International Polymer Processing, Vol. 23 (2), pp. 192-199.
7. S.S. Mahapatra, **Amar Patnaik**, Alok Satapathy, and R.R.Dash. 2008 "Taguchi Method Applied to Parametric Appraisal of Erosion Behavior of GF-Reinforced Polyester Composites'' Wear, 265, pp. 214–222.
8. **Amar Patnaik**, Alok Satapathy, S.S. Mahapatra and R.R.Dash, 2007 "A Modeling Approach for Prediction of Erosion Behavior of Glass Fiber-Polyester Composites" Journal of Polymer Research, DOI 10.1007/s10965-007-9154-2.
9. **Amar Patnaik,** Alok Satapathy, S.S. Mahapatra and R.R.Dash. "Modified Erosion Wear Characteristics of Glass-Polyester Composites by Silicon Carbide Filling: A Parametric Study using Taguchi Technique'' International Journal of Materials and Product Technology (IJMPT) (Special Issue on: "Materials Processing Technology)-2007. (accepted)
10. **Amar Patnaik**,Alok Satapathy, S.S. Mahapatra and R.R.Dash. 2009, "Tribo-Performance of Polyester Hybrid Composites: Damage Assessment and Parameter Optimization using Taguchi Design'' Materials and Design, Vol.30, pp. 57-67.
11. **Amar Patnaik**, Alok Satapathy and S.S.Mahapatra, 2009, Study on Erosion Response of Hybrid Composites using Taguchi Experimental Design, Journal of Engineering Materials and Technology, ASME, Vol. 131, pp. 1-16.

Appendix A2

Brief bio-data of the author

The author, **Amar Patnaik**, born on 26-12-1977 graduated in Mechanical Engineering from Karnataka University in the year 2000. He completed his Post-graduate study in Mechanical Engineering with specialization in Production Engineering from the National Institute of Technology, Rourkela-769008, India in the year 2005. Immediately after completion of M.Tech programme, he joined as a Senior Lecturer in Gandhi Institute of Engineering and Technology, Gunupur, Orissa.

The author is engaged in active research in the area of composite materials since 2004. He has 28 research papers to his credit which have been published in various national and international journals of repute. He has also presented 11 research papers in the area of composites and non-conventional machining processes at various national and international conferences held in India and abroad.

At present, he is a faculty in the Department of Mechanical Engineering at the National Institute of Technology, Hamirpur (H.P), India.

******